Molecular pharmacological analysis of the human MrgD receptor

New insights into signaling

Dissertation

zur
Erlangung des Doktorgrades (Dr. rer. nat.)
der
Mathematisch-Naturwissenschaftlichen Fakultät
der
Rheinischen Friedrich-Wilhelms-Universität Bonn

vorgelegt von
Diana Magdy Fahim Hanna
aus
Kairo, Ägypten

Bonn, 2021

Angefertigt mit Genehmigung der Mathematisch-Naturwissenschaftlichen Fakultät der Rheinischen Friedrich-Wilhelms-Universität Bonn

Erstgutachter: Prof. Dr. med. Ivar von Kügelgen

Zweitgutachterin: Prof. Dr. Christa E. Müller

Fachnaher Gutachterin: PD. Dr. Anke Schiedel

Fachfremder Gutachterin: Prof. Dr. Dorothea Bartels

Tag der Promotion: Donnerstag 29. Juli 2021

Erscheinungsjahr: 2021

Table of contents

List of abbreviations

[^{3}H] cAMP	Tritium-labeled cyclic adenosine monophosphate
µl	Microliter
µm	Micrometer
µM	Micromolar
µs	Microsecond
µW	Microwatt
AC	Adenylyl cyclase
ACE	Angiotensin converting enzyme
Akt	Protein kinase B
AlphaScreen	Amplified luminescent proximity homogenous assay
AMPK	5`Adenosine monophosphate-activated protein kinase
ANOVA	Analysis of Variance
ATP	Adenosine triphosphate
bp	Base pair
BSA	Bovine serum albumin
cAMP	Cyclic adenosine monophosphate
cDNA	Complementary deoxyribonucleic acid
cGMP	Cyclic guanosine monophosphate
CHO	Chinese hamster ovary cells
DMSO	Dimethyl sulfoxide
DNA	Deoxyribonucleic acid
DNase	Deoxyribonuclease
COVID-19	Corona virus disease 2019

DPBS	Dulbecco’s phosphate salt buffered saline
DRG	Dorsal root ganglion
E. coli	Escherichia coli
EC_{50}	Half maximal effective concentration
ECL	Extracellular loop
EDTA	Ethylenediaminetetraacetic acid
eNOS	Endothelial nitric oxide synthase
ERK	Extracellular signal-regulated kinase
EtOH	Ethanol
FBS	Fetal bovine serum
Fluo-4-AM	Acetoxymethyl ester of Fluo-4
fM	Femtomolar
FRT	Flp recombination target
G protein	Guanine nucleotide-binding protein
GABA	γ–Aminobutyric acid
GDP	Guanosine diphosphate
GPCRs	G protein-coupled receptors
GRKs	G protein-coupled receptor kinases
GTP	Guanosine triphosphate
h	Hour
HBSS	Hanks balanced salt solution
HEK	Human embryonic kidney cells
hERG	Human ether-go-go related gene-channel
hMrgD	Human MAS-related gene member D
HTS	High throughput screening

HUVEC	Human umbilical vein endothelial cells
IB4	Isolectin B4
IC_{50}	Half maximal inhibitory concentration
ICL	Intracellular loop
IP3	Inositol triphosphate
IUPHAR	The International Union of Basic and Clinical Pharmacology
JNK	c-Jun N-terminal kinase
Kb	Kilo base (s)
Kd	Binding affinity
kDa	Kilodalton
KO	Knockout
LOCI	Luminescent oxygen channeling immunoassay
LSM	Laser scanning microscopy
MAPKs	Mitogen-activated protein kinases
MD	Molecular dynamics
min	Minute
ml	Milliliter
mm	Millimeter
mM	Millimolar
Mrgs	MAS-related genes
mRNA	Messenger ribonucleic acid
MS	Mass Spectrometry
NFAT	Nuclear factor of activated T-cells
nm	Nanometer
nM	Nanomolar

NMDA	N-methyl-D-aspartate
NO	Nitric oxide
ns	Nanosecond
ºC	Degree Celsius
PI3K	Phosphoinositide 3-kinase
PKA	Protein kinase A
pK_B	Affinity constant
PLC	Phospholipase C
PTX	Pertussis toxin
RAS	Renin-angiotensin system
RLU	Relative light unit
RNA	Ribonucleic acid
RNase	Ribonuclease
rpm	Revolutions per minute
RT	Room temperature
s	Second
SARS-CoV-2	Severe acute respiratory syndrome coronavirus 2
SEM	Standard error of the mean
SNSRs	Sensory neuron-specific receptors
TAE	Tris-acetate-EDTA buffer
TM	Transmembrane
TRIS	*Tris*(hydroxymethyl)aminomethane
UV	Ultraviolet
WHO	World Health Organization

1. Introduction

1.1. G protein-coupled receptors “GPCRs”

1.1.1. Classification of GPCRs

Mammalian Guanine nucleotide-binding protein (G protein)-coupled receptors (GPCRs) constitute the largest family of signaling proteins, encompassing approximately 850 unique members so far identified in the human genome of which 342 are non-olfactory (Fredriksson et al., 2003). The occurrence of GPCRs and G-protein signaling dates back ~1.2 billion years, which is before plants, fungi and animals emerged from a common ancestor as suggested by evolutionary studies (Schöneberg et al., 2007). Characteristics of this family includes big size, ubiquitous expression, and participation in nearly every (patho)physiological process in mammals. This unsurprisingly makes the human GPCRs the target for ~ 30% of the currently marketed drugs including β-blockers, angiotensin receptor blockers, opioid agonists and histamine receptor blockers and many others (Santos et al., 2017; Erlandson et al., 2018).

Two overlapping classifcation systems have been used to sort out this superfamily. One based on sequence homology and denotes the classes A–F, of these, classes D and E are not found in vertebrates (Kolakowski, 1994). An alternative classification scheme is based on phylogenetic analysis by using the Hidden Markov Model approach for analysis of multiple sequence alignments of all GPCRs from 13 eukaryotic genomes (Fredriksson et al., 2003). This divides vertebrate GPCRs into five classes which are named after the prototypical members “can be shortened to the acronym GRAFS" **(Table 1).**

Rhodopsin (class A receptors) includes a vast variety of ligands as peptides, amines, and purines. Class A is by far the largest group with about 700 members, of whom about 240 are non-olfactory receptors. It was further subdivided into 4 groups (α, β, γ and δ) in which the largest cluster of members, the olfactory receptors, is found in the δ-group (Fredriksson et al., 2003; Lagerström and Schiöth, 2008). Furthermore, the rhodopsin family has the largest number of receptors which are targeted by clinically used drugs (Tyndall and Sandilya, 2005). Secretin (class B receptors) represent a small family of GPCRs in which all members have an extracellular hormone-binding domain and bind peptide hormones. Secretin is named after the first receptor which was discovered in this family (Ishihara et al., 1991). Glutamate (class C receptors) are receptors for the main neurotransmitters glutamate and gamma-aminobutyric

acid (GABA), for calcium (Ca^{2+}), for sweet and amino acid taste compounds, and for some pheromone molecules, as well as for odorants in fish (Pin et al., 2003). With regards to GRAFS GPCRs classification system, the fourth class (Adhesion family), represents the second largest GPCR family in humans and includes 33 members (Fredriksson et al., 2003). This family is also named as the LNB7TM (Foord et al., 2005), where LN stands for their long N-termini and B7TM for their 7 transmembrane region sequence similarity to those of class B secretin receptors (Stacey et al., 2000). In 1989, the first report on a seven hydrophobic domain-containing protein, assigned to the tissue polarity locus (frizzled) in *Drosophila* was published (Vinson et al., 1989). Following that discovery, 10 human homologues of the *Drosophila* frizzled were further cloned and characterized (all references are mentioned in the review Lagerström and Schiöth, 2008). Together with smoothened and Taste 2 receptors, the fifth class "Frizzled"/Taste 2 family is complete.

GPCR family	Representative members	Biological functions
G (Glutamate)	Metabotropic glutamate receptors, $GABA_B$ receptor, Ca^{2+}-sensing receptors, and taste1 receptors.	• Neurobiological roles • Gustatory roles (sweet and savory tastes)
R (Rhodopsin)	**α-group** includes histamine receptors 1 and 2, dopamine receptors 1 and 2, serotonin receptors 1A, 1D and 2A, adrenoceptors 1A, 2A, B1 and B2, muscarinic receptor 3, prostanoid receptors (TP, EP1, EP3, IP1 and FP), and cannabinoid receptor 1.	• Senses of vision and olfaction • Biogenic amine and neurotransmitter signaling • Immunological roles • Cardiovascular roles • Gastrointestinal roles • Neurobiological roles • Endocrinological roles
	β-group includes mainly peptide-binding receptors as: neuropeptide FF receptors, neuropeptide Y receptors, endothelin-related receptors, gastrin-releasing peptide receptor, thyrotropin releasing hormone receptor, the ghrelin receptor, arginine vasopressin receptors, gonadotropin- releasing hormone receptors, and oxytocin receptor.	
	γ-group includes receptors for both peptides and lipid like compounds as: the three opioid μ, δ, and κ receptors, somatostatin receptors 2 and 5, angiotensin receptor 1, and chemokine receptors.	
	δ-group includes MAS-related receptor cluster (MAS1 and MAS-related receptors), glycoprotein receptors, purine receptors and olfactory receptors.	

A (Adhesion)	Latrophilins, cadherin EGF LAG seven-pass G-type receptors.	• Immunological roles • Cancer • Developmental biology of the central nervous system
F (Frizzled/Taste2)	Frizzled receptors, Smoothened receptor, and taste2 receptors.	• Developmental biology • Cancer • Perception of bitter taste
S (Secretin)	Calcitonin and calcitonin-like receptors, corticotropin-releasing hormone receptors, glucagon receptor, gastric inhibitory polypeptide receptor, glucagon-like peptide receptor, growth-hormone-releasing hormone receptor, adenylate cyclase activating polypeptide receptor, parathyroid hormone receptors, secretin receptor, and vasoactive intestinal peptide receptors	• Endocrinological roles • Metabolic roles • Central homeostatic roles

Table 1: A summary of GPCR families with representative members and biological functions (Modified from Fredriksson et al., 2003; Lagerström and Schiöth, 2008; Erlandson et al., 2018).

1.1.2. Structural architecture and breakthrough in analysis of crystal structures of GPCRs

GPCRs are normally bound to the plasma membrane, representing the eyes and ears of the cell (Gurevisch and Gurevisch, 2019). GPCRs share a distinctive structural feature which can be divided into three parts. “A” The extracellular region, which consists of the N-terminus and three extracellular loops (ECL1–ECL3). “B” The transmembrane region (TM), which consists of seven α-helices (TM1–TM7). “C” The intracellular region, comprising three intracellular loops (ICL1–ICL3), an intracellular amphipathic 3-4 turn α-helix (H8), and the C-terminus (Ji et al., 1998; Flower, 1999; Venkatakrishnan et al., 2013). This common structural organization greatly contrasts the structural diversity of the natural GPCR ligands ranging from subatomic particles (a photon) to ions (H^+ and Ca^{2+}), to small organic molecules, to peptides and proteins (Ji et al., 1998). Generally, the extracellular region regulates ligand entry. The TM region forms the structural core which binds ligands and conveys extracellular signals to the intracellular region through conformational changes. Lastly, the intracellular region interfaces with cytosolic signaling proteins (heterotrimeric G-proteins, arrestins, G protein-coupled receptor kinases (GRKs) and other down-stream signaling effectors).

The machinery of how the 7TM helices of a GPCR are arranged into a bundle was imagined based on the low-resolution model of frog rhodopsin; the prototypical GPCR responsible for light perception from cryo-electron microscopy studies of the two-dimensional crystals (Unger et al., 1997). Recent advances in GPCRs structural biology have approved the initial idea and further deciphered the molecular mechanisms beyond ligand binding and GPCRs-mediated signaling. That was nearly by the end of the 20th century, when the first high-resolution crystal structure of a GPCR was solved by X-ray crystallography. That was for bovine rhodopsin in complex with 11-*cis*-retinal (Palczewski et al., 2000). The structure was not a surprise except for the presence of an additional cytoplasmic helix H8 and a precise location of a loop covering retinal binding site. However, it served as a scaffold which was hoped to be a universal template for homology modeling and drug design for other GPCRs. Seven years later full of extensive research and technology development, the high-resolution crystal structure of the human β2–adrenergic receptor (β2-AR) was decoded and that was the first structure for a GPCR with a diffusible ligand (Cherezov et al., 2007; Rasmussen et al., 2007). Interestingly, the structure had a quietly different shape on the extracellular side as compared to that of rhodopsin. Furthermore, the ligand binding site was much more spacious

and was open to the exterior. Other receptors which were shortly crystallized afterwards showed more easily accessible ligand binding sites. Past few years witnessed progress in membrane protein engineering and crystallography with subsequent exponential growth in GPCR structure determination. Crystal structures of GPCR-effector complexes showed up answering inquiries on the machinery of GPCR-mediated signaling. The first high-resolution view of transmembrane signaling by a GPCR was unraveled in 2011, when the structure of the ternary agonist occupied β2-AR–Gs-complex was solved (Rasmussen et al., 2011a). In 2015, the crystal structure of a constitutively active form of human rhodopsin bound to a pre-activated form of the mouse visual arrestin was provided by serial femtosecond X-ray laser crystallography (Kang et al., 2015). Subsequently, the adenosine receptor A2AAR–Gs complex was crystallized (Carpenter et al., 2016). Further recent complex structures include: calcitonin CTR–Gs (Liang et al., 2017), glucagon-like peptide Glp1R–Gs (Zhang et al., 2017), opioid μOR–Gi (Koehl et al., 2018), serotonin 5-HT1BR–Go (Garcı´a-Nafrı´a et al., 2018), adenosine A1AR–Gi (Draper-Joyce et al., 2018), and rhodopsin–Gi (Kang et al., 2018). So far, recent advances in GPCRs structural biology resulted in resolving more than 229 high-resolution structures of 136 distinct GPCRs-ligand complexes of 48 different GPCRs (Vass et al., 2018). Solved GPCRs crystal structures are reviewed in (Trzaskowski et al., 2012; Katritch et al., 2013; Venkatakrishnan et al., 2013; Zhang et al., 2015a; Lu and Wu et al., 2016; Lee et al., 2018; Vass et al., 2018). Altogether, these structures elucidated several issues regarding structural similarity and diversity of the GPCR superfamily and molecular basis of GPCR ligand recognition, activation, allosteric modulation, dimerization, and signaling. Nevertheless, structural studies of GPCRs remain challenging and difficult due to deficiency in a naturally abundant source of proteins, multiple conformation states of the receptor and the relatively small structured polar surface for forming crystal lattice contacts (Zhang et al., 2015a; Lu and Wu et al., 2016).

1.1.3. Diversity in ligand binding pockets and modes among GPCRs

A characteristic feature of class A receptor family is the ability to interact with diverse endogenous ligands that have different shapes, sizes, and chemical properties and to convey signals related to each ligand. Even though the receptor family shares common structural architecture, however, sizes, shapes and electrostatic properties of the ligand-binding pockets are extensively distinct between different receptors. Moreover, ligand binding modes can vary even within the same receptor family with a high overall structural similarity depending on receptor subtypes.

In class A GPCRs which represents the majority of receptors, the ligand binding pocket exist between the helices. The pocket could be either close to the extracellular surface or buried nearly to half the depth of the membrane. The pocket size and location are dependent on the ligand molecule (Erlandson et al., 2018; Lee et al., 2018). For example: ligands of peptide receptors such as chemokine receptors and opioid receptors, have a shallower and more open ligand-binding pockets as compared to other receptors with endogenous small-molecule ligands such as aminergic receptors. This could be attributed to the fact that peptides are much larger molecules that cannot enter deeply into the 7TM bundle and need more binding space as compared to small-molecule ligands (Zhang et al., 2015a). In most members of other families of GPCRs, the ligand binding pockets are very lipophilic and more open with the orthosteric site existing in large extracellular domains (Bartuzi et al., 2017). In the peptide interacting class B GPCRs, the high-affinity part of the ligand-binding pocket exist in their large N-termini, while the pocket between the helices constitutes the lower-affinity part (Lagerström and Schiöth, 2008; Erlandson et al., 2018). Class C GPCRS are dimers with two 7TM domains. The ligand-binding pocket is a cavity which is formed between the two lobes of the N-terminus, so called "Venus fly trap" (Fredriksson et al., 2003; Goudet et al., 2004; Lagerström and Schiöth, 2008). This domain was found homologous to bacterial periplasmic binding proteins involved in transporting amino acids, ions, and sugars in the periplasm of gram-negative bacteria (O'Hara et al., 1993).

Besides the orthosteric ligands, GPCRs are also affected by an array of endogenous allosteric modulators such as lipids, ions, waters, and sterols (Chini and Parenti, 2009). Allosteric binding pockets can be found in different locations of the receptor, that are generally less conserved than the orthosteric binding site. That explains the higher selectivity of allosteric ligands as compared to orthosteric ligands which makes them highly valuable therapeutic candidates with fewer adverse effects. Solved GPCRs structures reveal allosteric binding sites within the 7TM helical bundle as in chemokine CCR5, and glutamate mGluR1, and mGluR5 receptors, or in the extracellular region of the receptor as in muscarinic M2 receptor, or on the external lipidic interface of the 7TM domain as in purinergic $P2Y_1$ receptor (Zhang et al., 2015b). Orthosteric and allosteric sites of M2, mGluR3 and mGluR5 receptors were shown in a diagrammatic comparison in (Bartuzi et al., 2017), and of β2-AR, A2AAR, and CCR5 in (Lee et al., 2018). First observation on the allosteric modulatory role of sodium (Na^+) ions came from the structure of inactive A2AAR, which uncovered a tight water-filled channel linking the extracellular and intracellular sides of the receptor (Liu et al., 2012a). Specific

cholesterol binding sites were observed in the β2-AR (Hanson et al., 2008) and A2AAR (Liu et al., 2012a) structures with modulatory activity for the receptors thermostability and binding affinity for inverse agonists.

Receptors which belong to the same subfamily, show also distinct ligand-binding modes. One example is the structures of $P2Y_1$ and $P2Y_{12}$ receptors binding their nucleotide-like ligands. Although they recognize the same endogenous ligand ADP, they display different binding features. In the $P2Y_1$R-MRS2500 structure, the adenine group of the nucleotide-like antagonist MRS2500 is close to TMs 6, and 7. Whereas the adenine ring of the nucleotide agonist 2MeSADP in the $P2Y_{12}$R-2MeSADP complex structure reaches deep into the binding pocket and interact with TMs 3, and 4 (Zhang et al., 2014; Zhang et al., 2015b). Another example is observed in the structures of chemokine receptors CXCR4 and CCR5. In CXCR4-IT1t complex structure, the antagonist IT1t occupies part of the binding pocket formed by TMs 1, 2, 3, and 7 and ECL2. However, in CCR5-maraviroc complex structure, the HIV entry inhibitor; maraviroc is found located in deeper binding site and occupies a larger area of the pocket formed by TMs 1, 2, 3, 5, 6 and 7 without any contact with extracellular loops (Wu et al., 2010; Tan et al., 2013).

Furthermore, the approach routes through which the GPCRs ligands enter the binding pockets are different among receptors. In most of GPCRs structures, a large extracellular vestibule exist which is a part of an extended hydrophilic channel leading to the orthosteric binding pocket. However, in the lipid-activated GPCRs as sphingosine-1-phosphate S1P1 receptor, the N-terminus or extracellular loops make a cap-like structure which covers the ligand-binding pocket, therefore occluding the extracellular access by the ligand (Hanson et al., 2012). In these receptors, most likely the ligands get access through lipid bilayer. An identical approach route was observed in the P2Y1R-BPTU bound structure where the non–nucleotide antagonist BPTU was found to bind to an allosteric pocket on the external receptor interface with the lipid bilayer. BPTU presents the first structurally characterized selective GPCR ligand located entirely outside the helical bundle (Zhang et al., 2015b).

Despite the diversity, a systematic comparison of the receptor-ligand interactions approved the sharing of some common structural features in all class A GPCRs. Despite penetrating to different depths within the pocket, most of ligand-interacting residues are located on the inner side of the TM helices except for peptidic ligands (Venkatakrishnan et al., 2013). While TM1 is not directly involved in contact with the ligand, the topologically equivalent residues of

TMs 3, 6, and 7 specifically interact with diverse ligands in most of the receptors. Especially, 3.32, 3.33, 3.36, 6.48, 6.51, and 7.39 residues (Ballesteros-Weinstein numbering system; Ballesteros and Weinstein, 1995) are generally common among class A GPCRs (Lee et al., 2018).

1.1.4. Conserved structural features among class A GPCRs

It is generally believed from biophysical, biochemical, and structural data that most of GPCRs exist in a dynamic equilibrium between two conformation inactive and active states. The inactive states include R; inactive ground state, and R'; inactive low-affinity agonist bound state. The active states include R"; active high-affinity agonist bound state, and R*; active state with initial binding to the effector partner. This can be converted to the full ligand-receptor-effector-complex signaling state "R^{*G} for G proteins; G^{GRK} for GRKs; and G^{A} for arrestins" (Katritch et al., 2013). In ligand free receptors, the shifting between the different states can greatly differ, which explains their variable basal activity levels (Seifert and Wenzel-Seifert, 2002; Kobilka and Deupi, 2007). Stimulating the receptors with ligands, shifts the equilibrium between inactive and active states in an efficacy-based manner. Full agonists tend to bind and stabilize the active conformation, thus shifting the equilibrium to active states. Partial agonists are less effective in shifting equilibrium towards active states as they have some affinity for both active and inactive states. Inverse agonists bind and stabilize the inactive conformation, thus shifting equilibrium to inactive states, whereas the neutral antagonists do not affect basal equilibrium (Kobilka and Deupi, 2007; Katritch et al., 2013).

"Molecular micro-switches" is the name given to some conserved functionally important signature sequence motifs in the 7TM helical bundle of class A GPCRs. These are believed to act as switches between the active and inactive states of the receptors, thus regulating receptor activation and signaling (reviewed in Nygaard et al., 2009; Trzaskowski et al., 2012; Katritch et al., 2013; Zhang et al., 2015; Lee et al., 2018; Erlandson et al., 2018). One of the most conserved motifs is the aspartic acid (glutamic acid)-arginine-tyrosine (D[E]$R^{3.50}$Y) motif in TM3 which makes an interhelical salt bridge with D/$E^{6.30}$ in TM6 forming an "ionic lock". Such ionic lock has been suggested as a characteristic feature of the inactive conformation of GPCRs where it maintains the inactive state by locking helices 3, and 6 with subsequent blocking of G-protein binding at the cytoplasmic region. That was first observed in the structures of bovine rhodopsin, stabilizing the receptor in its fully inactive state (Vogel et al., 2008). A mutational disruption of the D[E]$R^{3.50}$Y motif has shown to increase the basal

activity of rhodopsin (Palczewski et al., 2000; Vogel et al., 2008). The lock seems to be broken upon activation of receptors as observed in rhodopsin (Palczewski et al., 2000; Scheerer et al., 2008), and A2AAR (Xu et al., 2011) active structures as well as in the model of agonist induced activation of 5-HT2A receptor (Shapiro et al., 2002). Based on mutagenesis study in 2001, it was suggested that the disruption of the ionic bond between TMs 3, and 6 is a consequence for the activation of the β2-AR (Ballesteros et al., 2001). An observation which was further confirmed by molecular dynamics simulations (MD) of the wild-type β2-AR (Vanni et al., 2009). However, in the human β2-AR crystal structure, the $R^{3.50}$- $E^{6.30}$ ionic lock was found absent; instead, a hydrogen bond between the highly conserved tyrosine $Y^{3.60}$, and histidine $H^{6.31}$ was present. Meanwhile, the $R^{3.50}$ residue was found to adopt a different conformer and forms a hydrogen bond with glycine $G^{6.36}$ in TM6 which can also link TMs 3, and 6 to some extent (Rasmussen et al., 2011a; Bang and Choi, 2015). Some attributed the absence of this ionic bond despite of the presence of the residues to the inclusion of T4L fusion protein in crystal structures, which may affect the interactions in TM6.

Moreover, the residue $R^{3.50}$ (which has 96% conservation among class A GPCRs) forms another intra-helical salt bridge to the neighboring acidic side chain $D/E^{3.49}$, which was noticed as a property of inactive-state GPCRs structures (Vogel et al., 2008). Surprisingly, some active state GPCR structures showed an intact $R^{3.50}$- $D^{3.49}$ salt bridge as in β2-AR-nanobody complex (Rasmussen et al., 2011b), as well as in the activated ($R^{"}$) A2AAR structures (Xu et al., 2011; Lebon et al., 2011). The $R^{3.50}$- $D^{3.49}$ salt bridge was found to be broken in the active-state rhodopsin (R*) and β2-AR (R^{*G}) structures with subsequent changes in the rotamer conformation of the $R^{3.50}$ guanidine for interaction with the C-terminal helix of the Gα subunit (Scheerer et al., 2008; Choe et al., 2011; Rasmussen et al., 2011a; Standfuss et al., 2011). This suggests that the presence of a G-protein is a pre-requisite for the switch in $R^{3.50}$ (Katritch et al., 2013).

Another conserved feature in several high-resolution structures of class A GPCRs, is a hydrated Na^+ ion specifically bound in the middle of the 7TM bundle between TMs 2, 3, and 7. It has been described to act as a negative allosteric modulator important for stabilizing the inactive conformations. Such effect is terminated upon receptor activation with an agonist through a conformational collapse of the sodium ion pocket (Katritch et al., 2014). The first direct experimental evidence of the existence of Na^+/water cluster in the 7TM core region was observed in the high-resolution structure of A2AAR (Liu et al., 2012a). Another high-

resolution inactive crystal structures of other GPCRs also revealed the presence of Na^+ ion in the same position as protease-activated receptor PAR1 (Zhang et al., 2012a), β1-AR (Miller-Gallacher et al., 2014) and δ-OR (Fenalti et al., 2014). A common feature among class A GPCRs is the Na^+ ion binding to a highly conserved $D^{2.50}$ residue (Katritch et al., 2014). In the inactive state of the receptor, an allosteric pocket is formed by $D^{2.50}$ residue and is composed of a bound Na^+ ion and a cluster of structurally ordered water molecules which make hydrogen bonding with other highly conserved class A residues. These include leucine $L^{2.46}$, alanine $A^{2.49}$, tryptophan $W^{6.48}$, and asparagine $N^{7.45}$, and $N^{7.49}$ residues (Liu et al., 2012a). $D^{2.50}$ allosteric pocket collapse is necessary for binding of ligand and activation of GPCRs. This results in structural rearrangement of TM helices with an inward shift of the asparagine-proline-xx-tyrosine ($N^{7.49}P^{7.50}xxY^{7.53}$) motif in TM7 and subsequent narrowing of the binding pocket which can accommodate a maximum of three water molecules but not Na^+ ion (Liu et al., 2012a). The 100 ns time scale MD simulations done for A2AAR in the presence or absence of Na^+ ion showed the mutual exclusivity for binding of the ions and the high-affinity agonist to the receptor which emphasize the negative allosteric modulatory effects of Na+ ion on conformational dynamics and activations profiles of GPCRs (Gutierrez-de-Teran et al., 2013). Furthermore, extensive recent MD simulations performed on the muscarinic M3 receptor showed the binding of Na^+ ion to the deprotonated but not protonated $D^{2.50}$ residue. As a consequence of binding to the deprotonated $D^{2.50}$, the flexibility of the M3R is reduced and receptor conformation is shifted towards the inactive state. On the contrary, a protonated $D^{2.50}$ M3R is more flexible with significantly larger conformational space, resulting in its activation (Miao et al., 2015).

One more common microswitch is the transmission switch (previously called rotamer toggle switch) within the cysteine-tryptophan-x-proline ($C^{6.47}W^{6.48}xP^{6.50}$) motif in TM6. The highly conserved $W^{6.48}$ residue was hypothesized to “toggle” or flip between active and inactive states of the receptor. Comparison of the two conformation states of GPCRs showed no real flip but a shift in $W^{6.48}$ side chain towards TM5, thus serving as a link between the ligand binding site and the movement of TMs 5, and 6 via the rearrangement of the TMs 3, 5, and 6 interfaces. That supports the early observation in rhodopsin structure that activation of GPCRs is accompanied by the outward movement of the TMs 5, and 6 (Farrens et al., 1996). In opsin (Park et al., 2008) and A2AAR structures (Xu et al., 2011), a conformational shift of the side chain of $W^{6.48}$ was induced by ligands binding with subsequent movement of TM6. However, in β2-AR structures, $W^{6.48}$ seems to have an indirect role in receptor activation. The

conformational change that promotes TM6 motion is mainly mediated via polar interactions between agonists and serine $S^{5.42}$, and $S^{5.46}$ residues in TM5. This results in a rotamer switch in isoleucine $Ile^{3.40}$, which is, in turn, coupled with a 4 ˚A movement of the phenylalanine $Phe^{6.44}$ side chain and a subsequent swing of TM6 (Rasmussen et al., 2011a and b; Bang and Choi, 2015). Interestingly, the magnitude of such so called "swinging" motion of TM6 was found to vary among different GPCRs and different activated states. For example, the intracellular tip of helix 6 moves ∼3.5 ˚A in ($R^{¨}$) state of A2AAR (Xu et al., 2011), ∼6 ˚A in ($R^{¨}$ and R^{*}) states of opsin (Park et al., 2008), and as much as 14 ˚A in (R^{*G}) state of β2AR-Gs complex (Rasmussen et al., 2011a). Furthermore, the extent of such activation-induced movement was shown to vary based on the effector molecule binding to the activated GPCR. Gi-coupled GPCRs show smaller activation-induced movement as compared to Gs-coupled GPCRs (Van Eps et al., 2018). Moreover, substantial rearrangements in the G-protein itself together with GDP release were observed to control the final positioning of the intracellular tips of TMs 5, and 6 in the active signaling state (R^{*G}). Altogether, these findings suggest the crucial role of TM5 and TM6 concerted movements in G-protein binding and activation and that these movements are most likely conserved in all class A GPCRs. Noteworthy, in PAR-1 structure, the $W^{6.48}$ is replaced by $Phe^{6.48}$ and showed different conformation as compared to other class A GPCRs (Zhang et al., 2012a).

Another important site of conformational changes in the binding pocket involves TMs 3, and 7, so called "3-7 lock switch" as the link between TMs 3, and 7 is broken during activation. Although essential but receptor specific (Katritch et al., 2013). In rhodopsin, light activation breaks down the salt bridge between glutamate $E^{3.28}$ and lysine $K^{7.43}$ Schiff base linked to retinal, corresponding to an increase of the distance between TMs 3, and 7 by approximately 2–3 ˚A (Park et al., 2008). On the other hand, in A2AAR, the ribose rings of agonists form a strong hydrogen-bond networking with threonine $T^{3.36}$ and Serine/histidine ($S^{7.42}$/$H^{7.43}$). This in turn decreases the distance between TMs 3 and 7 by ∼2 ˚A compared with A2AAR in complex with an inverse agonist (Xu et al., 2011; Lebon et al., 2011). In β2-AR, in both agonist and antagonist complexes, asparagine $N^{3.32}$ and aspartic acid $D^{7.39}$ are bridged by an ethanolamine tail, and the distance between these residues seems not to extensively change between the active- and inactive-state crystal structures (Rasmussen et al., 2011a and b; Bang and Choi, 2015).

The intracellular region of GPCRs has a relatively conserved conformations which can be related to the limited types of downstream binding effectors. In most of the solved GPCR structures, the C-terminus contains a 3-4 turn α-helix (H8), which runs parallel to the membrane and is characterized by a common [F(RK)xx(FL)xxx] amphiphilic motif (Zhang et al., 2015a). Additionally, the $N^{7.49}P^{7.50}xxY^{7.53}$ motif which is positioned in the cytoplasmic end of TM7 was also proposed as one of the important micro-switches. It has shown to form a hydrogen bond between tyrosine $Y^{7.53}$, and $Y^{5.58}$ moieties, synchronized by a bridging water molecule forming a "water lock" as shown in adrenaline-β2-AR solved structure (Ring et al., 2013). Such water lock is important in stabilizing the receptor in its active state, just like the ionic lock which stabilize receptor in its inactive state. The $N^{7.49}P^{7.50}xxY^{7.53}$ motif has shown to constrain TM7 with TM1, and TMs 2, and 7 with the amphipathic H8. In the structure of ligand-free opsin, the $Y^{7.53}$ residue rotates to face the TM helical bundle, preventing the back movement of TM6 toward TM3 and hence the adoption of inactive conformation (Park et al., 2008). The significance of the $Y^{7.53}$ residue in packing the interaction of $R^{3.50}$ (D[E]$R^{3.50}$Y motif) with the G-protein binding partner was also shown in the active structure of β2-AR-Gs complex, suggesting the coordinated activity of both motifs (Rasmussen et al., 2011a). Interestingly, the tyrosine $Y^{5.58}$ side chain was found to behave differently in different active-state structures. In rhodopsin, it shifts from outside to inside of the helical bundles, while in A2AAR, it makes an opposite switch from inside to outside, and in all β2-AR complexes, it remains in the interior of the 7TM bundle. Mutagenesis studies suggested the important active-state stabilizing role for $Y^{5.58}$ via its indirect hydrogen bond with $Y^{7.53}$ as observed in rhodopsin structure, where point mutation of $Y^{5.58}$ residue to phenylalanine $Phe^{5.58}$ caused reduction in the active state lifetime (Goncalves et al., 2010). Furthermore, point mutation of tyrosine $Y^{5.58}$ to alanine contributes to the stabilization of β1-AR in its inactive state (Warne et al., 2009), reduction of basal activity in the muscarinic M3 (Li et al., 2005) and thyrotropin (Biebermann et al., 1998) receptors.

The three extracellular loops of GPCRs play key role in molding the entryway to the ligand-binding pockets (Lu and Wu, 2016). ECL2; the largest extracellular loop is structurally different between receptors, however, has conserved conformation specific to each receptor subfamily. For example, structures related to adrenergic receptor showed an α-helical display of ECL2 and a hairpin display in peptide receptors-related structures. On the other hand, ECL1 and 3 are relatively short and lacking characteristic secondary structural elements. The extracellular loop regions in class A GPCR structures have some highly conserved motifs as

well. In most of GPCR structures, a highly conserved disulfide bond exists linking the cysteine $C^{3.25}$ residue at the extracellular tip of TM3 and a cysteine residue in ECL2. This disulfide bond was found essential to stabilize the conformation of the extracellular region and to shape the entrance to the ligand-binding pocket. An exception is the S1P1R structure, where it lacks the highly conserved $C^{3.25}$ residue, the corresponding disulfide bridge, and the secondary structure in ECL2 (Hanson et al., 2012). Another exception was observed in the structure of $P2Y_{12}R$ bound to the antagonist AZD1283. The $P2Y_{12}R$ structure has the conserved $C^{3.25}$ residue but lacks the disulfide bridge between TM3 and ECL2. This could be due to the lability of the bridge in the native structure (Zhang et al., 2014).

1.1.5. GPCRs signal transduction pathways

GPCRs-mediated signaling pathways are involved in numerous physiological events from vision, olfaction, taste to neurological, cardiovascular, endocrine, and reproductive functions thus making the GPCR superfamily a major target for therapeutic interventions (Tyndall and Sandilya, 2005; Overington et al., 2006). Multiple subforms of G proteins together with receptors, effectors, and various regulatory proteins represent the components of a highly versatile signal transduction system. As required for completing the signal transduction and for other receptor modulatory functions, the intracellular C-terminus and ICLs of GPCRs interact with effector molecules either in a G protein-dependent or G protein-independent manner. GPCRs signaling has been framed in two distinct signaling pathways **(Figure 1)**. One pathway is G protein-dependent/β-arrestin-independent and the other is β-arrestin-dependent/G protein-independent. However, it was recently shown that reality is way beyond such characterization and the phrase "G proteins are genuine drivers of GPCR-mediated transduction" came to show up. Research groups have provided evidence for the G protein dependency for β-arrestin-mediated signaling (Alvarez-Curto et al., 2016; Grundmann et al., 2018).

1.1.5.1. G protein-mediated signaling at GPCRs

The classical pathways downstream of GPCRs comprise the coupling to a heterotrimeric G protein which regulates various cellular events once activated. G proteins are composed of Gα, Gβ and Gγ subunits with a nucleotide binding pocket located in the α-subunit. In mammals, at least 16 different α-subunit genes (Wilkie et al., 1992; Hurowitz et al., 2000), 5 different β-subunit genes (Watson et al., 1994; Hurowitz et al., 2000; Wettschureck and

Offermanns, 2005), and 12 different γ-subunit genes (Morishita et al., 1995; Hurowitz et al., 2000; Wettschureck and Offermanns, 2005) have been encoded. The Gα subunit has different isoforms divided in subfamilies: $G\alpha_{i/o}$, $G\alpha_{s}$, $G\alpha_{q/11}$ and $G\alpha_{12/13}$. In the guanosine diphosphate (GDP)-bound conformation, nucleotide release is hindered by the βγ dimer with subsequent stabilization of α, β and γ heterotrimer. Agonist binding to the extracellular and/or transmembrane regions of the receptor is a pre-requisite for subsequent interactions with heterotrimeric G proteins. Following interaction, the receptor behaves as a guanine nucleotide exchange factor which catalyzes the exchange of GDP attached to the Gα subunit for guanosine triphosphate (GTP) followed by dissociation of the Gα and Gβγ subunits (Wettschureck and Offermanns, 2005). Different effectors will subsequently get bound and activated by G-protein subunits: adenylyl cyclase (AC) activation by $G\alpha_{s}$; AC inhibition by $G\alpha_{i/o}$; phospholipase C (PLC) activation followed by increased intracellular (Ca^{2+}) by $G\alpha_{q/11}$, and control of the regulators of the actin cytoskeleton, so called Rho GTPases by $G\alpha_{12/13}$. Subsequently, second messengers are generated which modulate further downstream effectors. Following dissociation from the heterotrimeric complex, the Gβγ subunit can also bind to and regulate certain downstream effectors as ion channels and PLC (Ritter and Hall, 2009; Chapman et al., 2014). In addition, βγ subunit seems to play role in receptor mediated phosphorylation by GRKs through binding the C-terminal of cytoplasmic GRKs and drawing them closer to the receptor membrane where it can phosphorylate the ligand-occupied receptor (Nestler and Duman, 1998; Smrcka, 2008). Description and characterization of mammalian G proteins and their cell-type specific functions can be found in reviews (Wettschureck and Offermanns, 2005; Campbell and Smrcka, 2018).

1.1.5.2. β-Arrestin-mediated desensitization, trafficking, and signaling at GPCRs

The arrestin family of proteins consists of four members and an array of splice variants. Two visual arrestins (arrestin-1 and arrestin-4) exist which were found localized in rods and cones of retinal tissues, respectively (Smith et al., 2000). The other two isoforms are ubiquitously expressed arrestins named β-arrestin-1 (arrestin-2; Lohse et al., 1990), and β-arrestin-2 (arrestin-3; Attramadal et al., 1992). The amino acid sequence of these two β-arrestin isoforms are 78% identical with most differences in the C-terminus. The name β-arrestin comprise a “beta”-prefix, which refers to the β2-adrenergic receptor; their first reported receptor substrate and an “arrestin” suffix, referring to their main function which is to arrest signaling via G proteins (Benovic et al., 1987).

As a physiological feedback mechanism protecting against both acute and chronic overstimulation, the receptor uncouples from its cognate G proteins. The primary mechanism to regulate GPCRs activity is through the phosphorylation of activated receptors at serine and threonine residues in their ICL3 and C-terminal tail domains by GRKs. This enables the high affinity binding of GPCRs to β-arrestins which prevent further coupling of G proteins to the activated receptor, potentially through a steric hinderance mechanism thus desensitizing the G protein signaling (Benovic et al., 1987). Both β-arrestins can desensitize GPCRs, however it has been reported that β-arrestin-1 is localized in the cytoplasm and nucleus while β-arrestin-2 is mainly distributed in the cytoplasm. This is owing to the presence of leucin-rich nuclear export signal in the C-terminus of β-arrestin-2 which is lacking in β-arrestin-1 (Scott et al., 2002). Therefore, β-arrestin-1 may play more important role in GPCR-mediated nuclear signaling.

Receptor internalization is an important feature of GPCR life cycle. For many GPCRs, interactions between the C-terminal tail of GPCR-activated β-arrestin and the cell membrane endocytic proteins, clathrin and adapter protein-2 will mediate the receptor-β-arrestin-kinase complex internalization forming by this an intracellular "signalosome" (Goodman, 1996; Laporte et al., 1999). Interestingly, a recently reported distinct and additional mechanism of β-arrestin activation showed that transient engagement of the GPCR core is sufficient for activating β-arrestin which is then able to bind to membrane phosphoinositides that link it to the cell membrane for endocytosis into signaling vesicles lacking the receptor (Eichel et al., 2018). Once internalized, GPCR-β-arrestin vesicles are trafficked to degradative or recycling pathways within the cell via the binding of β-arrestins to E3 ubiquitin ligases and deubiquitinases, modulating by this receptor cell surface expression (Shenoy et al., 2001; Shenoy, 2007). Such trafficking activity of β-arrestins is an important way through which these multifunctional proteins modulate GPCR signaling and cellular responses. GPCRs are divided into two distinct categories based on their association with β-arrestins and trafficking. Class A receptors interact transiently with β-arrestins (receptors recycle rapidly) and have higher affinity for β-arrestin-2 compared to β-arrestin-1. Examples include adrenergic (β2, α-1B), μ opioid, endothelin A, and dopamine D1A receptors. Class B receptors interact more stably with β-arrestins (receptors recycle slowly) and have equal affinities for both. These involve angtiotensin Ang II, vasopressin V2, neurotensin NTS1 and neurokinin NK1 receptors (see Sharma and Paramesvaran, 2015).

Independent of G proteins, β-arrestins are also signal transducers which initiate distinct signaling patterns by acting as scaffold proteins that couple the receptor to a growing list of signaling intermediates many of which are kinases. Thus, resulting in unique cellular, physiological, and pathophysiological consequences. β-arrestins were reported to scaffold mitogen-activated protein kinases (MAPKs) such as extracellular signal-regulated kinase (ERK), c-Jun N-terminal kinase (JNK), and p38 kinase. Moreover, phosphoinositide 3-kinase (PI3Ks) / protein kinase B (Akt), tyrosine kinases (as proto-oncogene tyrosine protein kinase Src), E3 ubiquitin ligases (such as atrophin-1-interacting protein 4, and elements of nuclear factor κb (see Shenoy and Lefkowitz, 2011; Ghosh et al., 2015; Sharma and Paramesvaran, 2015; Peterson and Luttrell, 2017).

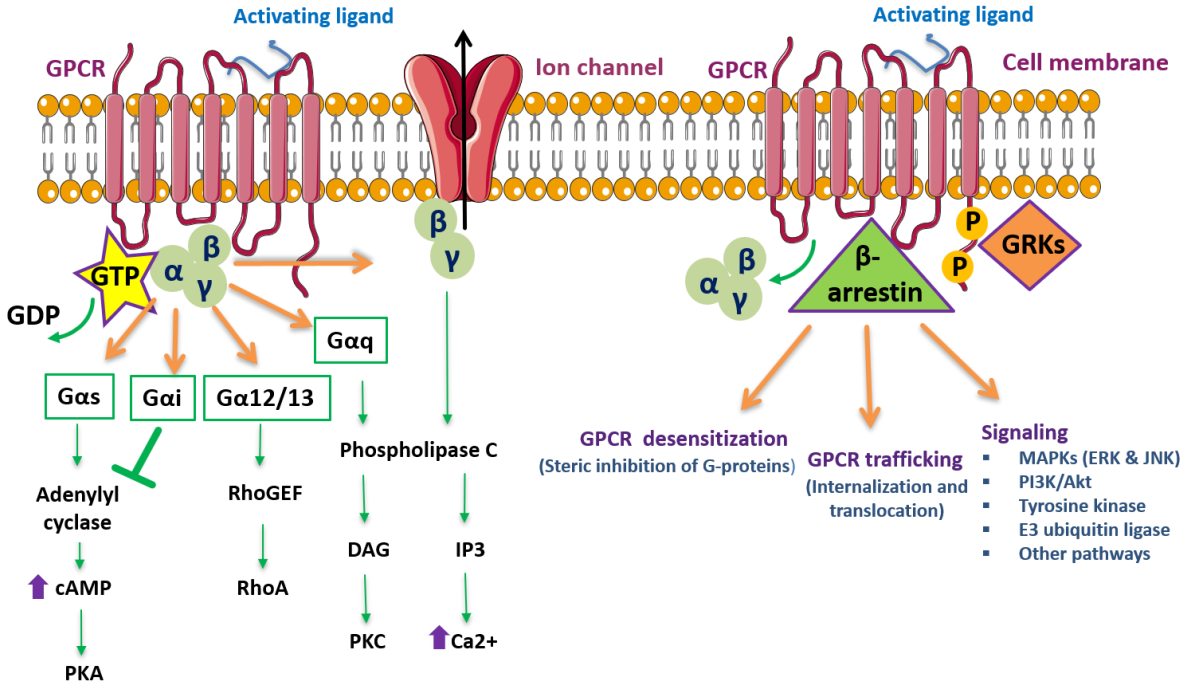

Figure 1: Simplified schematic of GPCRs-mediated signaling pathways. Binding of an activating ligand (agonist) induces a conformational change of the GPCR to activate it. Activated receptors then couple to heterotrimeric G proteins composed of Gα, Gβ and Gγ subunits. Subsequently, the GTP-bound Gα subunit dissociates from the Gβγ complex, and both subunits activate their respective cytoplasmic effectors resulting in a modulation of intracellular second messenger levels. GPCR kinases then phosphorylate the activated receptors. Phosphorylated receptors recruit the multifunctional adaptor proteins; β-arrestins which block further G protein–GPCR coupling resulting in receptor desensitization. β-Arrestins also mediate clathrin-dependent endocytosis of activated GPCRs as well as independent signaling pathways downstream of GPCRs. (Modified from Ritter and Hall, 2009; Chapman et al., 2014; Ghosh et al., 2015; Zhao et al., 2016). The receptor and membrane were used from the website "https://smart.servier.com".

1.1.5.3. Biased signaling of some GPCRs-ligand systems

The long-term goal of current drug discovery efforts is to improve therapies for more than 50 established GPCR targets and to expand the list of targeted GPCRs as well (Allen and Roth, 2011; Lappano and Maggiolini, 2011). Besides activating GPCRs with agonists and inhibiting GPCR signals with antagonists and inverse agonists, the discovery of allosteric and/or functionally selective modulators that bias downstream signaling toward specific G protein–activated or β-arrestin-activated pathways has become involved in the trends in modern pharmacology. Basically, it was believed that the majority of the ligands which bind to 7TM receptors are equally signaling through G proteins and β-arrestins pathways, in other words have balanced or unbiased signaling activity. However, some receptor-ligand systems preferentially signal through either G proteins or β-arrestin-mediated pathway which means that they display bias towards one pathway over the other (Violin and Lefkowitz, 2007). Such behavior can be termed as biased agonism, collateral efficacy, functional selectivity, or stimulus trafficking (Kenakin, 2007; Rajagopal et al., 2010).

One of the earliest characterizations of ligand bias was reported when several α2-adrenergic receptor agonists showed differing relative efficacies for Gαs and Gαi coupling, resulting in the hypothesis that different ligands could engage distinct receptor conformations (Eason et al., 1994). Another early example of ligand-selective signaling was shown when carbachol and pilocarpine, two agonists for the muscarinic acetylcholine receptor, experienced distinct signaling preferences. Carbachol-mediated receptor activation resulted in a balanced response mediated by Gαs and Gαq. On the other hand, pilocarpine showed only Gαq-mediated PLC activation without any Gαs-mediated responses (Gurwitz et al., 1994). Targeting specific G protein subunits downstream of GPCRs rather than directly targeting GPCRs has provided a way in developing new GPCRs therapeutic mechanisms. In this approach, GPCRs are biased by blocking selected post-receptor signaling pathways. Therefore, leaving pathways which are essential for normal cell functioning, while avoiding other detrimental signaling pathways. Out of this concept, specific and selective pharmacological inhibitors for the Gαq, and Gβγ protein subunits have been developed (see review Campbell and Smrcka, 2018).

Indeed, biased agonism is a characteristic of the ligand-receptor complex, therefore either a ligand or a receptor may be biased. As compared to the endogenous ligand, which is neutral (balanced or unbiased), a biased ligand is the one which prefers one response over another like G protein-or β-arrestin-biased ligands. A biased receptor is the one which can only signal

through a limited subset of pathways that are commonly available to the class to which the receptor belongs. For example, G protein-biased receptors which lack the C-terminal phosphorylation sites which are necessary for β-arrestin signaling. These receptors will preferentially signal via G proteins even though they were stimulated by unbiased ligands. There is also system bias which results from the differential expression of certain transducer elements. Higher expression of GRK and β-arrestin isoforms for example would subsequently result in β-arrestin signaling bias (see review Smith et al., 2018). Different Mechanisms of signaling bias are represented in **Figure 2.**

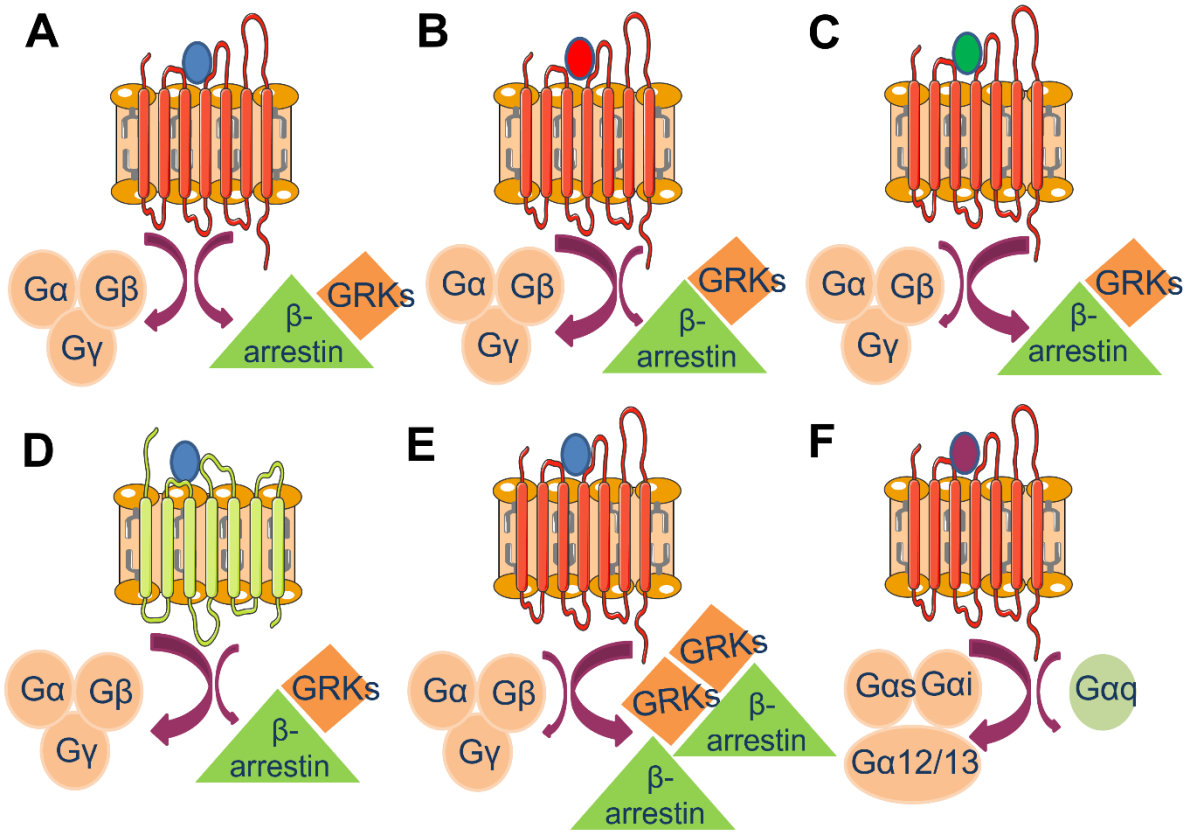

Figure 2: Simplified schematic of the different mechanisms of signaling bias. A) An unbiased ligand binding to a balanced receptor in a neutral system with equivalent preference to both G-protein and β-arrestin pathways. B) A G protein-biased ligand. C) A β-arrestin-biased ligand. D) A G protein-biased receptor in the presence of unbiased ligand and unbiased system. E) A β-arrestin-biased system overexpressing GRKs and β-arrestin isoforms. F) A specific Gαq-inhibitor with subsequent downstream signaling bias. (Modified from Campbell and Smrcka, 2018; Smith et al., 2018). The receptor and membrane were used from the website "https://smart.servier.com".

Functional selectivity results in a markedly different signaling profile with subsequent different functions (Rajagopal et al., 2010). It is well reported that the design of "biased"

drugs that cause GPCRs to favor or avoid arrestins stimulation relative to stimulation of G proteins could result in more effective and safer treatments for a wide range of diseases (Ilter et al., 2019). One of the best studied examples of ligand bias is the Angiotensin II-type 1 receptor (AT1R). Applying a potent, selective, β-arrestin-biased competitive ligand "TRV027" showed an increased cardiomyocyte contractility and meanwhile protection from cardiac apoptosis in preclinical studies (Violin et al., 2014). This new class of ligands would greatly benefit in blocking harmful AT1R effects (which are mediated through Gαq pathway) while preserving or enhancing beneficial effects (mediated through β-arrestin pathway) (Violin et al., 2014). An example of beneficial G protein-biased signaling is mediated by the selective ligand "TRV130" through the μ-opioid receptor. TRV130 could maintain the powerful opioid analgesia (which is Gαi-dependent) while maintaining safety and tolerability by avoiding the respiratory and gastrointestinal dysfunction (β-arrestin-dependent) (Violin et al., 2014). Recently, cell penetrating lipidated peptides derived from the the ICLs of the β2AR, so called "pepducins" showed a β-arrestin biased activity with subsequent coupling to the contractile machinery and prosurvival signaling pathways. These serve as a pharmacological template for the next generation of heart failure therapeutics (Carr et al., 2016; Grisanti et al., 2018).

1.1.5.4. Structural and molecular insights on GPCRs-G protein/-arrestin complex formation.

Understanding this critical event of GPCR-G protein/arrestin complex formation on the molecular basis is of great importance since abnormalities in GPCR´s function is accompanied by many diseases and GPCRs are major targets of drug development.

1.1.5.4.1. GPCR-G protein complex

The visual cascade of the rod cell represents one of the best characterized heterotrimeric G protein-coupled pathways (Hurley, 1992; Pfister et al., 1993). The cascade begins with the absorption of a photon by the 11-*cis*-retinal chromophore of the photoreceptor rhodopsin. This is followed by rapid photoisomerization to all-*trans*-retinal which triggers structural changes resulting in the formation of the activated intermediate meta-rhodopsin II. Meta-rhodopsin II then binds the heterotrimeric guanosine diphosphate (GDP)-bound form of transducin (Gtαβγ.GDP) and catalyses the exchange of GTP for GDP with subsequent dissociation of the complex into (Gtα.GTP + Gtβγ). Gtα.GTP then binds and activates a potent cyclic guanosine

monophosphate (cGMP) phosphodiesterase with subunits $\alpha\beta\gamma_2$ by displacing the inhibitory γ subunits. Consequent to decreased second messenger cGMP concentration, the cation-specific cGMP-gated channels close and hyperpolarization of the rod outer segment membrane happens. Gtα is then inactivated by hydrolysis of GTP to GDP by the intrinsic GTPase activity, returning by this the system to its resting state (Lambright et al., 1994).

The solved crystal structures of the rhodopsin heterotrimeric Gt (Noel et al., 1993; Coleman et al., 1994; Lambright et al., 1994; Mixon et al., 1995; Wall et al., 1995; Lambright et al., 1996) have highlighted and unravelled the nature and mechanism of the conformational switches and structural interfaces for interaction with the GPCR and the functional implications for interactions with other components of the signaling cascade. Furthermore, these structures revealed that the overall topology is greatly similar and likely typical for all heterotrimeric G proteins. The Gα subunit is composed of two conserved domains. One of them is the GTP-ase domain which mediates the hydrolysis of GTP and serves as a binding surface for the βγ dimer, GPCR and effector proteins. In the crystal structure of the GTP-ase domain, three flexible loops called switch I, II and III were identified and showed the most significant conformational differences in both active and inactive structures of Gα, suggesting their most likely key role in the GDP/GTP exchange during the activation process (Noel et al., 1993; Lambright et al., 1994; Lambright et al., 1996; Jastrzebska, 2013). The other conserved domain is the Gα-helical domain which consist of six α-helices on top of the nucleotide-binding pocket located within the GTP-ase domain, thus maintaining the nucleotide in the protein core. Generally, the GTP-ase and helical domains as well as the guanine nucleotide in the active GαGTP resemble their counterparts in the inactive GαGDP except for significant changes where the GTP-ase domain approaches Gβγ (Lambright et al., 1996). Another component of the Gα- subunit is the N-terminal helix which projects away from the Gα-subunit where it was found lacking in some structures as in Gtα.GTPγS (Noel et al., 1993) and Gtα.GDP (Lambright et al., 1994). Moreover, it was found disordered in $Gi\alpha_1$GTPγS (Coleman et al., 1994) with a conformation different from that in $Gi\alpha_1$GDP (Mixon et al., 1995). The Gβ-subunit consist of an N-terminal helix that is followed by a repeating module of seven similar β-sheets, each with four anti-parallel strands which constitute the blades of a β-propeller structure (Lambright et al., 1996). This β-propeller structure forms the structural unit which corresponds to the highly conserved repeating units which ends with tryptophan-aspartic acid residues referred to as “WD” sequence repeats (Neer et al., 1994; Lambright et al., 1996). The Gγ-subunit has two helices where the N-terminal helix forms a coiled-coil wih

the N-terminal helix of Gβ-subunit while the remaining of Gγ makes thorough interactions with the β-propeller of the Gβ-subunit (Lambright et al., 1996). Despite the absence of direct contacts between the Gα and Gγ subunits, however their modified N-and C-termini respectively are in close proximity and in charge of membrane association (Jastrzebska, 2013).

The very early information of the contacting interfaces in the activated GPCR-G protein complex was obtained using site-directed cysteine mutagenesis together with cross linking. These studies showed what parts are needed for complex assembly which includes ICLs 2, and 3, helix H8 in the photoactivated rhodopsin, and the C-and N-termini of Gtα (Cai et al., 2001; Itoh et al., 2001). Furthermore, the C-terminus of Gγ-subunit was found to interact as well with rhodopsin's helix H8 (Kisselev and Downs, 2006). Since these two subunits of Gt are interacting with the receptor and are located quite far apart, it is unlikely that a single receptor could afford such a large surface for interaction with both structural regions. Most likely, a rhodopsin dimer is needed to accomodate the Gt heterotrimer. Such assumption was proved to be correct when a dimer of bovine rhodopsin was detected in its first resolved crystal structure (Palczewski et al., 2000; Jastrzebska, 2013). Observations from the crystal structures of opsin (Scheerer et al., 2008) and Meta II-like rhodopsin (Choe et al., 2011) bound to the C-terminal of Ctα came supporting to the early predictions. In these structures, receptor activation triggers structural re-arrangements of ICLs2 and 3 and opens a cleft at the cytoplasmic surface which enables G protein binding.

However, it was not until the first crystal structure of an intact GPCR-G protein complex was solved when the most detailed molecular determinants in the binding of GPCR and G protein were revealed. The β2AR-Gαs complex structure provided the structural basis for GPCR-mediated G protein activation and uncovered GPCR-Gαs interfaces and conformational changes upon complex formation (Rasmussen et al., 2011a). Extensive interaction was found to exist only between ICL2, TMs 5, and 6 of the receptor and GTP-ase domain of the α-subunit (Jastrzebska, 2013; Du et al., 2019). As compared to Meta II-like rhodopsin, the conformational changes in TMs 5 and 6 are smaller. Moreover, possibly due to the presence of more extensive contacts in case of intact G-protein, the position of the α5-helix of Gt is tilted ~30° relative to the position of the same region of Gs (Choe et al., 2011; Rasmussen et al., 2011a; Jastrzebska, 2013). Surprisingly, no interactions were detected between the single β2AR and either β or γ-subunits of the G protein which supports the possibility that these interactions occur only in dimerized receptors (Jastrzebska, 2013). Subsequently, crystal

structure of A2AR in complex with engineered Gαs subunit was solved (Carpenter et al., 2016). Other complex structures were recently solved including: CTR-Gs (Liang et al., 2017), Glp-1R-Gs (Zhang et al., 2017), μOR-Gi (Koehl et al., 2018), 5-HT_{1B}R-Go (García-Nafría et al., 2018), A_1R-Gi (Draper-Joyce et al., 2018) and rhodopsin-Gi (Kang et al., 2018). All these structures represent the nucleotide-free state of the receptor which has the stability needed for crystallography and cryo-electron microscopy.

Several distinct receptors can couple to the same Gα-protein for example, β1AR (Frielle et al., 1987) and 5-HT_6R (Ruat et al., 1993) can both couple to and activate Gαs resulting in increase in heart muscle contraction and excitatory neurotransmission, respectively. Moreover, some receptors show multiplicity in G protein coupling for example, the β2AR primarily couples to Gαs inducing smooth muscles relaxation, couples to Gαi to inhibit that response and can differentially couple to Gq (Wenzel-Seifert and Seifert, 2000). Regulation of gene expression in a cell-type specific manner and altering expression levels can lead to coupling selectivity, however many different receptors and Gα-proteins are simultaneously expressed in several cell types (Flock et al., 2017). For better understanding of structural basis of coupling specificity (why a particular GPCR prefers a specific G protein isoform) and the temporal sequence of coupling events as process of GDP release, recent studies have addressed that issue using representative class A β2AR-Gs and A2AR-Gs structures (Flock et al., 2017; Du et al., 2019; Liu et al., 2019). To get better insight into GPCR-G-protein coupling specificity, a recent study performed protein sequence analysis and identified several residues on the α5 helix which represent a part of the G protein-specific bar code (Flock et al., 2017). It suggested that receptors which belong to different subtypes can read the same selectivity barcode presented by Gαs however in different manners (in other words different receptors use different sets of residues to read distinct parts of the same Gαs selectivity barcode) (Flock et al., 2017). The investigation of sequence of events during GPCR-mediated GDP release using hydrogen-deuterium exchange mass spectrometry (MS), and radiolytic X-ray footprinting MS in a time-resolved manner revealed that GDP release occurs within seconds of mixing the purified β2AR with Gs.GDP. However, the formation of the stable β2AR-Gs nucleotide free complex noticed by crystallography takes much longer time (Du et al., 2019).

In agreement and completion to the previous two studies, another reported the occurrence of a relatively large conformational arrangement of Gs on the β2AR during transition from the GDP-bound complex to the nucleotide-free complex (Liu et al., 2019). In this study, the α5-helix interacts with the β2AR in two completely different orientations, each includes two Gs

bar code amino acids. An intermediate state via E392Gαs and R389Gαs which interact with the highly conserved DRY motif of the β2AR and a full stable nucleotide free state via Y391Gαs and H387Gαs. Mutations of E392Gαs and R389Gαs reduced the coupling efficiency, suggesting the importance of this intermediate complex in the process of Gαs activation which is most likely taking place in all class A GPCRs (Liu et al., 2019).

1.1.5.4.2. GPCR-arrestin complex

In 2013, the crystal structure of an active β-arrestin-1 bound to a fully phosphorylated peptide derived from a GPCR was reported and revealed a receptor-interacting interface on β-arrestin (Shukla et al., 2013). Two years after, the first crystal structure of arrestin in complex with an active GPCR was published (Kang et al., 2015). In order to acheive such a stable complex, activating mutations were introduced to both binding partners (mouse arrestin-1 and human opsin), and the N-terminus of arrestin was fused to the C-terminus of the receptor by means of a flexible linker. Despite of the modifications and lack of receptor phosphorylation, that solved crystal structure gave insight into the link between the conformational changes upon arrestin activation and coupling to the active receptor (Kang et al., 2015).

Structurally, arrestins consist of near symmetric amino N-and C-domains which look like two crescent-shaped beta sandwitches or in another description like two clamshells placed end to end (Lally et al., 2017; Scheerer and Sommer, 2017). The basal conformation of arrestins is stabilized by extensive interactions between a long C-terminal tail and the N-domain. Arrestins are activated for binding to the receptor through the phosphorylated C-terminus of the receptor, forming an initial low-affinity interaction called a pre-complex in which the phosphorylated C-terminus displaces the arrestin acidic C-tail. Such displacement allows gaining more access to the numerous basic residues in the N-domain. Furthermore, rotation (~21°) of the N-and C-domains against each other takes place with subsequent increase in flexibility in receptor binding loops in the central crest region (finger loop region) of arrestins. These conformational changes allow the second binding step which is the tight binding step and formation of the high-affinity complex (Kim et al., 2013; Shukla et al., 2013; Kang et al., 2015; Lally et al., 2017). According to recent studies, the receptor binds arrestin at two distinct interfaces: the phosphorylated receptor tail binds within a pool of positively charged residues in the arrestin N-domain, meanwhile the transmembrane helices and loops of the receptor (receptor core) bind between the arrestin's N and C domains (Kang et al., 2015; Zhou et al., 2017). Activation of arrestins for receptor binding can also be acheived by C-tail

truncation, as in the naturally occurring splice variant of arrestin-1 (p44) which lacks the regulatory C-tail and can bind an active receptor independent of receptor phosphorylation (Pulvermüller et al., 1997; Schröder et al., 2002; Lally et al., 2017).

It is worth to mention that some studies have concluded that the phosphorylated tail of the receptor is able to stimulate arrestin conformational change and signaling on its own without the need for the receptor core (Cahill et al., 2017; Kumari et al., 2017). Most recently, applying extensive all-atom molecular dynamic simulations of arrestins, either free or bound to various parts of the receptor suggested that the active conformation of arrestin can be stabilized and functions of arrestin can be maintained by the presence of either the receptor core alone or the receptor phosphorylated tail alone and is further stabilized if both are present (Eichel et al., 2018; Latoracca et al., 2018). Interestingly, different conformation states of GPCRs-β-arrestin complexes can carry out distinct functions. Creating a mutant form of β-arrestin which lacks the finger-loop region so can only acquire the tail conformation was shown to preserve its ability to mediate receptor internalization and β-arrestin signaling but not the desensitization of G protein signaling (Cahill et al., 2017).

Classification of GPCRs based on their arrestin-binding properties into class A, and class B receptors can be explained to be strongly correlated to the phosphorylation codes which exist in the C-terminal tails of GPCRs. Recent studies were interested to figure out the phosphorylation codes in the C-terminal tail of rhodopsin which play role in arrestin-1 binding and activation (Zhou et al., 2017; Mayer et al., 2019). In these studies, a set of phosphorylated threonine and serine residues were found to be essential for the formation of high-affinity complex between arrestin and GPCR. Zhou and colleagues reported some important phosphorylated residues (pT336, pS338 and pS334) in rhodopsin C-terminus which can form extensive electrostatic interactions together with other negatively charged rhodopsin residues and positively charged arrestin residues (Zhou et al., 2017). These phosphorylated sites together with pT338 were recently referred to as “modulator sites” by Mayer and colleagues because of their influence on the global conformation and flexibility of arrestin (Mayer et al., 2019). Two other phosphorylated residues (pT340 and pS343) were discovered and referred to as “key sites” because of their necessity for high-affinity rhodopsin-arrestin interactions, and an “inhibitory site” which lies between the two key sites (pT342) that can abrogate arrestin binding (Mayer et al., 2019)

Studies on the other interface of interaction as noticed from the crystal structure of rhodopsin-arrestin-1 reported three parts of arrestin are needed for binding the core of the receptor. These include the arrestin finger loop which embed into the helical bundle of the receptor, the C-loop in the C-domain of arrestin, and neighboring residues in the N-domain which interact with ICL2 of the receptor, and Arginine (R318) in the back loop of C-domain which ionically interacts with gluatamate (E239) in the ICL3 of the receptor (Kang et al., 2015). Each of these three elements undergo different conformational changes upon interaction with the receptor's core. The finger loop presents the largest conformational change which extensively contributes to arrestin-GPCR binding. However, it has a restricted role in triggering arrestin activation. On the other hand, the conformational changes acquired by the other two elements which are in contact to ICLs 2, and 3 are mainly related to the activation state of arrestin (Latoracca et al., 2018). This supports previous observations in certain GPCRs on the ability of phosphorylated or acidic residues on ICL3 to trigger arrestin binding and activation (Tobin, 2008).

Crystal structures of GPCRs have showed that G protein C-terminal helix and the arrestin finger loop bind to the same pocket between TMs 3, 5, 6, and 7 which triggers G protein activation (Dror et al., 2015) and limited triggering of arrestin activation (Latoracca et al., 2018). Despite maintaining similar conformations of the receptor core in existing crystal structures of complexes with G proteins and arrestins, certain receptor core conformations might prefer G protein stimulation over arrestin or vice versa. This provides new and complementary structural basics for designing functionally selective (biased) GPCRs targeted ligands.

1.1.6. Orphan GPCRs

GPCRs are major regulators of intercellular interactions. They need to be activated by a broad panel of natural ligands to exert their actions. Each GPCR recognize its ligand in a highly selective manner (Civelli et al., 2006). Conventionally, ligands were discovered first and served in the pharmacological characterization of the receptors. That was until the 1980s, when receptors were discovered first due to the homology screening approaches which helped in the molecular identification of receptors (Civelli et al., 2006; Chung et al., 2008). Until a ligand is identified GPCRs are called "orphan CPCRs" and they provide a valuable and novel field of targets for the development of new drugs with unique therapeutic properties (Civelli, 2005; Civelli et al., 2006). To date, approximately 120 GPCRs remain orphans with poorly

understood physiological functions and potential roles in diseases (Diaz et al., 2018). If the orphan GPCR of interest was found to be activated by a yet unknown endogenous ligand, the discovery of that ligand would be of great importance. However, the need for an endogenous ligand for every orphan GPCR is not clear as some of them instead rely upon constitutive activity or heteromerization for activation (Civelli et al., 2013). Despite their endogenous means of stimulation and modulation of receptor activity, recognition of surrogate (non-natural) ligands will be invaluable in understanding orphan GPCRs pharmacology and function (Ngo et al., 2016).

The earliest trials to deorphanize GPCRs started in the latter half of 1980 together with the development in molecular biological techniques like low-stringency hybridization and degenerate polymerase chain reaction which helped in the successful cloning of orphan GPCRs (Civelli et al., 2013). Furthermore, with modern cloning technology, researchers were able to express orphan GPCRs in cell lines to be tested in signal transduction assays using potential exogenous or endogenous ligands (Civelli et al., 2013). One of the traditional approaches that has been used in the 1990's to identify endogenous and/or surrogate ligands for orphan GPCRs is reverse pharmacology which is defined as "the science of integrating documented clinical experiences and experiential observations into leads, through transdisciplinary exploratory studies and further developing these into drug candidates through robust preclinical and clinical research" (Vaidya, 2014). This paradigm shift from the conventional drug discovery was proved to be successful in matching many orphan GPCRs with their cognate ligands including; orexin-A for orexin receptor type 1, orexin-B for orexin receptor type 2 and ghrelin for the growth hormone secretagogue receptor (Wise et al., 2004; Yoshida et al., 2012; Civelli et al., 2013). As a consequence of the increasing availability of GPCR structural input, a shift from traditional high throughput (HTS) methods to cheaper and efficient virtual ligand screening approaches has occurred facilitating the identification of novel ligands at GPCRs (Ngo et al., 2016).

1.2. MAS and MAS-related GPCRs

More than thirty years ago, the human MAS gene was isolated from the DNA of human epidermoid carcinoma cell line (Young et al., 1986). Computer analysis of the MAS amino acid sequence proposed the involvement of this protein to the class of GPCRs with seven transmembrane domains (Young et al., 1986). Because of the ability of the MAS to transform fibroblast cells "NIH3T3" upon transfection, it was thought to be a proto-oncogene (Young et

al., 1986). Independent experiments approved the finding but meanwhile challenged the tumorigenic potential of MAS (Janssen et al., 1988; van't Veer et al., 1993). An explanation to the activation of MAS gene in the tumorigenicity assay was assumed to be due to the rearrangement of the 5´-noncoding sequence which happened during transfection. Therefore, MAS is not an oncogene, however it can transform cells when artificially overexpressed (van't Veer et al., 1993; Bader et al., 2014). Interestingly, the MAS receptor was early believed to be a functional Ang II receptor when there were responses to angiotensin I, II, and III in *X*enopus frog oocytes injected with MAS RNA (Jackson et al., 1988; Jackson and Hanley, 1989). However, other study showed that the responses to angiotensins occurred only in MAS-transfected cells which endogenously express Ang II receptor (Ambroz et al., 1991). Furthermore, cloning of the AT-1 receptor disapproved the initial hypothesis (Murphy et al., 1991; Sasaki et al., 1991).

Later in 2001, and 2002, two independent working groups discovered a group of orphan GPCRs which are predominantly expressed in the sensory neurons of the dorsal root ganglia (DRG) and with amino acid sequence closely related to that of MAS (Dong et al., 2001; Lembo et al., 2002). These receptors were named after their founder gene and known to be MAS-related G Protein-coupled receptors (formerly called MAS related genes "Mrgs"), also known as sensory neuron-specific receptors "SNSRs" (Dong et al., 2001; Lembo et al., 2002).

Phylogenetic analysis revealed that MAS and Mrgs belong to one of four main branches of the δ group of rhodopsin-like class A GPCRs (Fredriksson et al., 2003) see **Table 1 above (page 3)**. Coding genes for more than 50 Mrgs in mouse, rat, human, and macaque were identified from the screening of cDNA libraries and bioinformatic analysis of databases (Dong et al., 2001; Wittenberger et al., 2001; Lembo et al., 2002; Takeda et al., 2002; Zylka et al., 2003). Mrgs are a complex family of receptors with dozens of members (Meixiong and Dong, 2017). The mammalian family of Mrgs can be subclassified based on sequence similarities into nine main separate subfamilies designated by capital letters (A to H, and X), and individual subtypes which are indicated by numbers; MrgA1–A22, MrgB1–B13, MrgC1–C14, MrgX1-X4 (Dong et al., 2001; Zylka et al., 2003). Only in rodents the subfamilies A, B, C exist. Beside expression in rodents, the MrgH has been identified in the genome of birds; so, called Gallus gallus (Solinski et al., 2014). Subfamily X was found to be specifically expressed in primates including human, macaque and rhesus monkey (Dong et al., 2001; Lembo et al., 2002; Zhang et al., 2005; Burstein et al., 2006). On the other hand, subfamilies D to G were found to be conserved in different mammalian species involving rodents and

primates (Dong et al., 2001; Lembo et al., 2002; Zylka et al., 2003). In lower vertebrates, there is no evidence for the expression of Mrgs genes up to now, which could be attributed to the less progress in gene sequencing and annotation of lower vertebrate genomes (Solinski et al., 2014).

For every species, the genes coding for Mrgs are located on a single chromosome (Solinski et al., 2014). All genes for Mrgs are located on human chromosome 11, rat chromosome 1 and mouse chromosome 7 (Dong et al., 2001). Exception includes MAS, which is located on chromosome 6 in human, chromosome 17 in mouse, and MrgH, which is located on chromosome 17 in mouse (Bader et al., 2014). The number of protein-encoding genes differs among subfamilies and species. While having only one gene in rats, the MrgA harbors eighteen protein-encoding genes as well as several pseudogenes in mice (Dong et al., 2001; Zylka et al., 2003). The MrgB subfamily involves seven protein-encoding genes in rats, nine in mice with several pseudogenes in both (Dong et al., 2001; Zylka et al., 2003). In rats, the MrgC subfamily comprises only one gene, however, in mice there is one protein-encoding gene beside 13 pseudogenes (Han et al., 2002; Zylka et al., 2003). The MrgD (Dong et al., 2001; Lembo et al., 2002; Zylka et al., 2003), together with MrgE to H subtypes (Zylka et al., 2003) comprise only one protein-encoding gene per species. It was reported that MrgX subfamily consist of four distinct genes which are all located on chromosome 11p15.1 in humans (Dong et al., 2001).

Nociceptive sensory neurons in the DRG are classified into peptidergic (marked by the neuropeptide Calcitonin Gene-Related Peptide and substance P), and nonpeptidergic (marked by the isolectin B4 (IB4)) subsets (Molliver et al., 1997; Hunt and Mantyh, 2001; Woolf and Ma, 2007). All of MrgA, MrgB4, MrgB5, MrgC to H, and MrgX are expressed in nonpeptidergic $IB4^+$ small-diameter somatosensory afferents, representing nearly half of the nociceptors per DRG (Dong et al., 2001; Lembo et al., 2002; Zylka et al., 2003; Zhang et al., 2005; Cox et al., 2008; Liu et al., 2009). Such expression reflects their important roles in pain perception and modulation. Mrgs were also found to be involved in neuronal signaling pathways mediating pruritis (Meixiong and Dong, 2017). Besides the highly selective expression in small-diameter primary sensory neurons, Mrgs were found to be expressed in other tissues. Of notice, mouse MrgB2 and human MrgX2 receptors are the only members with specific cell-type expression outside the nervous tissue. The two receptors are expressed in mast cells with subsequent contribution to neurogenic inflammation, pain, and itch (Tatemoto et al., 2006; Subramaninan et al., 2016; Alkanfari et al., 2018). For detailed

information on Mrgs pharmacology, signaling, and physiological implications in pain and itch, see reviews (Bader et al., 2014; Solinski et al., 2014; Meixiong and Dong, 2017).

1.2.1. MAS-related gene member D "MrgD"

One of the members of Mrg family is the MrgD, also referred to as hGPCR45 (Takeda et al., 2002) or TGR7 (Shinohara et al., 2004) with orthologues in rodents and primates (Dong et al., 2001; Shinohara et al., 2004; Zhang et al., 2005). The single copy encoding MrgD gene was found located on chromosome 11q13.3 in human (Hao et al., 2012), chromosome 1 in rat and chromosome 7 in mouse (Zylka et al., 2003). The amino acid sequences of MrgD receptors are not highly conserved among species but yet closely related (Shinohara et al., 2004). The MrgD receptor is composed of 321 amino acids in human, 321, and 319 in mouse, and rat, respectively (Shinohara et al., 2004). Analysis of gene bank sequences of mouse, rat, rhesus monkey and chimpanzee revealed 59.8%, 63.7%, 88.1% and 96.6% sequence homology to that of the human receptor, respectively (Shinohara et al., 2004). The predicted 2-dimensional structure model of the human MrgD (hMrgD) receptor is shown in **Figure 3.**

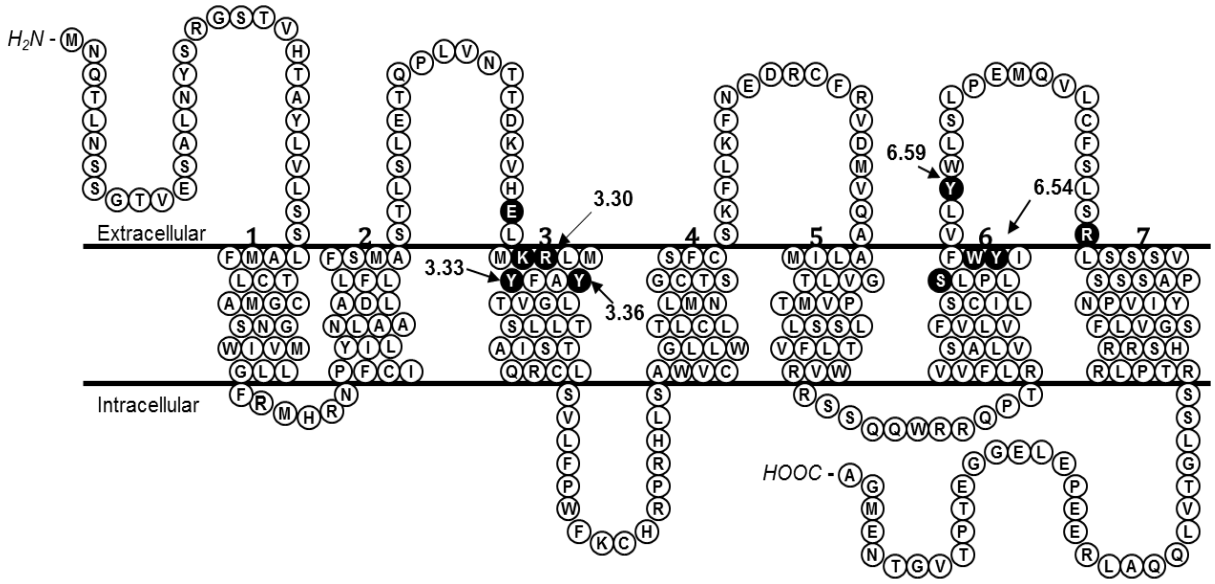

Figure 3: Predicted two-dimensional structural model of the hMrgD receptor. 1 to 7 denotes the seven transmembrane helices, extracellular and intracellular regions are marked. Amino acids previously studied by site-directed mutagenesis are indicated by filled circles (Müller, 2014; Arbogast et al., 2018). The model was created with TeXtopo in LaTeX (Beitz, 2000) by (Müller, 2014).

MrgD is expressed in ~75% of all $IB4^+$ nonpeptidergic nociceptive neurons and within the DRG, MrgD was found co-localized with ATP-gated ion channel purinoceptor P2X3 and vanilloid receptor-1 (Dong et al., 2001; Zylka et al., 2003; Shinohara et al., 2004). Both of which are cation channels that function as nociceptors of importance in detecting noxious stimuli (Chen et al., 1995; Caterina and Julius, 1999). $MrgD^+$ neurons selectively innervate the most superficial layer of epidermis in the skin (stratum granulosum) and terminate in lamina II (the substantia gelatinosa) of dorsal spinal cord as revealed by axonal tracer studies (Dong et al., 2001; Zylka et al., 2003; Zylka et al., 2005). Beside innervating the epidermis, a minor population (20%-26%) of IB4+ sensory neurons were detected by different retrograde tracers to innervate the colon (Robinson et al., 2004; Christianson et al., 2006; Hockley et al., 2014). Recently, MrgD mRNA and protein expressions were detected in sensory DRG projecting to the mouse colon (Bautzova et al., 2018; Hockley et al., 2019). On the cardiovascular level, MrgD expression was detected in arterial smooth muscle cells, endothelial nitric oxide synthase (eNOS) positive endothelial cells, and in atherosclerotic plaques (Habiyakare et al., 2014). Another study localized the receptor in blood vessels, membrane, perinuclear and nuclear regions of cardiomyocytes, and the cardiovascular center of the mouse brain (Oliveira et al., 2019). MrgD is recently reported to be expressed in the retinal neurons, retinal vasculature, Müller glial and retinal pigment epithelial cells (Zhu et al., 2020). Investigations of clinical cancer tissues revealed high expression levels of MrgD in lung cancer, suggesting the tumorigenic potential of MrgD (Nishimura et al., 2012).

1.2.2. Agonists of MrgD

1.2.2.1. β-Alanine

β-Alanine is a non-proteinogenic β-amino acid which exists in several different forms in vivo (Derave et al., 2010). Within the body, β-alanine is produced from the breakdown of pyrimidines, decarboxylation by gut microbes of L-aspartate, and transamination with 3-oxopropanate by L-aspartate (Gojkovic et al., 2001; van Kuilenburg et al., 2004; Tiedje et al., 2010). Moreover, β-alanine is generated from the breakdown of the dipeptide carnosine by the enzyme carnosinase (Stellingwerff et al., 2012). As a free amino acid within the nervous tissue, β-alanine has been thought to act as a neurotransmitter or neuromodulator (Wu et al., 1993; Tiedje et al., 2010). Owing to the structural similarity to glycine and GABA, β–alanine can bind to hippocampal N-methyl-D-aspartate (NMDA), GABA-A, GABA-C, and glycine receptors to help in learning of new information (Suzuki et al., 2002; Artoli et al., 2009). As a

component of coenzyme A, β–alanine is important for the metabolism of fatty acids, and functionality of the citric acid cycle in the heart (Hayaishi et al., 1961). Within the muscle cells, β–alanine is the rate limiting amino acid in the production of carnosine, which is an effective intramyocellular buffering agent that decreases fatigue and enhances exercise performance (Baguet et al., 2010; Derave et al., 2010). In the liver in the presence of β-alanine-α-ketoglutarate transaminase or β-alanine-pyruvate transaminase, β-alanine is degraded to malonate semialdehyde. The latter is further transformed to acetyl coenzyme A to be used by the citric acid cycle (Yamada et al., 1960) or converted back to β-alanine in the brain by the action of GABA transaminase (Tiedje et al., 2010).

β-Alanine is the first putative ligand described for the MrgD receptor in human, rat, mouse, and monkey, where high concentrations (in the micromolar range) of the amino acid are needed to activate the receptor (Shinohara et al., 2004). In recombinant chinese hamster ovary (CHO) cells, β-alanine caused activation and internalization of MrgD with subsequent increases in intracellular Ca^{2+} levels, and inhibition of forskolin-induced cAMP production, suggesting the receptor coupling to Gαq and Gαi proteins, respectively (Shinohara et al., 2004). Further reports in CHO cells supported the same findings (Zhang et al., 2007; Ajit et al., 2010; Müller, 2014; Arbogast et al., 2018). In human embryonic kidney 293 (HEK293) cells, β-alanine-induced activation of the MrgD receptor, caused increase in intracellular Ca^{2+} concentrations (Milasta et al., 2006; Uno et al., 2012), and stimulated ERK1/2 phosphorylation (Milasta et al., 2006). β-Alanine-induced activation of MrgD in Xenopus oocytes proved the functional coupling between MrgD and calcium-activated chloride channels which was reported to be mediated through the Gαq/PLC/IP3/Ca^{2+} pathway (Zhuo et al., 2014).

The possible interaction between MrgD and voltage sensitive KCNQ/M-type potassium channels has been addressed using β-alanine. Neuronal M-channels are present in the DRG (Passmore et al., 2003), consisting of KCNQ2/3 subunits (Wang et al., 1998), and have been involved in pain sensation (Blackburn-Munro and Jensen, 2003; Passmore et al., 2003). β-Alanine-induced activation of MrgD caused a robust inhibition of KCNQ2/3 currents with subsequent excitation of DRG neurons, and enhancement of the signaling of primary afferent nociceptive neurons (Crozier et al., 2007). Genetic ablation of $MrgD^{+}$ mouse neurons was reported to reduce the behavioral sensitivity to noxious mechanical stimuli (Cavanaugh et al., 2009). In vivo DRG recordings showed that β-alanine-sensitive neurons represent ~40% of total $MrgD^{+}$ neurons and respond to heat stimuli. On the other hand, the β-alanine-insensitive

$MrgD^+$ neurons are insensitive to heat (Liu et al., 2012b). Moreover, a subset of MrgD-expressing neurons was found involved in β-alanine-induced itch and possess a distinct physiological profile (Liu et al., 2009; Liu et al., 2012b). Together, that suggests the heterogeneity and functional diversity of $MrgD^+$ neurons and makes MrgD an experimentally tractable therapeutic target for pain and itch.

1.2.2.2. Alamandine

The renin-angiotensin system (RAS) is a very complicated and dynamic system which includes a series of enzymes and peptides, necessary for many physiological processes such as cardiovascular and renal control (Ferrario, 1990; Bader et al., 2001; Fraga-Silva et al., 2013). In the last decades, new peptides, enzymes, and receptors with biological activities have been discovered and characterized as components of the RAS (Etelvino et al., 2014; de Souza-Neto et al., 2018). In 2013, the newest peptide of the RAS was identified so-called Ala^1-Ang-1–7 "alamandine" (Lautner et al., 2013). The heptapeptide alamandine was detected in plasma of rats and humans, and in the aorta of mice and rats (Lautner et al., 2013). High plasma levels of alamandine were detected in patients with nephropathy suggesting the role of this peptide in pathological conditions (Lautner et al., 2013). Endogenously, alamandine is produced either from the octapeptide angiotensin A by the action of angiotensin converting enzyme 2 "ACE2" or through the decarboxylation of the N-terminal Asp1 of angiotensin 1–7 into Ala1 (Lautner et al., 2013). Metabolically, alamandine as well as angiotensin 1-7 preferentially hydrolyze to angiotensin 1-4 via angiotensin 1-7 peptidase which was found expressed in the sheep cortex, and isolated tubules, and in human HK-2 renal epithelial cells (Wilson et al., 2015). In the pioneering discovery article, MrgD was described as the functional receptor for alamandine where the peptide can activate it at nanomolar concentrations, mediating beneficial effects (Lautner et al., 2013). An oral formulation of an inclusion compound of alamandine/β-hydroxypropyl cyclodextrin produced long-term antihypertensive effects in spontaneous hypertensive rats, and anti-fibrotic effects in isoproterenol treated rats (Lautner et al., 2013). Since that discovery, several studies addressed the antihypertensive and cardioprotective effects of alamandine (Soares et al., 2017; de Souza-Neto et al., 2018; Jesus et al., 2018; Li et al., 2018; Liu et al., 2018; Park et al., 2018; de Souza-Neto et al., 2019; Hekmat et al., 2019; Song et al., 2019; Wang et al., 2019). It became established that the ACE2/alamandine/MrgD axis together with ACE/angiotensin II/AT-2, and ACE2/angiotensin 1-7/MAS axes, represent the three protective arms of RAS which counteracts the classical ACE/angiotensin II/AT-1 axis **(Figure 4).**

Mechanistically, alamandine-induced vasodilatory effects are mediated via stimulation of eNOS and enhanced nitric oxide (NO) release (Lautner et al., 2013; Li et al., 2018). An effect described to be protein kinase A "PKA" dependent (Liu et al., 2018; Qaradakhi et al., 2017). The Gαs/cAMP/PKA pathway was reported to be the primary intracellular pathway of alamandine signaling at MrgD receptor (Tetzner et al., 2018). In cardiomyocytes, alamandine reversed Ang II-induced hypertrophy, and sepsis-induced cardiac dysfunction via 5`adenosine monophosphate-activated protein kinase (AMPK)/NO pathway (Jesus et al., 2018), and inhibition of MAPK signaling (Li et al., 2018), respectively. Other actions of alamandine include decreased expression of leptin in adipose tissue in a Gq/PLC dependent manner (Uchiyama et al., 2017). Furthermore, alamandine showed anti-inflammatory actions in retinal tissues (Duan et al., 2018; Zhu et al., 2020).

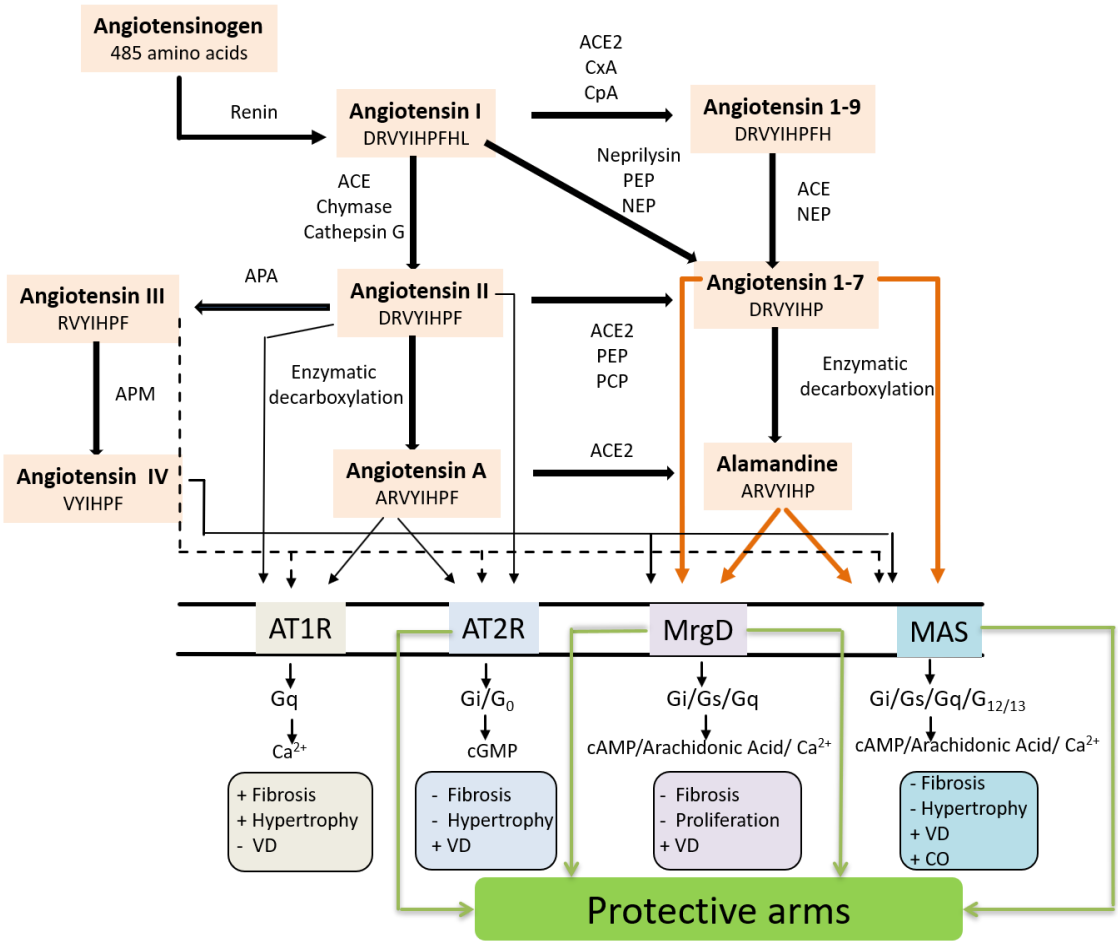

Figure 4: Simplified view of the RAS cascade showing the protective arms composed of ACE/angiotensin II/AT2-R, ACE2/angiotensin 1-7/MAS, and ACE2/alamandine/MrgD axes. ACE; angiotensin converting enzyme; ACE2; angiotensin converting enzyme 2, CxA; carboxypeptidase A, CpA; cathepsin A, PEP; prolylendopeptidase, NEP; neutral endopeptidase, APA; aminopeptidase A, APM; aminopeptidase M, VD; vasodilation, CO; cardiac output. Modified from (Mendoza-Torres et al., 2015 and Karnik et al., 2017).

1.2.2.3. Other agonists

In addition to β-alanine, other amino acids were reported to be MrgD agonists. These include 3-aminoisobutyric acid (Müller et al., 2012; Uno et al., 2012), GABA (Shinohara et al., 2004; Ajit et al., 2010; Müller et al., 2012), and 3-aminobutyric acid (Müller et al., 2012). Other compounds involve the puridazine 121145 (Zhang et al., 2007), the thiazole 011531 (Zhang et al., 2007), 5,7, dihydroxytryptamine creatinine sulfate (Ajit et al., 2010), the negative enantiomer and racemic mixture of 3-amino-1-hydroxy-pyrrolidin-2-one; HA 966 (Ajit et al., 2010), and diethylstilbesterol (Uno et al., 2012). All of which have lower potency as compared to β-alanine. The heptapeptide angiotensin 1-7 (Gembardt et al., 2008; Tetzner et al., 2016), and the polyunsaturated keto acid 5-oxo-6,8,11,14-eicosatetraenoic acid "5-Oxo-ETE" (Bautzova et al., 2018) were reported to activate the MrgD receptor.

1.2.3. Antagonists of MrgD

The antipsychotic drugs (R)–propylnorapomorphine (Ajit et al., 2010), chlorpromazine (Ajit et al., 2010; Müller et al., 2012), thioridazine (Ajit et al., 2010; Müller et al., 2012), rimcazole (Müller et al., 2012), and levomepromazine (Müller et al., 2012) showed antagonistic potentials at the MrgD receptor. The potential anticancer agent MU-6840 displayed antagonistic activity at the hMrgD receptor (Uno et al., 2012). With the discovery of alamandine as an agonist at the MrgD receptor, the Ang 1-7 antagonist "D-Pro^7 angiotensin 1-7" and the AT-2 receptor antagonist "PD123319", were characterized as MrgD antagonists (Lautner et al., 2013; Tetzner et al., 2016; Tetzner et al., 2018). Furthermore, the compound "THV201" designed by the group of Prof. Christa E. Müller (Medicinal Chemistry, University of Bonn) was identified by our group as MrgD antagonist (unpublished data).

2. Aim of work

By virtue of its cross-species conservation as a single copy gene as well as its predominant expression in small diameter nociceptive neurons, MrgD represents an attractive target to be further investigated. However, up to date there are no three-dimensional structures available for any of the members of the Mrgs family. Aim of the present work was to provide additional molecular pharmacological characterization of the hMrgD receptor using the putative ligand "β-alanine". Discovered as a novel component of the RAS, we were additionally interested to investigate more about the hMrgD signaling in response to activation with the newest RAS peptide member "alamandine". Other compounds with reported activity at the MrgD receptor were further studied. These include the peptide "angiotensin 1-7", the polyunsaturated fatty acid "5-Oxo-ETE", and small molecule structural analogues of β-alanine as 3-aminoisobutyric acid, 3-aminobutyric acid, GABA, and carnosine. Beside agonists, we aimed to identify new antagonists at the hMrgD receptor and to further investigate known ones.

To reach our goal, CHO Flp-In cells were chosen as the stable expression system for our receptor. Functional experiments targeting the Gαq coupling and signaling of the hMrgD as Fluo-4 Ca^{2+} and NFAT luciferase reporter gene assays were applied. The Gαi or Gαs downstream signaling was addressed using the AlphaScreen cAMP assay. As a control to our experiments, β-alanine was investigated in parallel as a positive control and similar experiments were performed in non-transfected CHO cells. For the first time, data showing the Gα protein-independent signaling through coupling of the hMrgD receptor to the β-arrestin pathway are presented. That was achieved using the highly sensitive PathHunter β-arrestin recruitment assay.

Together with previous investigations done on the hMrgD receptor by our group, the data provided here add on better understanding of the hMrgD signaling and function. The information offered here modify our vision to the specificity of alamandine/MrgD signaling and subsequent functional effects. In addition, data would help in the future in developing biased pharmaceuticals for the management of pain and diseases related to the MrgD receptor.

3. Materials and Methods

3.1. Materials

3.1.1. Laboratory glassware and consumables

Table 2. Laboratory glassware and consumables.

Item	Catalogue number	Company
Autoclavable waste plastic bags 600x780x0,050 MM	646201	Greiner Bio-One GmbH, Frickenhausen, Germany
Biosphere® Filter tips (10 µl / 100 µl / 1000 µl)	70.1115.210 / 302-08-151 / 302-01-151	Sarstedt, Nümbrecht, Germany
Brown tissues 38X58 cm	16004	Lohmann and Rauscher GmbH & CO.KG, Germany
Cell culture flasks (75 cm^2)	658175	Greiner Bio-One GmbH, Frickenhausen, Germany
Cell culture well plates (6 / 24 / 96 wells)	65716/ 662160 / 655073	Greiner Bio-OneGmbH, Frickenhausen, Germany
Combitips advanced (0.5 ml / 1 ml / 2.5 ml / 5 ml)	0030089421 / 0030089430 / 0030089448 / 0030089458	Eppendorf Biopur GmbH, Germany
Corning® Costar® Stripette® serological pipettes, individually paper/plastic wrapped (1ml / 2ml / 5ml / 10ml / 25ml	CLS4485 / CLS4486 / CLS4487 / CLS4488 / CLS4489	Sigma-Aldrich, Saint-Louis, USA
Disposable filter unit (Filtropur V50 500ml)	83.1823.001	Sarstedt, Nümbrecht, Germany
Epindorfs (1.5 ml)	72.690.001	Sarstedt, Nümbrecht, Germany
Falcons (15 ml / 50ml)	62554502 / 62547254	Sarstedt, Nümbrecht, Germany
Filtropur S 0.2 membrane filter	83.1826.001	Sarstedt, Nümbrecht, Germany

Gloves	1286M	Nitril, BestGen, Meditrade GmbH, Germany
Microscope Cover slips 25 mm, MENZEL-GLÄSER	0110650	Invitrogen, Thermo Fisher Scientific, Waltham, USA
Parafilm™	2016904	Labomedic GmbH, Germany
Pippette tips (10 µl / 200 µl / 1000 µl)	70.1115 / 70.760.012 / 70.762	Sarstedt, Nümbrecht, Germany
Tissue culture (TC) dish 100, standard.	83.3902	Sarstedt, Nümbrecht, Germany

3.1.2. Molecular biology reagents and chemicals

Table 3. Molecular biology reagents and chemicals.

Item	Catalogue number	Company
Agarose broad range	11404	SERVA Electrophoresis GmbH, Heidelberg, Germany
Ampicillin sodium salt	13399	SERVA Electrophoresis GmbH, Heidelberg, Germany
Blue Juice™ Gel Loading Buffer (10X)	10816015	Invitrogen, Thermo Fisher Scientific, Waltham, USA
Dinatrium-EDTA x 2 H2O	11280	SERVA Electrophoresis GmbH, Heidelberg, Germany
DNA Ladder (1 kb plus)	10787018	Invitrogen, Thermo Fisher Scientific, Waltham, USA
DNase/RNase-free distilled water	15230089	Invitrogen, Thermo Fisher Scientific, Waltham, USA
Ethanol ROTIPURAN® ≥ 99.8 %	9065.3	Roth, Karlsruhe, Germany
Isopropanol Rotipuran ≥ 99.8 %	6752.3	Roth, Karlsruhe, Germany
LB Agar (Lennox Agar)	22700	Invitrogen, Thermo Fisher Scientific, Waltham, USA

LB Broth	10855001	Invitrogen, Thermo Fisher Scientific, Waltham, USA
One Shot Top10 E. coli	404003	Invitrogen, Thermo Fisher Scientific, Waltham, USA
SERVA DNA stain G	39803.01	SERVA Electrophoresis GmbH, Heidelberg, Germany
S.O.C medium	15544034	Invitrogen, Thermo Fisher Scientific, Waltham, USA
TRIS (Base) PUFFERAN® ≥ 99.9 %	5429.3	Roth, Karlsruhe, Germany

3.1.3. Cell culture reagents and chemicals

Table 4. Cell culture reagents and chemicals.

Item	Catalogue number	Company
Acetic acid, water free ROTIPURAN®	3738.4	Roth, Karlsruhe, Germany
BSA; Bovine Serum Albumin	A7030	Sigma-Aldrich, Saint-Louis, USA
DMSO; Dimethylsulfoxide	D5879	Sigma-Aldrich, Saint-Louis, USA
DMSO sterile	D2650	Sigma-Aldrich, Saint-Louis, USA
DPBS (Dulbecco's Phosphate Salt Buffered Saline; without Ca^{2+} und Mg^{2+}) 1x	14190169	Invitrogen, Thermo Fisher Scientific, Waltham, USA
FBS; Fetal Bovine Serum	10270106	Gibco, Thermo Fisher Scientific, Waltham USA
Forskolin	F-6886	Sigma-Aldrich, Saint-Louis, USA
Ham's F12 Nutrient Mix, GlutaMAX™	31765068	Invitrogen, Thermo Fisher Scientific, Waltham, USA

HBSS (Hanks Balanced Salt Solution)	14025100	Invitrogen, Thermo Fisher Scientific, Waltham, USA
HEPES (1M)	15630-106	Gibco, Thermo Fisher Scientific, Waltham, USA
Hygromycin B	10687010	Invitrogen, Thermo Fisher Scientific, Waltham, USA
Immersol™ 518F CarlZeiss	12737327	Invitrogen, Thermo Fisher Scientific, Waltham, USA
Lipofectamine™ 2000 Reagent	11668019	Invitrogen, Thermo Fisher Scientific, Waltham, USA
OptiMEM®I + GlutaMAX™I reduced serum medium, no phenol red	11058021	Gibco, Thermo Fisher Scientific, Waltham, USA
pNFAT-luc	219088-51	Stratagene, Amsterdam, N
Sodium hydroxide pellets	1.06498	Merck, Darmstadt, Germany
Trypsin-EDTA (0.05%), phenol red	25300054	Gibco, Thermo Fisher Scientific, Waltham USA
Tween 20	P2287	Sigma-Aldrich, Saint-Louis, USA
Zeocin	R25001	Invitrogen, Thermo Fisher Scientific, Waltham, USA

3.1.4. Molecular and cellular biological kits

Table 5. Molecular and cellular biological kits.

Item	Catalogue number	Company
AlphaScreen cAMP assay kit	6760635M	PerkinElmer, Baesweiler, Germany
Bright-Glo™ luciferase assay system	E2620	Promega, Mannheim, Germany
EndoFree plasmid maxi kit	12362	Qiagen, Hilden, Germany
Fluo-4-direct™ Ca^{2+} assay kit	F10471	Invitrogen, Thermo Fisher Scientific, Waltham, USA
PathHunter®eXpress MRGPRD CHO-K1 β-arrestin GPCR assay (1000 dp (10 x 96-well)	93-0926E2CP2L	Eurofins DiscoverX, Fremont, CA, USA

3.1.5. Buffers

Table 6. Buffer I (TRIS-EDTA Puffer 10x).

Reagent	Amount	Concentration
TRIS (Base)	48,456 g	400 mM
Dinatrium-EDTA x 2 H2O	3,723 g	100 mM

All substances were dissolved in distilled water. The pH was adjusted to 8.3 with water-free acetic acid, the volume was made up to 1000 ml and the solution was filtered. Storage took place at room temperature. For use, the solution was diluted 1:10 with water.

Table 7. Buffer II (Lysis buffer).

Reagent	Volume	Final
Milli-Q water	19 ml	
BSA	20 mg	0.1%
10% Tween 20	600 µl	0.3%
1M HEPES	100 µl	5 mM

pH was adjusted to 7.4 with 1M NaOH. Volume was completed to 20 mL with Milli-Q H20. The buffer was prepared fresh on day of use and kept on ice.

3.1.6. Cell lines

Table 8. Cell lines used in this work

Cell line	Catalogue number	Provider
Flp-In™-CHO (chinese hamster ovary) Cell line	R75807	Invitrogen, Thermo Fisher Scientific, Waltham, USA
Flp-In™-CHO stably transfected with a short variant of hMrgD	-	Kindly provided by Prof. von Kügelgen Produced by (Müller, 2014)

3.1.7. Culture media

Culture medium I (Medium for non-transfected CHO Flp-In-cells)

- Ham's F12 Nutrient Mix, GlutaMAX
- 10 % FBS (heat inactivated)
- 100 µg/ml Zeocin

Culture medium II (Medium for stably transfected CHO Flp-In-cells)

- Ham's F12 Nutrient Mix, GlutaMAX
- 10 % FBS (heat inactivated)
- 500 µg/ml Hygromycin B

Culture medium III (Medium for transient transfection for the luciferase assay)

- Ham's F12 Nutrient Mix, GlutaMAX
- 10 % FBS (heat inactivated)

3.1.8. Test substances

3.1.8.1. Agonists

Table 9. Agonists tested in this work.

Agonist	Solvent	Catalogue No	Company
5-OxoETE	EtOH	34250	Cayman chemical, Michigan, USA
Alamandine; Angiotensin A (1-7) trifluoroacetate salt	H_2O	SML1374	Sigma-Aldrich, Saint-Louis, USA
Angiotensin fragment 1-7 acetate salt hydrate	H_2O	A9202	Sigma-Aldrich, Saint-Louis, USA
DL-3-Aminobutyric acid	HBSS	A44207	Sigma-Aldrich, Saint-Louis, USA

DL-3-Aminoisobutyric acid	HBSS	217794	Sigma-Aldrich, Saint-Louis, USA
GABA	HBSS	A5835	Sigma-Aldrich, Saint-Louis, USA
L-Carnosine	HBSS	C9625	Sigma-Aldrich, Saint-Louis, USA
β-Alanine	HBSS	146064	Sigma-Aldrich, Saint-Louis, USA

3.1.8.2. Antagonists

Table 10. Antagonists tested in this work.

Antagonist	Solvent	Catalogue No	Company
Chlorpromazine HCl	H_2O	C8138	Sigma-Aldrich, Saint-Louis, USA
D-(+)-3-Phenyllactic acid	HBSS	376906	Sigma-Aldrich, Saint-Louis, USA
D-Phenylalanine	HBSS	P1751	Sigma-Aldrich, Saint-Louis, USA
D-Tryptophan	HBSS	T9753	Sigma-Aldrich, Saint-Louis, USA
L-Lysine monohydrochloride salt	HBSS	L5626	Sigma-Aldrich, Saint-Louis, USA
Rimcazole 2HCl	H_2O	R-112	RBI Research Biochemicals International, USA
Thioridazine HCl	H_2O	T9025	Sigma-Aldrich, Saint-Louis, USA

- The solvents of the test substances are shown in the tables. All other substances were dissolved in distilled water unless otherwise specified. Dilutions of stock solutions were made in HBSS.
- For forskolin, a stock solution (10 mM) in DMSO / EtOH solvent mixture (1 : 7) was prepared. Dilution in HBSS (at 37 °C) was performed on the day of the experiment.

3.1.9. Chemical structures of test substances

3.1.9.1. Agonists

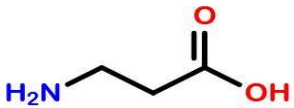

β-Alanine

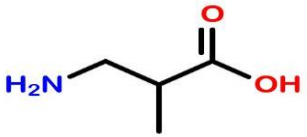

DL-3-Aminoisobutyric

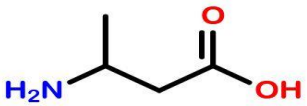

DL-3-Aminobutyric

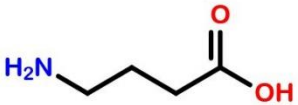

GABA

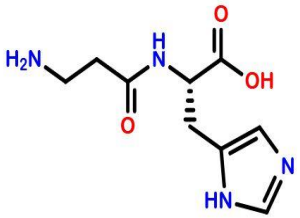

L-Carnosine

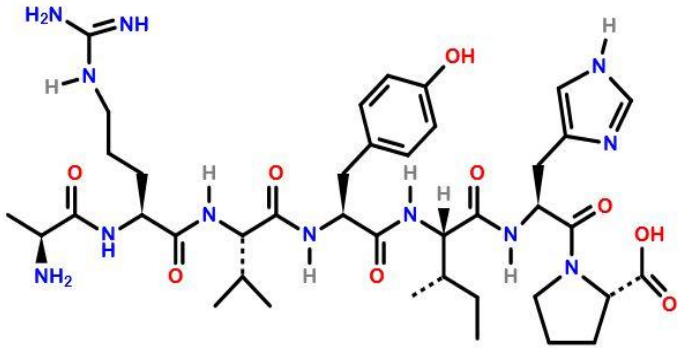

H-Ala-Arg-Val-Tyr-Ile-His-Pro-OH

Alamandine

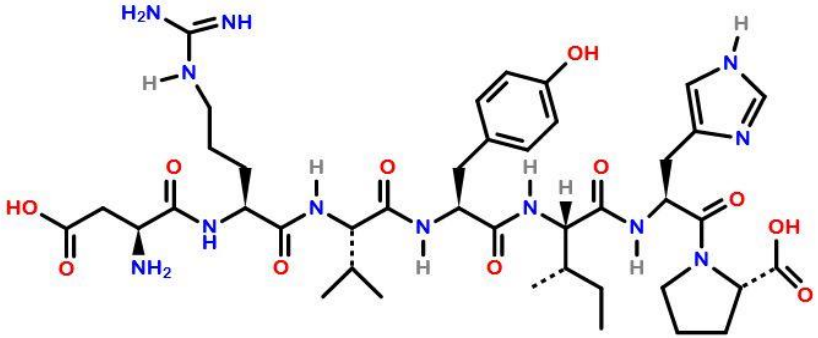

H-Asp-Arg-Val-Tyr-Ile-His-Pro-OH

Angiotensin 1-7

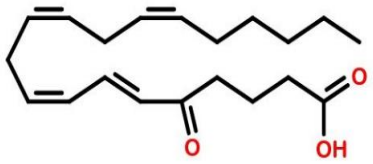

5-OxoETE

3.1.9.2. Antagonists

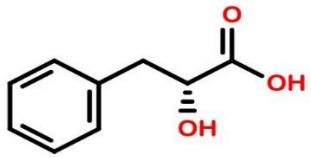

D+3-Phenyllactic acid

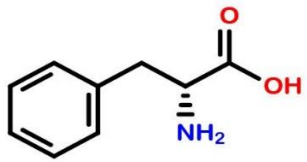

D-Phenylalanine

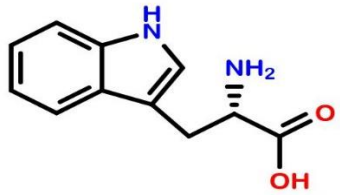

D-Tryptophan

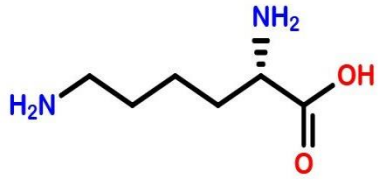

L-Lysine

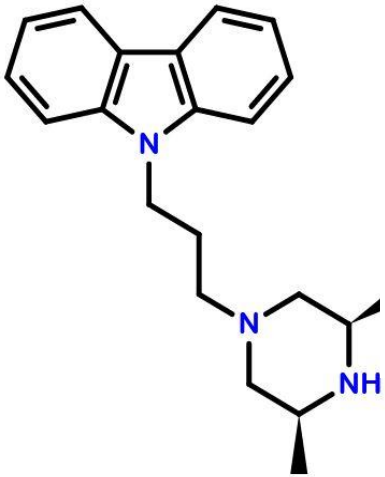

Rimcazole

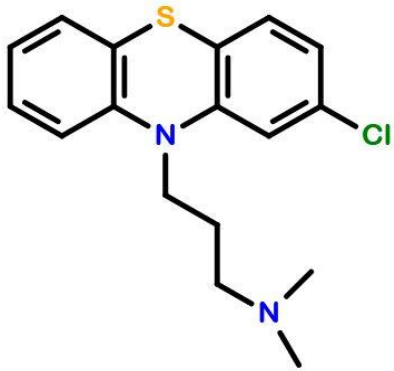

Chlorpromazine

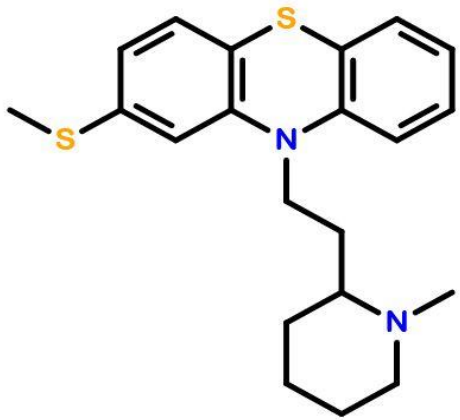

Thioridazine

3.1.10. Laboratory instruments and equipment

3.1.10.1. Devices

Table 11. Devices

Device	Company
Autoclave (VarioklavR (H+p))	Invitrogen, Thermo Fisher Scientific
Confocal Laser Scanning Microscope	observer Z.1/LSM 700; Zeiss, Jena
Cooling centrifuge	543OR; Eppendorf AG
FiveEasy™ PH-meter	Mettler Toledo
Gel DocTM XR+ Molecular Imager®	BIO-RAD laboratories; GmbH
Heracell CO2 incubator (HERACELL 150i)	Invitrogen, Thermo Fisher Scientific
Herasafe Cell culture hood (Heraeus instrument-HERA Safe)	Invitrogen, Thermo fischer scientific
Light microscope	IDO3; Zeiss
Micro plate reader, FLUO star Optima	BMG Labtech, Ortenberg
Micro plate reader, POLAR star Omega	BMG Labtech, Ortenberg
Minispin plus (centrifuge)	Eppendorf
Multi (automatic) pipette	Eppendorf
Sensitive balance	BP211D; Sartorius
Shaking incubator	Edmund Bühler GmbH
U-1900 spectrophotometer	HITACHI, Krefeld

Ultrapure distilled water device classic	PURELAB
UV-transilluminator	BIO-RAD laboratories; GmbH
Vacuum pump	ILMVAc
Vortex Mixer	VELP Scientifica
Weighing balance	TE601; Sartorius

2.1.10.2. Software

Table 12. Software.

Software	Company
Microsoft Excel 2010	MS Office
Microsoft Powepoint 2010	MS Office
Microsoft Word 2010	MS Office
OMEGA analysis software	BMG Labtech
OPTIMA analysis software	BMG Labtech
Prism 5.04	GraphPad Software; San Diego, USA
Quantity One® 1-D Analysis Software	BIO-RAD laboratories; GmbH
Zen 2012 imaging software	Zeiss Jena

3.2. Methods

3.2.1. Cell culture

Cells were grown using identical culture requirements in cell incubators, which were set to 37°C with an atmosphere of 5% CO2 and 96% humidity. Applied cell culture solutions and media were prewarmed at room temperature (RT). Cells culturing was carried out under aseptic conditions in a safety cabinet with laminar air flow.

3.2.1.1. Passaging cell lines

Cells were splitted routinely at least twice a week. For harvesting the cells, the growth medium was removed from the flask and cells were washed carefully with DPBS (RT) to remove remaining medium. For a 75 cm^2 flask, 2.5 ml of trypsin solution (RT) were added to the flask and incubated at 37°C until cells have detached (2-5 min). Trypsinization was stopped by addition of respective growth medium (see section 3.1.7). Cells were resuspended in an appropriate volume and transferred into a new culture flask, which was already filled with growth medium.

3.2.1.2. Cryopreservation of cell lines

To keep permanent stocks of the utilized cell lines, cells were grown until they nearly reached confluence (80-95%), using cell culture flasks (75 cm^2). Cells were washed with DPBS (RT) to remove residual medium and then trypsinized with trypsin (RT) until they have detached (2-5 min). Cells were then concentrated in low volume of the growth media (1-3 ml). Meanwhile, a freezing medium containing 20% of the cryoprotectant (DMSO) of the respective plain medium was freshly prepared. Then, to one cryo-vial, equal volumes of the cell suspension and the freezing media were added (0.9 ml). The labelled cryo-vial was then stored in the -20°C for 24 h after which it was transferred to liquid nitrogen tank for long term storage.

3.2.1.3. Revitalization of cell lines

For cell thawing after long-term storage, a vial of frozen cells was removed from the liquid nitrogen tank and rapidly unfrozen. Following complete defreezing, the content of one vial

(1.8) ml were added to a culture flask having a large volume (20 ml) of fresh respective growth media without antibiotics. This large volume of media was used to dilute DMSO to avoid its cytotoxic effects. Twenty-four hours later, medium was replaced by complete growth medium, including antibiotics. Usually, cells were cultured at least for one week before they were used for further analyses.

3.2.2. Methods in molecular biology

3.2.2.1. Heat shock transformation into chemically competent E. coli

Transformation is the process that occurs when a cell ingests foreign DNA from its surroundings. For proper presentation and replication of Nuclear Factor of Activated T-cells-luciferase (NFAT-luc) reporter plasmid, transformation into chemically competent E. coli was performed. First, the bacteria (One Shot Top 10 E. coli) were thawed on ice for 30 min. Meanwhile, a dilution (1:200) of the plasmid was prepared by adding 0,5 µl of NFAT-luc reporter plasmid to 100 µl of distilled water (DNase and RNase free). Then, 1 µl of this solution mixture was added to the bacteria and incubated together for 15 min on ice. After the incubation, the bacterial vial was heat shocked at 42°C for 30 s for pore formation and uptake of the plasmid directly followed by 3 min ice incubation. 200 µl S.O.C medium was then introduced to the vial and incubated for 1 h in a shaking incubator at 37°C. Agar plates with ampicillin (100 µg/ml) were used for streaking the bacteria (25 µl and 100 µl). Plates were then incubated overnight at 37°C, then stored in the refrigerator at 4°C until selection of the clones (Singh et al., 2010).

3.2.2.2. Plasmid DNA isolation (Maxi-preparation)

To obtain high purity and high concentration plasmid DNA, as required, for the reporter gene assay, a maxi-preparation was carried out. One day before the plasmid isolation, a single transformed bacterial (One Shot TOP10 E. coli, Invitrogen®) colony was selected from an LB agar plate and pre-cultured in 5 ml of LB Broth with ampicillin (100 µg / ml) at 36.5 °C with horizontal shaking (225 rpm) for 8 h. The starter culture was then diluted 1/500 into selective LB medium by inoculating 100 ml of LB broth with ampicillin (100 µg / ml) with 200 µl of the starter culture at 36.5 °C with horizontal shaking (225 rpm) overnight for 16 h. The immediately following maxi preparation was performed with the EndoFree Plasmid Maxi Kit (QIAGEN®) according to the manufacturer's instructions. An alkaline partial lysis of the

bacterial membrane caused pore formation and the DNA went into the lysate. Cell constituents were removed by filtration, then a special buffer was used to remove endotoxins and DNA was bound to an anion exchange column. RNA, proteins, and other low-molecular substances were removed by rinsing with different osmolar salt solutions. DNA elution was carried out with a high molar salt solution. The eluted DNA was precipitated using RT isopropanol followed by washing with ethanol for further purification and concentration. Finally, the air-dried DNA pellet was redissolved using suitable volume (50-100 µl) of a basic buffer. Samples were taken for sequencing and for agarose-gel electrophoresis and the original aliquot was stored at -20°C.

3.2.2.3. Agarose gel electrophoresis

Agarose gel electrophoresis is a simple and highly effective method for separating and purifying DNA fragments of different sizes (200-20,000 base pairs) (Vogelstein & Gillespie 1979). Molecules migrate through the agarose gel-matrix with varying speed, depending on their size and charge. The electrophoresis buffer TRIS-Acetate-EDTA (1x TAE) enables the charge migration due to its alkaline pH (pH 8.3), which causes the dissociation of the acidic phosphate groups of the DNA and migration from the negatively charged cathode to the positively charged anode upon applying a voltage to the electrophoresis chamber. The result is a separation by size of the molecules. It should be noted that due to its circular structure, plasmid DNA migrates faster than linear molecules of the same length as they do not interfere as much with the surrounding agarose gel matrix.

The gel was made of 1% agarose dissolved in 1x TAE buffer by heating to 100 °C. After cooling to about 50 °C, a fluorescent DNA intercalating dye (SERVA DNA stain G) was added to the gel (for each 20 ml of the gel, 1 µl of dye was added) and poured into a horizontal comb-shaped casting chamber. Once the gel had hardened (approx. 15 min), it was inserted in an electrophoresis chamber containing 1x TAE running buffer. Prior to loading, the samples were mixed with DNA gel loading buffer (10x Blue Juice gel loading buffer). Blue juice is a simple mixture of glycerol to raise the density of DNA sample and bromophenol blue dye to monitor the progress of the electrophoresis. A molecular-weight size marker (DNA ladder) of 1 Kb was added to run in parallel to the plasmid DNA samples. A voltage of 75 V was applied for 60 to 90 min after which the gel was taken for visualization by Bio-Rad Gel Doc XR^+ system. This device emits light in the UV range, which leads to the

fluorescence of the DNA intercelating dye. This fluorescence is detected by a camera and displayed with the Quantity One® 1-D Analysis Software (Bio-Rad Laboratories).

As can be seen from the gel image (**Figure 5**), the plasmid pNFAT-luc show clear bands in the upper fifth of the gel image and a weak band at the site of application. The size of the plasmid is around 4000 bp as compared to the reference 1 kb ladder running in parallel.

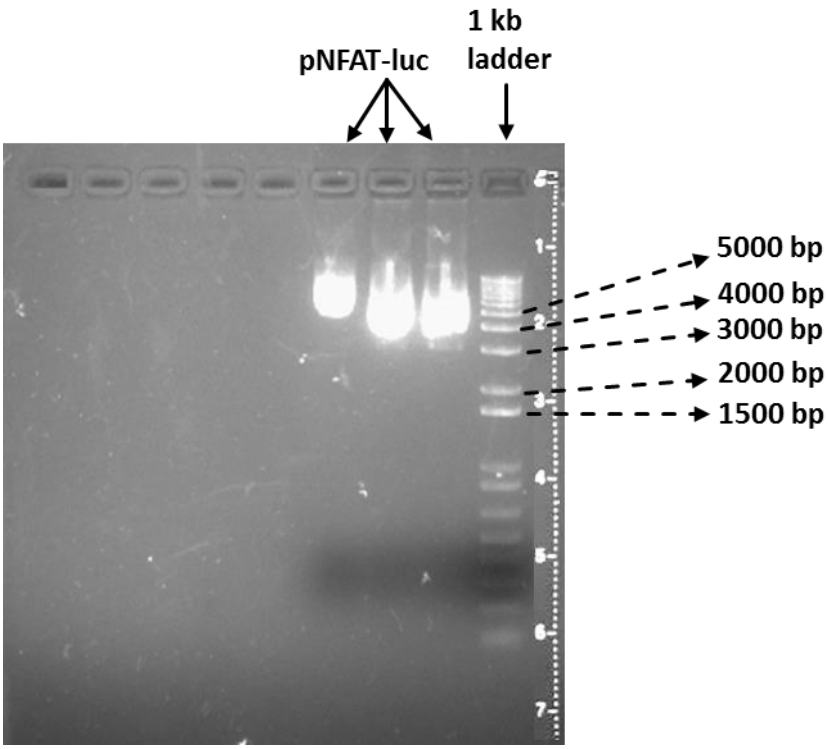

Figure 5: Agarose gel electrophoresis of maxi-prepared Nuclear Factor of Activated T-cells-luciferase (NFAT-Luc) plasmid. The DNA was stained with DNA intercelating dye (SERVA DNA stain clear G). To determine the DNA size, a 1 kb plus DNA ladder was used. The image was taken with a Universal Hood using the Quantity One 1-D Analysis Software (Bio-Rad Laboratories).

3.2.2.4. Plasmid DNA concentration and purity determination

The concentration and purity were determined using the UV-VIS spectrophotometer (HITACHI U-1900, Hitachi High Technologies, Krefeld). Absorbance was measured at two wavelengths (260 nm and 280 nm). First zero blank at both wavelengths was adjusted using 1 ml of distilled water. Using the same cuvette, 5 µl of the purified plasmid were added to 995 µl of distilled water (200 times dilution) and absorbance at 260 and 280 nm was measured.

Concentration of the plasmid DNA was determined according to the following formula:

$$\text{Concentration } (\mu g/\mu l) = \frac{\text{ABS (260 nm) x Dilution factor x 50}}{1000}$$

Purity of the plasmid DNA was determined according to the following formula:

$$\text{Measure for the purity} = \frac{\text{ABS (260 nm)}}{\text{ABS (280 nm)}}$$

The ratio should be > 1.8. Smaller values indicate a contamination with proteins or phenols (Wilfinger et al., 1997).

3.2.3. Functional experiments

3.2.3.1. Fluorescent Ca^{2+} sensitive indicators

Activation of Gq coupled GPCRs mediate increase in PLC activity followed by production of IP3 and Ca^{2+} release from intracellular stores. In order to study such a signaling pathway, fluorescent Ca^{2+}-sensitive dyes have been successfully developed to monitor changes in intracellular Ca^{2+} levels such as the UV light-excitable quin2 (Tsien et al., 1982) and the more fluorescing Fura-2 and Indo-1 (Grynkiewicz et al., 1985).

Later on, visible-light excitable Ca^{2+} indicators were developed for use in flow cytometry and confocal laser-scanning microscopy (LSM) such as Fluo-3 (Minta et al., 1989; Kao et al., 1989) and its more advanced analog Fluo-4 (Gee et al., 2000). Fluo-4 shows similarity to Fluo-3 in several aspects including spectral properties, stability, Kd (Ca^{2+}), convenience, easy of loading and high Ca^{2+}-dependent fluorescence increase. However, due to chlorine substitution with fluorine atoms in the fluorophore moiety, the absorption maximum of fluo-4 is blue-shifted about 12 nm, as compared with fluo-3 resulting in more efficient fluorescence absorption and excitation at 488 nm. Thereby generating more intense signal levels when used with confocal LSM, flow cytometry and microplate screening applications.

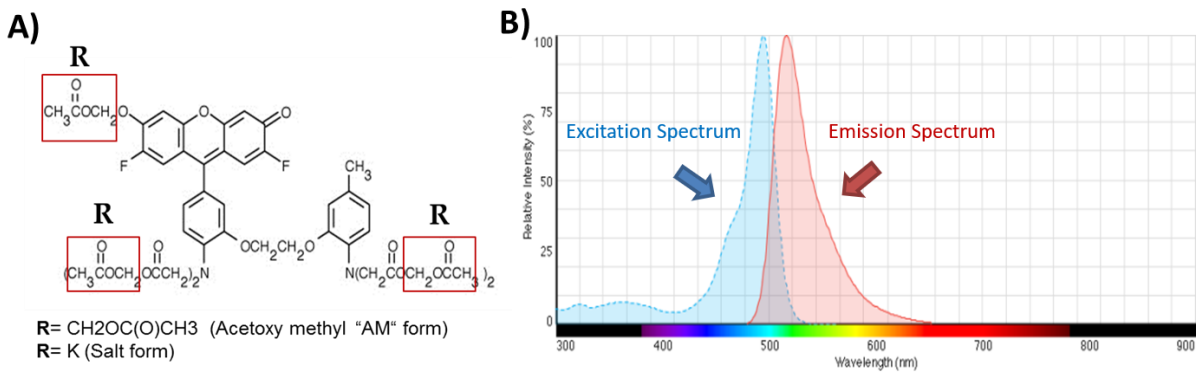

Figure 6: A) Chemical structure of Fluo-4 AM. B) Fluo-4 fluorescence spectrum (Gee et al., 2000; Invitrogen).

3.2.3.1.1. Fluo-4 Ca^{2+} mobilization assay

To prepare the cells for the assay, CHO cells were splitted as described above (see section 3.1.7), 50 µl from cell suspension with medium were added to the center of each coverslip in a 6 well plate. After 10 min the cells were attached to the surface of the coverslips and 2 ml of culture medium (see section 3.1.7) was added carefully to the wall of each well and incubated (37 °C, 5% CO2). After 24 hours, the assay was performed using Fluo-4 direct Ca^{2+} assay kit (Invitrogen). First, the media was removed from the cells then, HBSS buffer and Fluo-4 AM loading solution (prepared according to manufacturer's instructions) were added in a ratio of 9:1 (900 µl to 100 µl) respectively to each coverslip, and incubated (37 °C, 5% CO2) for 30 min. The coverslip was carefully placed inside a plastic coverslip holder fixed with a metal lock. Then it was washed with 1 ml HBSS (3x) and a final volume of HBSS was added and examined at the stage of a confocal LSM (observer Z.1/LSM 700; Zeiss, Jena) using the following parameters:

- Objective: Plan-Apochromat objective (40x/1.3 oil DIC M27)
- Dimensions: x: 1660, y: 1660, 16-bit color depth
- Image size: x: 159.95 µm, y: 159.95 µm
- Scan mode: plane, time series of 40 cycles with 15 s intervals
- Master gain: 700
- Digital gain: 9.97
- Filters: 493-1000
- Beam splitter: 492 nm
- Lasers: 488 nm & 2% laser power

Cells were consistently scanned with the laser beam for 40 cycles with 15 s intervals. At the fourth cycle of the experiment, either β-alanine (end concentration 300 µM and 3 mM) or alamandine (10 µM) or HBSS buffer (control) were added, and images were automatically captured along the whole time series. In alamandine experiments, β-alanine (600 µM) or HBSS were additionally given to the cells at the 30th cycle of the experiment. Evaluation was then performed using the Zen 2012 (Zeiss) software. At least two coverslips with cells were examined per treatment. For each field, 15 cells and a background region (without cells) were randomly selected using circles of the same dimensions. First, the measured pixel values were corrected for their background. Then, the percentage of ratio of ΔF (which is for each cell, the difference in fluorescence intensity between each cycle (F) and the starting baseline cycle which corresponds to zero time point (F0)) to F0 (ΔF/F0 %) was calculated and graphically represented. For each treatment curve, a paired-two-tailed t-test was performed to compare the difference in fluorescence between the pre-treatment cycle (cycle 3) and the following cycles post-treatment (starting from cycle 4). In order to compare each agonist to its control, a percentage of the ratio of ΔF (which is in this case, the difference between highest fluorescent signal elicited by each cell post treatment (F highest) and the pre-treatment fluorescent signal at cycle 3 which corresponds to 30 s time point (F30)) to F30 (ΔF/F30 %) was calculated and analyzed using unpaired-two-tailed t-test. In alamandine experiments, ΔF/F420 % was additionally tested to get the fluorescence difference between the highest fluorescent signal elicited by β-alanine and the base line signal which corresponds to 420 s time point (cycle 29).

The following equations apply to the examined fields:

$$\Delta F/F0\ \% = \left(\frac{F_{\text{each cycle}} - F0_{\text{cycle 1}}}{F0_{\text{cycle 1}}} \times 100\right) + 100$$

$$\Delta F/F30\ \% = \left(\frac{F_{\text{cycle with highest fluorescence}} - F30_{\text{cycle 3}}}{F30_{\text{cycle 3}}} \times 100\right) + 100$$

$$\Delta F/F420\ \% = \left(\frac{F_{\text{cycle with highest fluorescence}} - F420_{\text{cycle 29}}}{F420_{\text{cycle 29}}} \times 100 \right) + 100$$

3.2.3.2. Reporter gene system

Reporter gene system is a technology that aims to signal transcriptional activity in cells using genes which have been adapted as reporter genes. The activation of a specific signaling cascade of interests induces the expression of a reporter gene which can be monitored through its enzymatic activities linked with a variety of colorimetric, fluorescent, or luminescent read-outs (Cheng et al., 2010). Advantages of the reporter assay including inherent sensitivity, large signal dynamics and simplicity to set up, makes it a high throughput homogenous assay for screening GPCR targets linked to cAMP or Ca^{2+} signaling (Bronstein et al., 1994).

Luciferases are oxidative enzymes which are found in several species enabling them to bioluminesce. The most famous of these is the 61 kDa monomer firefly luciferase which catalyzes the mono-oxygenation of beetle luciferin to oxyluciferin together with light emission **(Figure 7).** The quantum yield is about 0.9, the highest of any known luminescent reaction (see Bronstein et al., 1994). In 1985, de Wet and colleagues reported the cloning of firefly luciferase cDNA (*luc*), following which has been incorporated into several reporter vectors. Luciferase reporter assays are sensitive, rapid, reliable, easy to perform and well suited to laboratory automation and HTS applications.

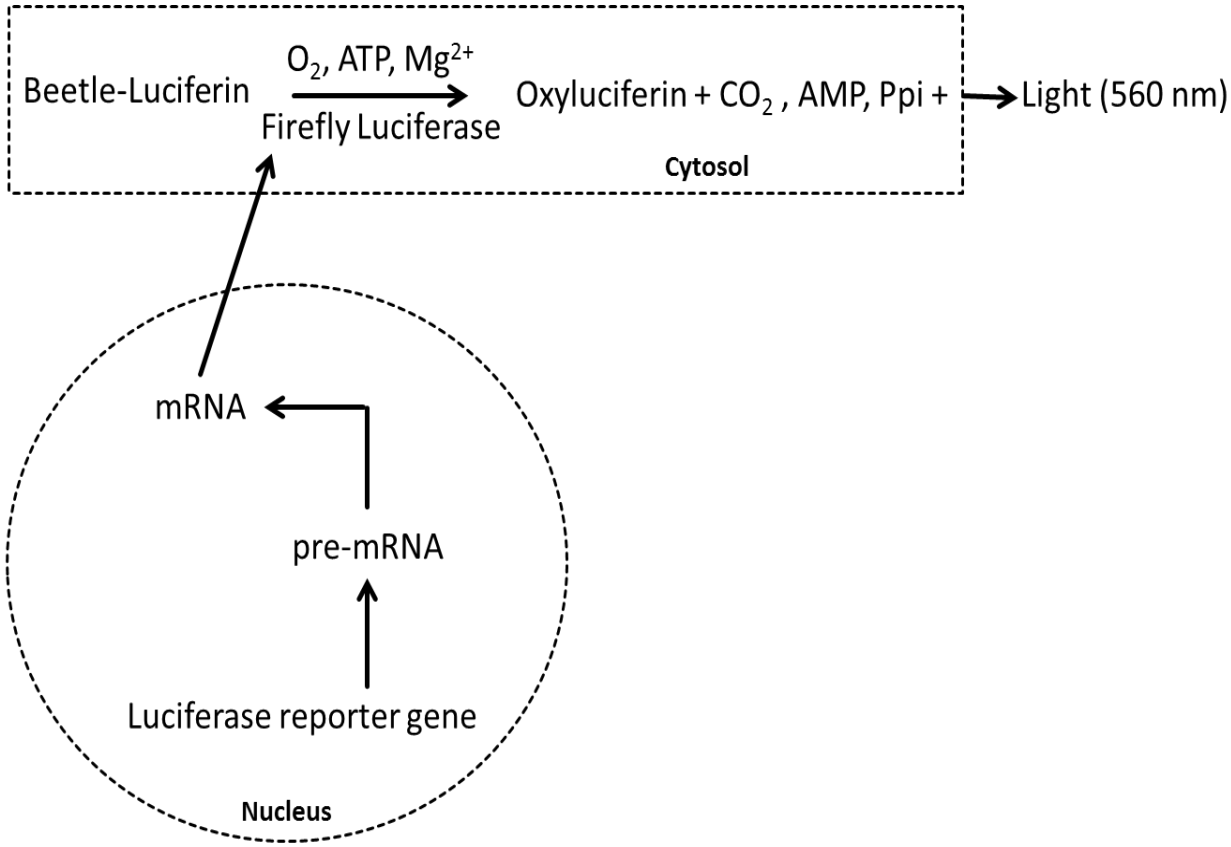

Figure 7: The luciferase bioluminescent reaction. Mono-oxygenation of luciferin is catalyzed by firefly luciferase in the presence of molecular oxygen, adenosine triphosphate (ATP) and magnesium (Mg^{2+}), yielding oxyluciferin, CO_2, adenosine monophosphate (AMP), inorganic pyrophosphate (Ppi), and light. Modified from (de Almeida et al., 2011).

3.2.3.1.1. NFAT-luciferase reporter gene assay

The NFAT-luciferase reporter gene assay is designed to monitor the activation of nuclear factor of activated T-cells (NFAT) and Ca^{2+} mediated signal transduction pathways downstream of Gαq protein activation. Increases in intracellular Ca^{2+} concentrations will induce the promotor activity through the activation of the phosphatase calcineurin. This is followed by the binding of endogenous transcription factors to NFAT; thus, initiating the transcription of the luciferase reporter gene **(Figure 8).**

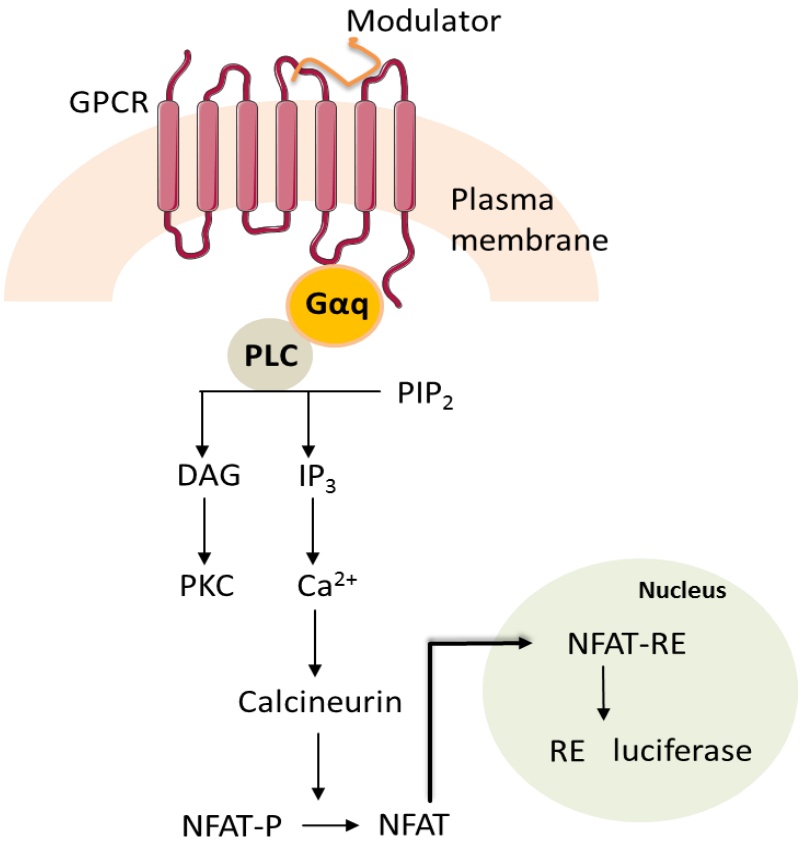

Figure 8: Schematic diagram showing NFAT signal transduction pathway. Gαq: Gq-Protein, PLC: Phospholipase C, PIP2: Phosphatidylinositol-4,5-bisphosphate, IP3: Inositol triphosphate, DAG: diacylglycerol, PKC: Protein kinase C, NFAT: nuclear factor of activated T-cells, RE: response element (Modified from Paguio et al., 2006). The receptor and membrane were used from the website "https://smart.servier.com".

For this experiment, CHO cells were transiently transfected with 10 µg pNFAT-Luc vector DNA (Stratagene, Amsterdam, NL) and 25 µl Lipofectamine 2000 (Invitrogen) per one tissue culture flask (75 cm^2). The vector and the lipofectamine were diluted with 500 µl OptiMEM®I (Gibco) each. After 5 min incubation at RT, both solutions were combined and incubated at RT for further 20 min. Then, the whole solution was added dropwise to a flask of approximately 80% cells confluency having medium without antibiotics (see section 2.1.7). 18 h after transfection, cells were splitted into 24-well cell culture plate (500 µl of cell suspension to each well). 24 h later, the medium was removed from the cells, the cells were then washed with 1 ml of warm (37 °C) HBSS (2x) and 900 µl of HBSS were finally introduced per well. After 1 h incubation in the incubator (37 °C, 5% CO2), 100 µl of the

agonist or the solvent (control) were added. In some experiments, antagonists were studied. These were added 20 min before the agonists. Pre-incubation with the antagonist should ensure even distribution as well as equilibration of the antagonist binding to the receptor. Cells were then incubated (37 °C, 5% CO2) for 3.5 h after which the buffer containing the tested substances was discarded and the reaction was stopped by adding to each well 50 µl HBSS and 50 µl of the luciferase substrate, Bright-GLO luciferase assay solution (Promega, Mannheim, Germany). After 3 min incubation at RT in the dark (as the luciferase substrate is light sensitive), 80 µl was transferred from each well to a corresponding well in a 96-well plate and measured in a luminometer (FLUOstar OPTIMA, BMG Labtech, Ortenberg, Germany). The plate measurement was repeated 3 times automatically and the output signal was in terms of relative light units (RLUs). For the evaluation, RLUs of the 3 cycles were averaged and data were presented as % of respective basal control.

3.2.3.3. AlphaScreen cAMP assay

The AlphaScreen (Amplified Luminescent Proximity Homogeneous) cAMP assay has been developed to directly measure levels of cAMP produced upon modulation of adenylate cyclase activity by GPCRs. The assay is efficient at measuring both agonist and antagonist activities on Gαi- and Gαs-coupled GPCRs by respectively activating or inhibiting adenylate cyclase (enzyme which catalyze the conversion of ATP to cAMP). In this assay cells are stimulated to either increase or decrease intracellular cAMP levels followed by a combined cell lysis / detection step (PerkinElmer, Waltham, MA, USA).

The principle of the assay as shown in **Figure 9** is based on the competition between endogenous cAMP and exogenously added biotinylated cAMP. There are two bead types in every AlphaScreen assay: acceptor beads and donor beads. Acceptor beads have a specific antibody conjugated to them to capture cAMP. Donor beads contain a photosensitizer, phthalocyanine, which upon illumination at 680 nm, converts ambient oxygen to an excited form of O2, singlet oxygen which has a limited lifetime (4 µs half-life) before it falls back to the ground state. During this lifetime if an acceptor bead is in proximity, singlet oxygen which can diffuse up to approximately 200 nm in solution will transfer its energy to thioxene derivatives within the acceptor bead producing light at 520–620 nm. Otherwise, singlet oxygen falls to ground state and no signal is produced.

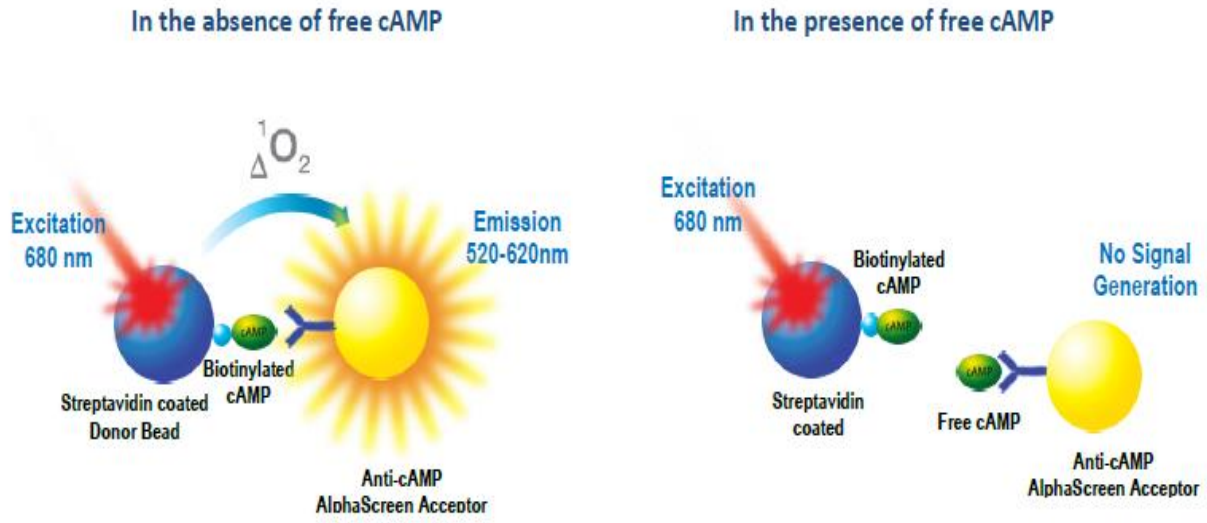

Figure 9: AlphaScreen cAMP assay principle. Modified from AlphaScreen cAMP User Manual, PerkinElmer®, Inc, 2010-2015.

Advantages of AlphaScreen cAMP assay includes:

- The very high sensitivity as each donor bead can release up to 60,000 singlet oxygen molecules per second resulting in a very high signal amplification.
- The very low backgrounds as the signal is read at a lower wavelength as compared to the excitation wavelength, where most of the background counts are found. Moreover, very few biological or assay substances will interfere owing to the very long illumination wavelength at 680 nm.

For this experiment, CHO cells were cultured on 24-well cell culture plates. 24 h later (cells approx. 90% confluent), the culture medium was removed, and cells in a well were washed with 1 ml HBSS (2x). 400 µl HBSS were finally applied into each well. The plate was then incubated (37 °C) in a water bath for 1 h after which 100 µl of agonists or solvent (control) were added to the cells. In experiments using forskolin, 300 µl of HBSS were introduced into each well. 100 µl of drugs were added first followed by 100 µl of forskolin. 10 min after forskolin addition, the reaction was stopped by removing the assay buffer and lysing the cells with 500 µl / well of cold lysis buffer (5 mM HEPES containing 0,1% bovine serum albumin (BSA) and 0,3% Tween-20, pH 7.4). BSA is a small, stable, moderately non-reactive protein which helps to reduce the assay background while Tween-20 is a nonionic surfactant which helps in forming pores in the cell membrane of the cells, releasing intracellular cAMP. After 3 min incubation on ice, the cell culture plates were swirled on ice for 30 min to allow

equilibration between intracellular and extracellular cAMP. 20 µl of the supernatant or cAMP standards (0,39 nM to 100 nM) or lysis buffer were then added to a 96-well cell culture plate having 20 µl of acceptor beads per well and incubated (RT) in the dark. After 30 min, 60 µl of donor beads-biotinylated cAMP detection mix were then added to all wells and incubated (RT) for 1 h after which the luminescence was measured using the luminometer (POLARstar Omega, BMG Labtech, Ortenberg, Germany). Acceptor beads and donor beads-biotinylated cAMP detection mix solutions in lysis buffer were prepared according to the manufacturer's instructions and kept in the dark for at least 30 min before using.

cAMP levels per well were calculated by regression analysis from a standard curve determined for each experiment. For the preparation of the calibration line defined concentrations of a cAMP standard (0,39 nM to 100 nM) were measured. The cAMP content of the measured samples was in the range of the calibration line. For the calculation of the cAMP content of the samples, first, the lysis buffer/sample (C0/Cx) ratio was determined for all values. Second, the cAMP concentration of the samples was estimated from the calibration curve (which is the correlation between cAMP concentration in nM (x-axis) versus the Lysis buffer/cAMP standard ratio (y-axis)). For the presentation of the results, the cAMP values in the presence of the agonist were calculated as percentage values of the respective control. In the presence of forskolin, data were presented as percentage values of positive control after subtraction of the basal cAMP content. The basal cAMP content was determined on each experimental day and corresponds to the cAMP content of a sample to which no forskolin and agonist were added.

3.2.3.4. PathHunter eXpress MRGPRD CHO-K1 β-arrestin GPCR assay

The PathHunter β-arrestin assays measure an essential pathway in GPCR activation, i.e., β-arrestin recruitment to activated GPCRs, enabling scientists to screen for and profile functional agonists and inhibitors of GPCRs (DiscoverX, Fremont, CA).

The principle of the assay is based on measuring β-arrestin translocation to the activated GPCR using β-galactosidase (β-gal) enzyme fragment complementation technology **(Figure 10).** In our assay, CHO-K1 cells are stably expressing the hMrgD receptor tagged with the small fragment of β-gal enzyme called ProLink^{TM} (PK). In co-expression is β-arrestin tagged with the other fragment of the β-gal enzyme called Enzyme Acceptor (EA). Independently, these fragments have no β-gal activity. Binding of an activating ligand to the hMrgD receptor

will stimulate the recruitment of the β-arrestin to the C-terminus of the Prolink™ tagged hMrgD, forcing the complementation of both enzyme fragments and resulting in the formation of an active β-gal enzyme. A substrate which is present in the PathHunter detection reagents will then be hydrolyzed by the functional enzyme, generating a chemiluminescent signal.

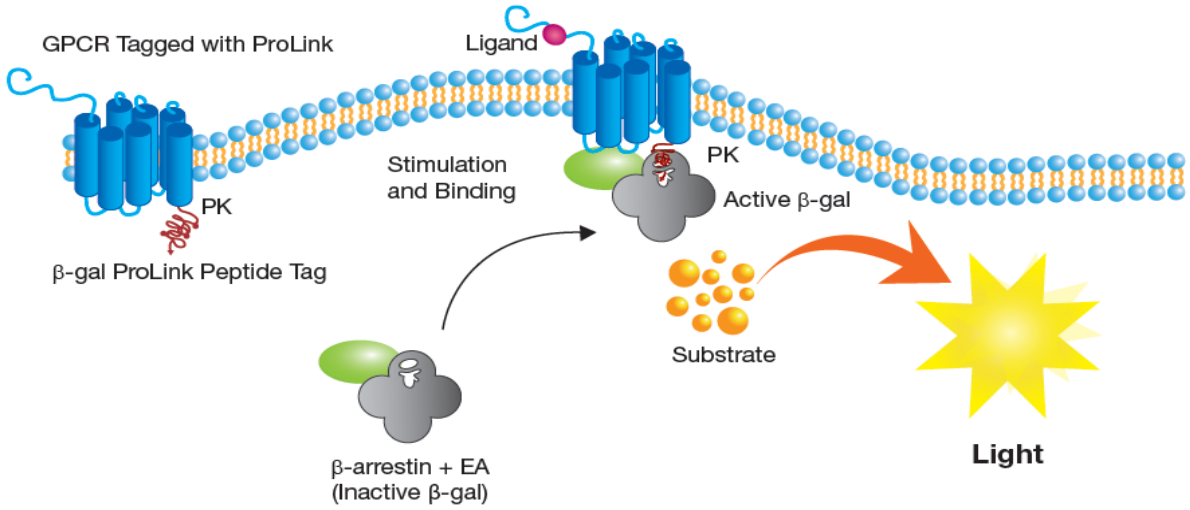

Figure 10: PathHunter β-arrestin GPCR assay principle. Modified from DiscoverX user manual, 2016 DiscoverX Corporation. 20460 111616.

Advantages offered by PathHunter β-arrestin GPCR assay include:

- A G protein-independent signaling pathway (suitable for all GPCRs; especially orphans with little information on their G protein signaling).
- A completely receptor specific response (no signal without enzyme complementation).
- An easy quantitative assay (read out is luminescence)
- Pliability for HTS.
- Robust
- Highly sensitive

To perform the assay, the conditions supplied with the kit manual were applied (PathHunter eXpress MRGPRD CHO-K1 β-arrestin GPCR assay data sheet, DiscoverX). CHO-K1 cells were plated in a 96-well plate in a density of 10000 cells per well (100 µl per well) using the AssayComplete™ Cell Plating 2 Reagent. Following 48 h of incubation (37°C, 5% CO_2), the cells were stimulated (10 µl per well) with either the solvent (HBSS) or the agonists (11x the final concentration) and incubated for 90 min (37°C, 5% CO_2) as recommended in the kit's

protocol. In some experiments, the antagonists were incubated with cells for 30 min before adding the solvent or agonists. For β-alanine and alamandine, shorter (60 min) and longer (120 min) incubation periods were additionally tested. Meanwhile, a PathHunter working detection solution was prepared (4.75 ml of cell assay buffer + 1.25 ml of Substrate reagent 1 + 0.25 ml of Substrate reagent 2) which is stable up to 24 h at room temperature. Once the detection mixture was added to the cells (55 µl per well), the plate was incubated for 1 h at room temperature in a dark place after which the plate was immediately measured in a luminometer (FLUOstar OPTIMA, BMG Labtech, Ortenberg, Germany) at 1 s per well. The output signal was in terms of relative light units (RLUs). For the evaluation, data were presented as % of respective basal control.

3.2.4. Statistical analyses

Data were presented as means ± SEM (standard error in relation to the mean value), for number of experiments (n). For most experiments, differences between means were tested for significance by an analysis of variance (ANOVA) followed by a Bonferroni post hoc test. For experiments without multiple comparisons, paired and unpaired two-tailed t-test were carried out for determination of significance differences. Fitting of data to bell-shaped (AlphaScreen cAMP experiments) or sigmoidal (β-Arrestin experiments) concentration-response curves were performed using GraphPad Prism 5.0 (GraphPad Software Inc, San Diego, CA). $P \leq 0.05$ were considered significant.

4. Results

4.1. Overview of the applied expression system

In the present work, CHO Flp-In cells were used as an expression system for the hMrgD receptor. CHO Flp-In host cell line has a single Flp recombination target (FRT) site which allows the integration and expression of the gene of interest at specific genomic location. Thus, generating stable and genetically identical cell line (Invitrogen; Sauer, 1994). Cloned CHO Flp-In cells stably expressing a short variant (short N-terminus) of the hMrgD receptor which were produced and functionally characterized by Müller, (2014), were further used in this work for studying of Gα-protein-dependent signaling pathways. The variant sequence was introduced into cells genome using the pcDNA5 / FRT / V5-His-TOPO vector (Müller, 2014). In parallel, non-transfected CHO Flp-In cells were tested for responses to exclude any non-specific signals. CHO Flp-In cells cells readily co-expressing the hMrgD and β-arrestin-2 provided by "DiscoverX" were used for β-arrestin recruitment assays.

4.2. Investigation of G protein-dependent signaling pathways downstream of the hMrgD receptor.

4.2.1. Experiments using Fluo-4 Ca^{2+} mobilization assay

4.2.1.1. Study of β-alanine-induced changes in intracellular Ca^{2+} levels

Investigation of the Gαq signaling downstream of the hMrgD was performed using the Fluo-4 direct Ca^{2+} assay in cloned CHO cells stably expressing a short variant of the receptor. Using this assay, alterations in intracellular Ca^{2+} levels were directly visualized by changes in fluorescence on the confocal LSM using the Fluo-4 Ca^{2+} sensitive dye.

In CHO-hMrgD cells, β-alanine in concentrations of [300 µM, 1 mM, and 3 mM] caused concentration-dependent, strong, and extended increases in intracellular Ca^{2+} levels using this assay according to Sargheini, (2017). In the current work, control experiments using β-alanine in concentrations of [300 µM, and 3 mM] were performed in non-transfected CHO cells. Addition of β-alanine either [300 µM] (**Figure 11**) or [3 mM] (**Figure 12**) to the non-transfected cells at the 4^{th} cycle of the 40 cycles time series experiment showed no visual increases in the fluorescence intensity. Comparing the pixel values "ΔF/F0 %" before addition

of β-alanine (cycle 3) and post-addition (cycles 4, 5, 6, 7, 8, 9, and 10) revealed no significant differences in fluorescence intensity in either of tested concentrations **(Figure 13)**. Similarly, when the solvent (HBSS) was added nothing changed. However, one could observe slower time-dependent photobleaching when treating the cells with β-alanine at [300 µM] concentration as compared to the faster bleaching produced by HBSS **(Figure 13 A)**

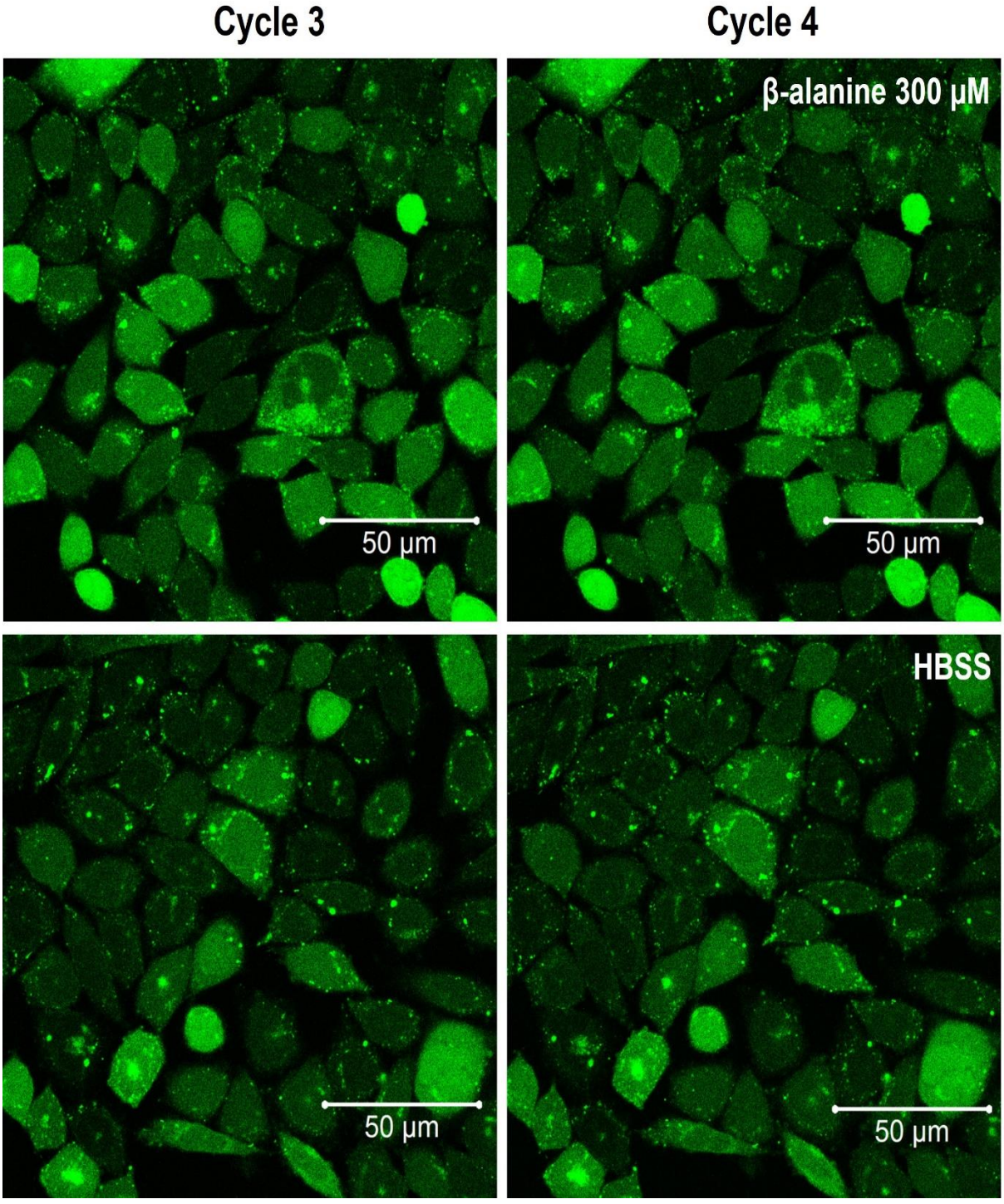

Figure 11: Photomicrographs of changes in intracellular Ca^{2+} levels after addition of β-alanine [300 µM] using the Fluo-4 Ca^{2+} sensitive dye in non-transfected CHO cells. The cells were incubated (37°C) with Fluo-4 AM loading solution for 30 min. At the 4th cycle, either β-alanine or HBSS were added to the cells. The images were taken under identical dyeing and recording conditions of 40x magnification, time series mode, 488 nm excitation wavelength, 492 nm beam splitter, and 2 % laser power on the confocal LSM using Zen 2012 software. Scale bar is 50 µm.

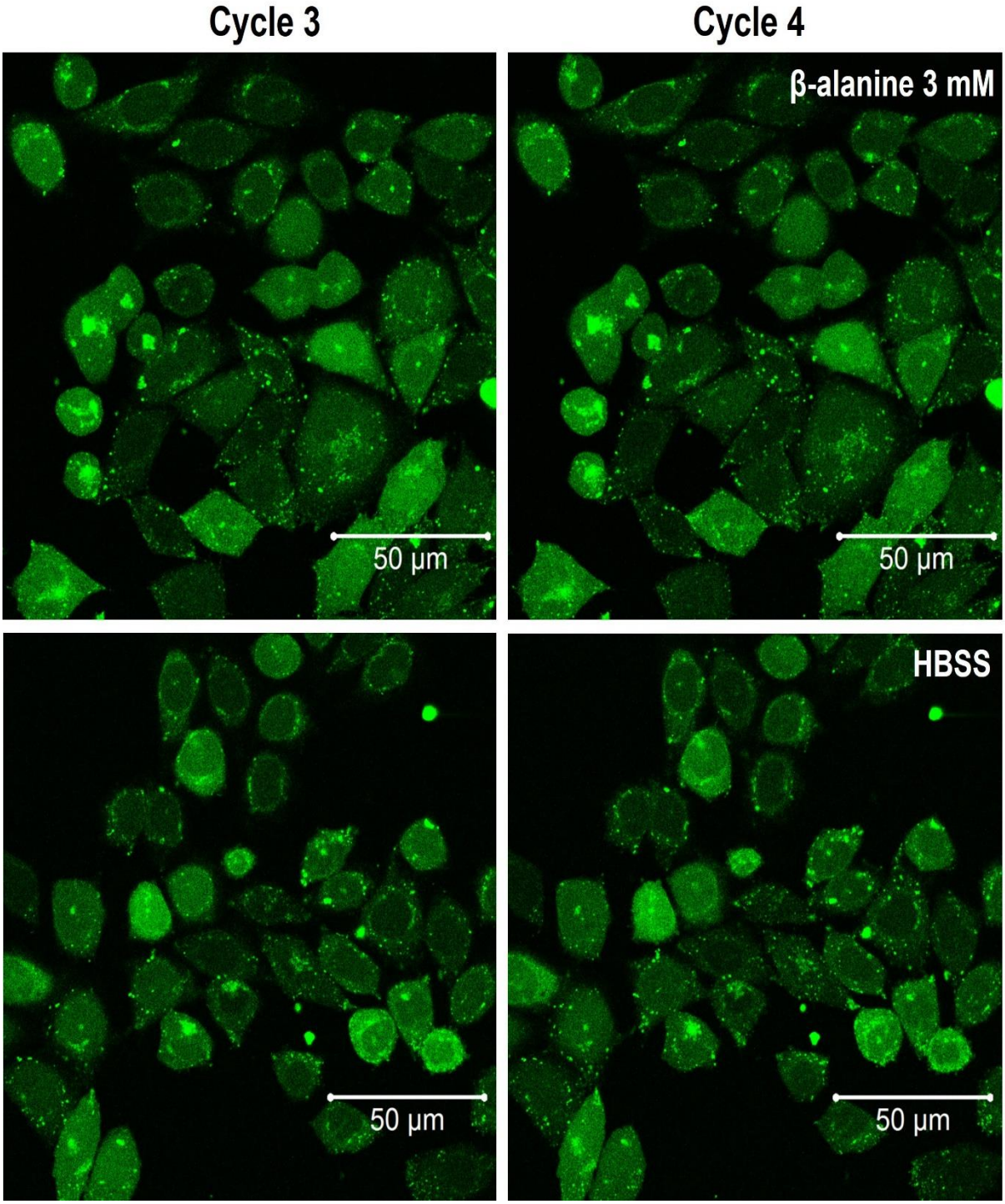

Figure 12: Photomicrographs of changes in intracellular Ca^{2+} levels after addition of β-alanine [3 mM] using the Fluo-4 Ca^{2+} sensitive dye in non-transfected CHO cells. The cells were incubated (37°C) with Fluo-4 AM loading solution for 30 min. At the 4th cycle, either β-alanine or HBSS were added to the cells. The images were taken under identical dyeing and recording conditions of 40x magnification, time series mode, 488 nm excitation wavelength, 492 nm beam splitter, and 2 % laser power on the confocal LSM using Zen 2012 software. Scale bar is 50 µm.

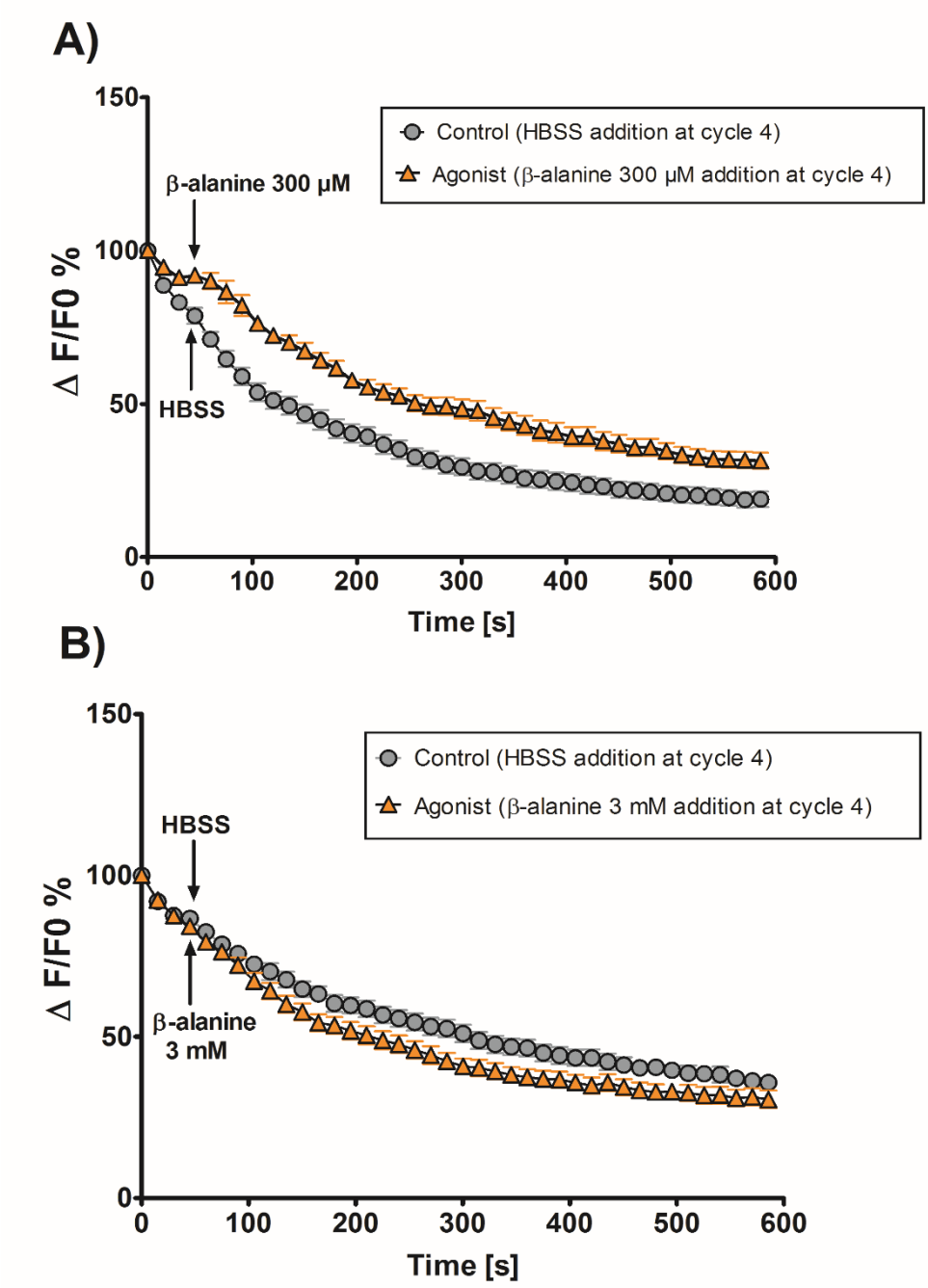

Figure 13: Graphical representation of the mean fluorescence intensity of Ca^{2+} mobilization in response to β-alanine [300 µM] (A), and β-alanine [3 mM] (B) in non-transfected CHO cells. The cells were incubated (37°C) with Fluo-4 AM loading solution for 30 min. At the 4th cycle, either β-alanine or HBSS was added to the cells. At least two coverslips with cells were examined (15 cells per field) for each treatment. Means ± SEM of 45 analyzed cells (β-alanine), and 30 analyzed cells (HBSS). Differences in mean fluorescence intensity in terms of "ΔF/F0 %" between cycle 3 (before addition) and cycles 4 to 10 (post addition) for each treatment were analyzed by paired two-tailed t-test.

Determination of the mean of ΔF/F30 % for each treatment and comparing to respective controls (HBSS) revealed a small increase in fluorescence of 1.1-fold (**p<0.01) by β-alanine [300 µM] which reflects the over-time delay in photobleaching, **(Table 13; Figure 13 A)**. No significant increases were found with β-alanine at [3 mM] concentration. Analyzing the mean ΔF/F30 % for β-alanine in CHO-hMrgD cells further approved graphical representation of Sargheini, (2017). Strong and concentration dependent increases in fluorescence by 3.1-fold (**p<0.01), 5.4-fold (***p<0.001), and 6.3-fold (***p<0.001), were elicited by β-alanine in concentrations of [300 µM], [1 mM], and [3 mM], respectively as compared to respective HBSS **(Table 13).**

Treatment	**CHO-hMrgD Pixel values (ΔF/F30 %)**		**Non-transfected CHO cells Pixel values (ΔF/F30 %)**	
	Mean ± SEM	**n**	**Mean ± SEM**	**n**
HBSS	115 ± 9.6	20	94.5 ± 1.7	30
β-Alanine [300 µM]	358.2 ± 69.9**	30	105.1 ± 2.5**	45
HBSS	101.7 ± 0.6	20	Not tested	
β-Alanine [1 mM]	552.3 ± 117.4***	20		
HBSS	103.6 ± 1.6	20	100.6 ± 1.6	30
β-Alanine [3 mM]	654.7 ± 71.2***	30	97 ± 1.2	45

Table 13: Mean fluorescent intensity of β-alanine-induced increases in intracellular Ca^{2+} levels in cloned CHO cells expressing a short variant of the hMrgD receptor and in non-transfected CHO cells. The cells were incubated (37°C) with Fluo-4 AM loading solution for 30 min. At the 4th cycle, either β-alanine [300 µM or 1 mM or 3 mM] or HBSS were added to the cells. At least two coverslips with cells were examined (10 or 15 cells per field) for each treatment. Pixel values are presented as a percentage of the fluorescence difference between the cycle with highest signal and the baseline cycle before treatment addition (cycle 3, corresponds to 30 s time point). Shown are means ± SEM for (n) cells analyzed. **p<0.01; ***p<0.001 significant differences from respective controls (HBSS). Unpaired two-tailed t-test.

4.2.1.2. Study of alamandine-induced changes in intracellular Ca^{2+} levels

Following establishment and proving the applicability of the Fluo-4 assay with our cell system, the peptide alamandine was tested**.** In CHO-hMrgD cells, addition of alamandine [10 µM] at the 4th cycle of the 40 cycles time series experiment, caused sudden small increases in the fluorescence intensity in some cells. The effect last only till the end of the cycle then disappeared **(Figures 14, and 16 A).** Similar increases were induced by alamandine in non-transfected CHO cells **(Figures 15, and 16 B).** HBSS treatment showed no signal changes in both cell lines. As the experiment runs, there was time-dependent bleaching of fluorescence signal. Once β-alanine [600 µM] was added at the 30th cycle of the experiment, strong fluorescence increases were observed in most of the cells of the field only in hMrgD stably transfected CHO cells **(Figure 14)**. In these cells, significant signal increases started at cycle 31, reached maximum at cycles 32, then started to gradually decrease till cycle 36 **(Figure 16 A).** In non-transfected CHO cells, both β-alanine [600 µM] and HBSS addition at the 30th cycle caused small responses which were not visually observed **(Figures 15, and 16 B)**.

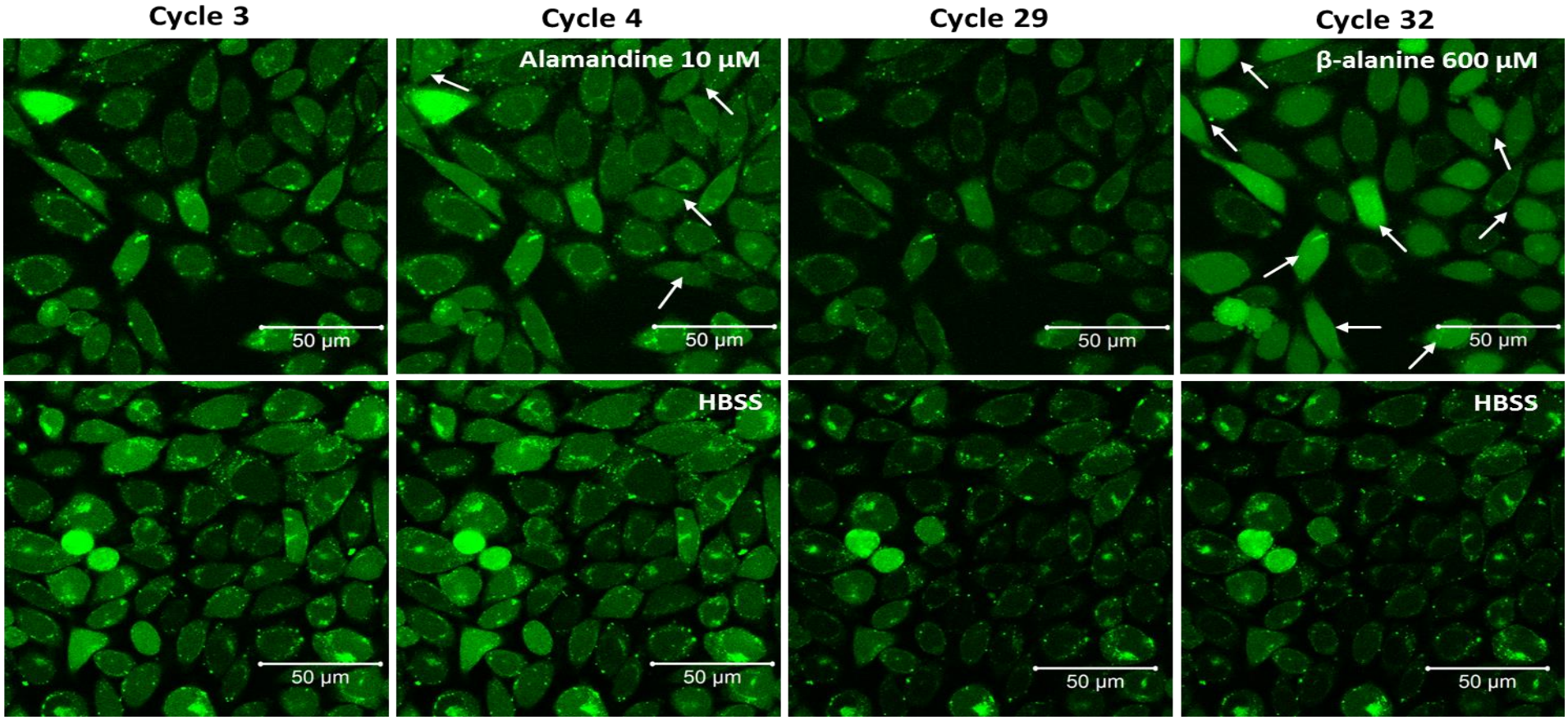

Figure 14: Photomicrographs of changes in intracellular Ca^{2+} levels in response to alamandine [10 µM] using the Fluo-4 Ca^{2+} sensitive dye in cloned CHO cells stably expressing a short variant of the hMrgD. The cells were incubated (37°C) with Fluo-4 AM loading solution for 30 min. At the 4th cycle, either alamandine or HBSS were added to the cells. This was followed by addition of β-alanine or HBSS at the 30th cycle. The images were taken under identical dyeing and recording conditions of 40x magnification, time series mode, 488 nm excitation wavelength, 492 nm beam splitter, and 2% laser power on the confocal LSM using Zen 2012 software. White arrows refer to cells with increases in fluorescence signal post treatment. Scale bar is 50 µm.

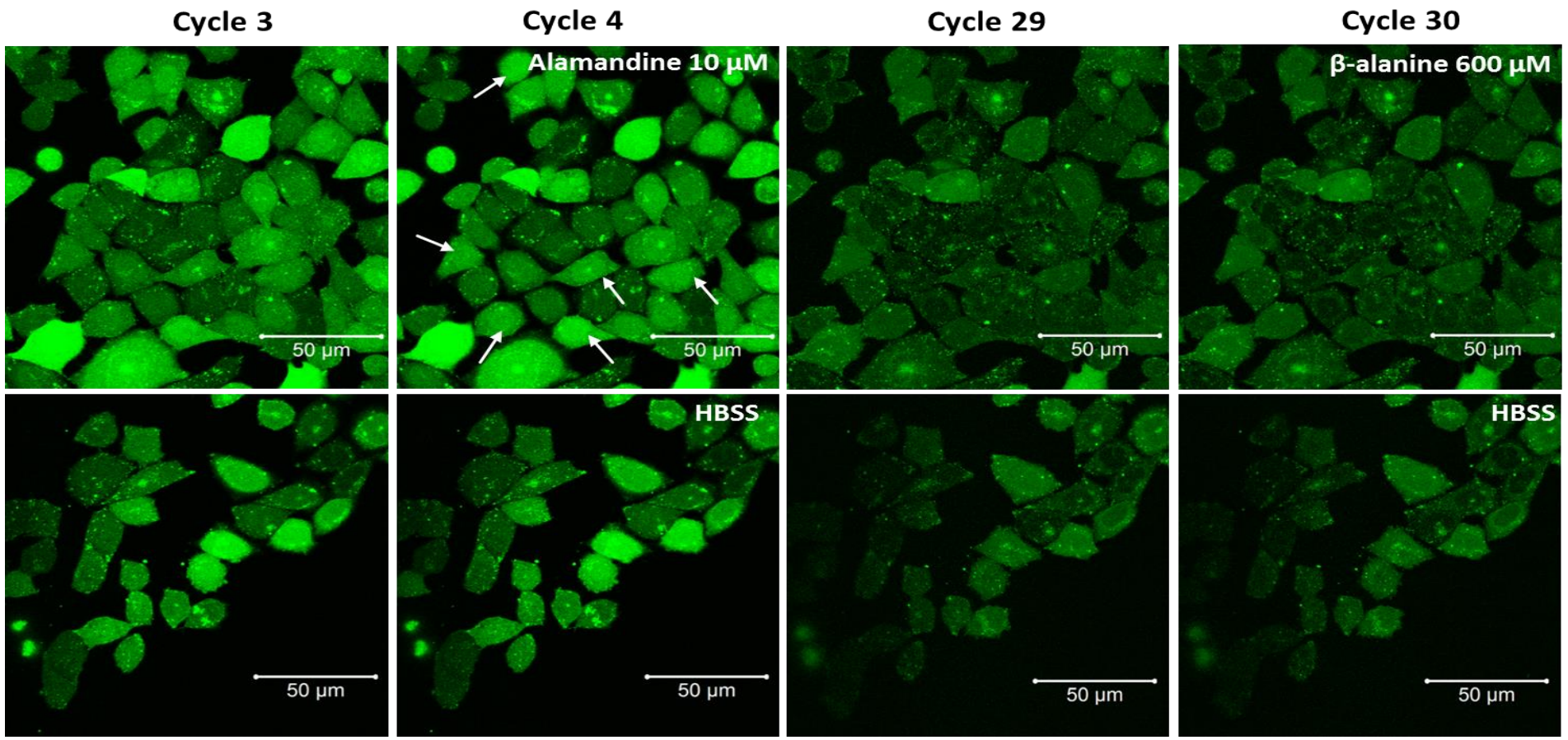

Figure 15: Photomicrographs of changes in intracellular Ca^{2+} levels in response to alamandine [10 µM] using the Fluo-4 Ca^{2+} sensitive dye in non-transfected CHO cells. The cells were incubated (37°C) with Fluo-4 AM loading solution for 30 min. At the 4th cycle, either alamandine or HBSS were added to the cells. This was followed by addition of β-alanine or HBSS at the 30th cycle. The images were taken under identical dyeing and recording conditions of 40x magnification, time series mode, 488 nm excitation wavelength, 492 nm beam splitter, and 2% laser power on the confocal LSM using Zen 2012 software. White arrows refer to cells with increases in fluorescence signal post treatment. Scale bar is 50 µm.

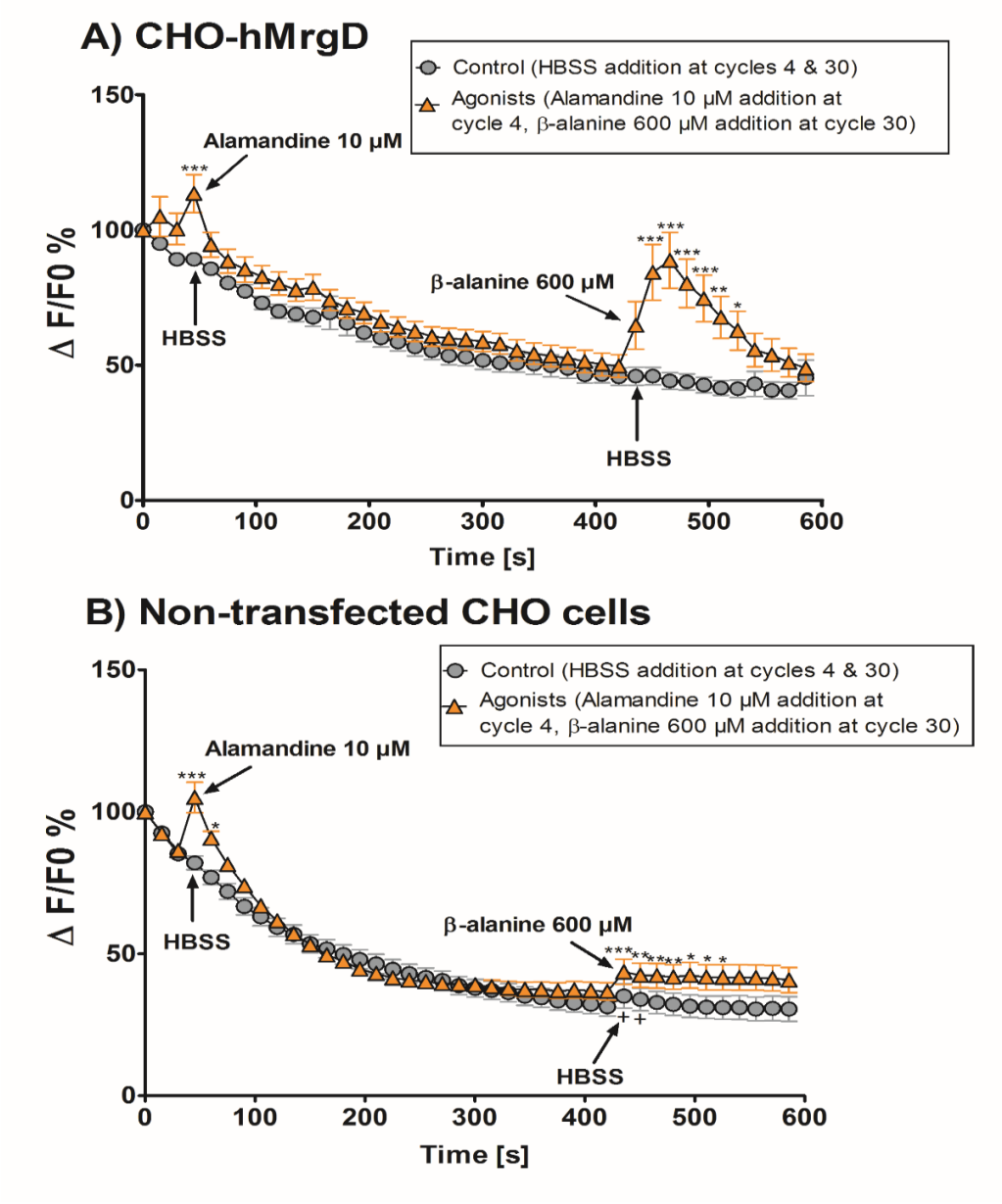

Figure 16: Graphical representation of the mean fluorescence intensity of Ca^{2+} mobilization in response to alamandine [10 µM] in cloned CHO cells stably expressing a short variant of the hMrgD (A) and in non-transfected CHO cells (B). The cells were incubated (37°C) with Fluo-4 AM loading solution for 30 min. At the 4th cycle, either alamandine or HBSS were added to the cells. This was followed by addition of β-alanine or HBSS at the 30th cycle. At least three coverslips with cells were examined (15 cells per field) for each treatment. Means ± SEM of 75 cells (alamandine), and 45 cells (HBSS). Differences in mean fluorescence intensity in terms of "ΔF/F0 %" between cycle 3 (before addition), and cycles 4 to 10 (post addition) for alamandine and HBSS, and between cycle 29 (before addition), and cycles 30 to 36 (post addition) for β-alanine and HBSS were analyzed by paired two-tailed t-test.

Comparing alamandine and β-alanine, each to their respective controls (HBSS) revealed significant fluorescence increases by 1.2-fold (**p<0.01), and 2.2-fold (***p<0.001), respectively, in CHO-hMrgD cells. In non-transfected CHO cells, alamandine significantly increased the signal by 1.3-fold (**p<0.01) over HBSS, however, β-alanine's response was significantly indifferent from that of HBSS **(Table 14)**.

Treatment	CHO-hMrgD Pixel values (ΔF/F30 %)		Non-transfected CHO cells Pixel values (ΔF/F30 %)	
	Mean ± SEM	**n**	**Mean ± SEM**	**n**
HBSS	101.4 ± 1.3	45	97.3 ± 2.2	45
Alamandine [10 µM]	117.7 ± 4.5**	75	122.2 ± 5.6**	75
Treatment	**CHO-hMrgD Pixel values (ΔF/F420 %)**		**Non-transfected CHO cells Pixel values (ΔF/F420 %)**	
	Mean ± SEM	**n**	**Mean ± SEM**	**n**
HBSS	105.5 ± 1.2	45	111.8 ± 3.7	45
β-Alanine [600 µM]	234.3 ± 23.4***	75	120.8 ± 4.1	75

Table 14: Mean Fluorescent intensity of alamandine-induced increases in intracellular Ca^{2+} levels in in CHO cells stably expressing a short variant of the hMrgD and in non-transfected CHO cells. The cells were incubated (37°C) with Fluo-4 AM loading solution for 30 min. At the 4th cycle, either alamandine or HBSS were added to the cells. This was followed by addition of β-alanine or HBSS at the 30^{th} cycle. At least three coverslips with cells were examined (15 cells per field) for each treatment. Pixel values are presented as a percentage of the fluorescence difference between the cycle with highest signal and the baseline cycle before treatment addition (cycle 3, corresponds to 30 s time point for alamandine; cycle 29, corresponds to 420 s time point for β-alanine). Shown are means ± SEM for (n) cells analyzed. **p<0.01; ***p<0.001 significant differences from respective controls (HBSS). Unpaired two-tailed t-test.

4.2.2. Experiments using AlphaScreen cAMP assay

4.2.2.1. Study of alamandine-induced changes in endogenous cAMP levels

To investigate the Gαi/s-dependent signaling pathway downstream of hMrgD receptor activation, endogenous cAMP levels were directly measured using the AlphaScreen cAMP assay. In cloned CHO cells stably expressing a short variant of the hMrgD receptor, alamandine [0.0001 nM to 10 nM] showed a bell-shaped concentration response curve with half maximal effective concentration (EC_{50}) of [0.0004 nM], and a half maximal inhibitory concentration (IC_{50}) of [0.2 nM] **(Figure 17 A)**. Alamandine maximally increased forskolin-induced increments in cAMP levels by 1.5-fold (*$p<0.05$) at [0.01 nM] concentration. Interestingly, in non-transfected CHO cells, alamandine [0.0001 nM to 1 nM] showed a similar pattern of response **(Figure 17 C)**. The bell-shaped curve has an EC_{50} of [0.0005 nM], and an IC_{50} of [0.04 nM]. In these cells, alamandine caused increases in cAMP levels by 2.4-fold (**$p<0.01$) and 3.1-fold (***$p<0.001$) over basal forskolin signal at [0.001 nM], and [0.01 nM] concentrations, respectively. On the other hand, β-alanine [300 µM] significantly inhibited forskolin-induced increases of cAMP by 2.6-fold (**$p<0.01$) only in CHO-hMrgD stably transfected cells **(Figure 17 B)**. The absolute basal and forskolin-induced cAMP values are represented in (**Table 15).**

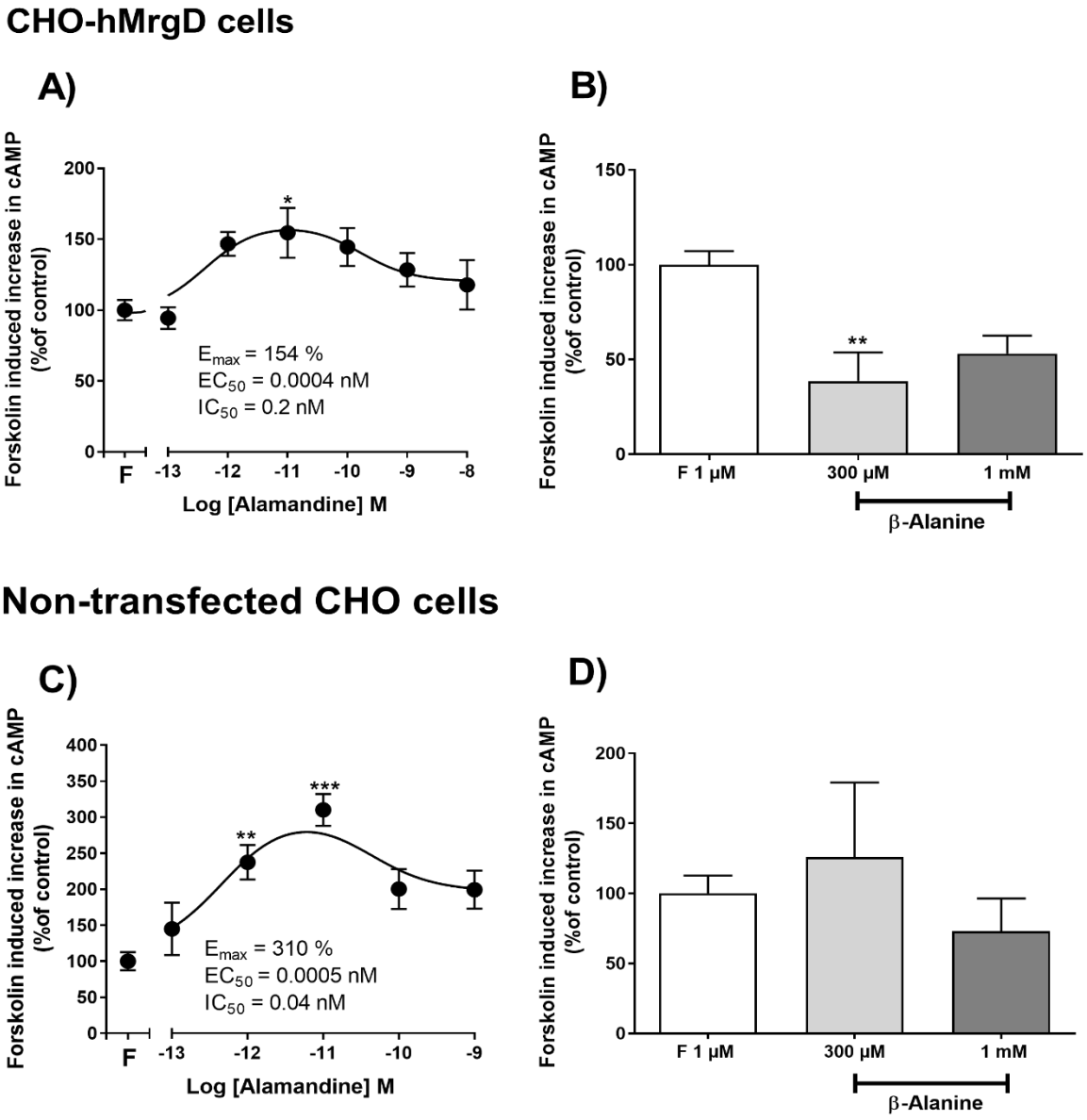

Figure 17: Cellular cAMP production in response to alamandine and β-alanine in cloned CHO cells stably expressing a short variant of the hMrgD receptor (A, and B) and in non-transfected CHO cells (C, and D). CHO cells were seeded in 24-well plates and incubated for 24 h. Cellular cAMP accumulation was induced by forskolin [1 µM] for 10 min. The data are presented as % of forskolin induced increase in cAMP (% of control, F; forskolin alone). Means ± SEM of 3-10 (CHO-hMrgD), 4-6 (non-transfected CHO) experiments. *p<0.05; **p<0.01; ***p<0.001, significant differences from respective control (F; Forskolin alone). ANOVA followed by Bonferroni post-hoc test.

Cell line	cAMP levels [nM/well]	
	HBSS	Forskolin [1 µM]
CHO-hMrgD	1.3 ± 0.1 (10)	4.1 ± 0.6 *** (10)
Non-transfected CHO cells	0.8 ± 0.1 (6)	1.1 ± 0.1 (6)

Table 15: Basal and forskolin-induced cAMP levels in experiments where alamandine and β-alanine were tested in cloned CHO cells stably expressing the hMrgD receptor and in non-transfected CHO cells. The cAMP levels are given as absolute concentration per well. Shown are means ± SEM for (n) wells analyzed. ***p<0.001 significant difference from respective control (HBSS). Unpaired two-tailed t-test.

4.3. Investigation of the coupling of the hMrgD to the β-arrestin pathway

4.3.1. Study of β-alanine-induced activation and recruitment of β-arrestin

For assay establishment and validation, β-alanine was tested in concentrations of [0,3 µM to 1 mM] in CHO-K1 cells stably co-expressing the hMrgD and β-arrestin-2. Following 90 min of incubation, β-alanine caused concentration-dependent increases in the recruitment of β-arrestin-2 to the activated receptor. The concentration-response curve has a maximal effect of 3.9-fold increase in response above basal. β-Alanine at concentration of [79.4 µM] induced increase in RLUs by 100% over basal **(Figure 18).**

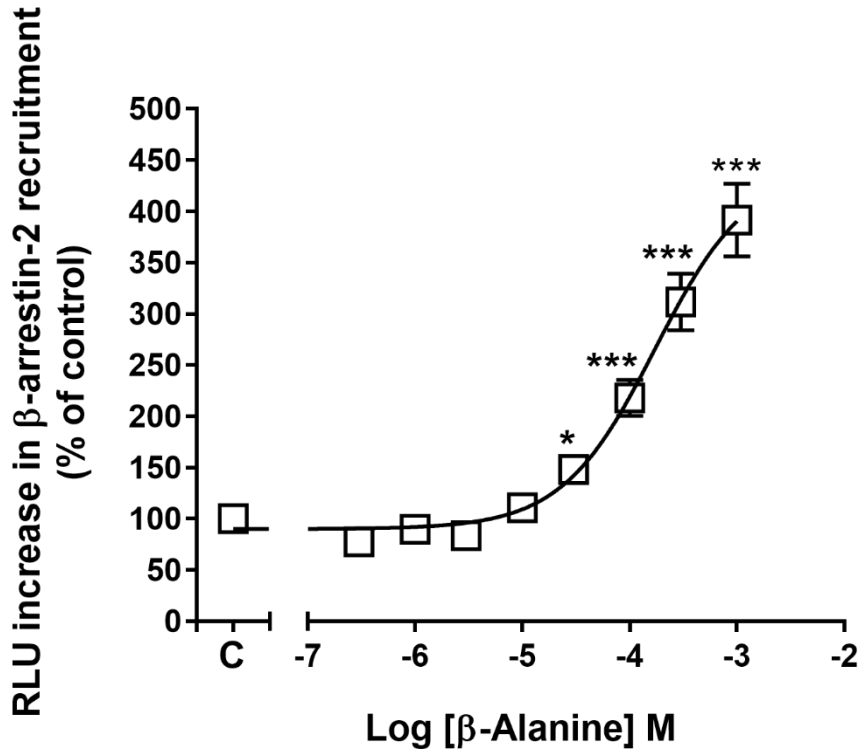

Figure 18: Concentration-response curve of β-alanine-induced receptor activation and recruitment of β-arrestin-2 in CHO-K1 cells stably co-expressing the hMrgD and β-arrestin-2. CHO-K1 cells were seeded in 96-well plates. After 48 h, agonists or solvent were added and incubated at 37°C for 90 min. A PathHunter detection mixture was then added and incubated at R.T. for 1 h followed by measuring RLUs using a luminometer. The data are presented as % of basal control (C, solvent). Means ± SEM of 10-22 experiments. *p<0.05; **p<0.01; ***p<0.001, significant differences from respective control (C, solvent). ANOVA followed by Bonferroni post-hoc test.

4.3.2. Study of alamandine-induced activation and recruitment of β-arrestin

A wide concentration range [0.00001 nM to 100 µM] of alamandine was tested. Following 90 min of incubation, alamandine caused only a weak response of 1.3-fold (*p<0.05) signal increase above basal at the [0.1 nM] concentration **(Figure 19)**. This is unlike the strong signal increases of 1.9-fold (***p<0.001), and 2.5-fold (***p<0.001), above basal elicited by [100 µM], and [300 µM] concentrations of β-alanine, respectively **(Figure 19).**

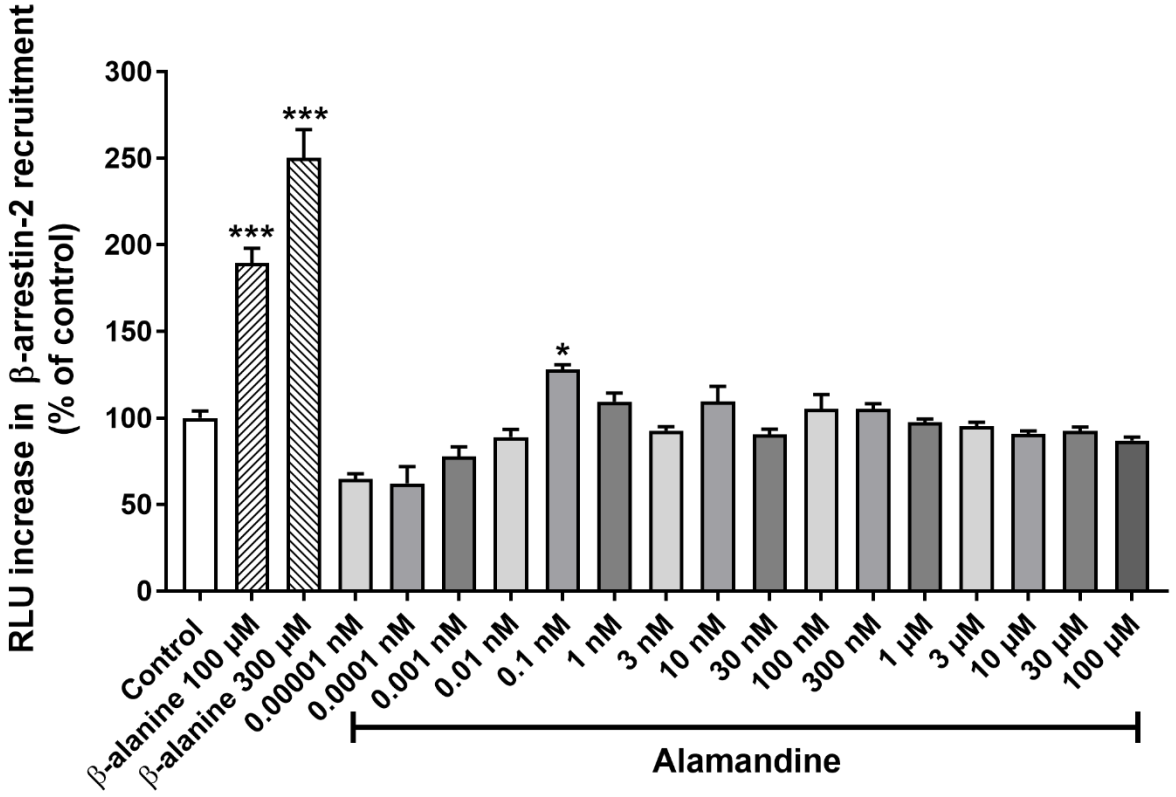

Figure 19: β-Arrestin activation and recruitment in response to alamandine in CHO-K1 cells stably co-expressing the hMrgD and β-arrestin-2. CHO cells were seeded in 96-well plates. After 48 h, agonists or solvent were added and incubated at 37°C for 90 min. A PathHunter detection mixture was then added and incubated at R.T. for 1 h followed by measuring RLUs using a luminometer. The data are presented as % of respective control (HBSS). Means ± SEM of 5-38 experiments. *p<0.05, ***p<0.001, significant differences from respective control (HBSS). ANOVA followed by Bonferroni post-hoc test.

To ensure that interaction kinetics are not responsible for such low signal, alamandine [0.001 nM to 1 µM] was tested following shorter (60 min) and longer (120 min) incubation periods with CHO cells co-expressing the hMrgD and β-arrestin-2. At both incubation periods, alamandine completely failed to elicit a response **(Table 16).** Despite keeping significances, the β-alanine signals at 60 min and 120 min were 2.1-fold and 1.8-fold lower as compared to the 90 min incubation, respectively **(Table 17).** This also approves the parameters set by the kit data sheet where 90 min of agonist incubation should be used for the best signal.

Treatment	RLU (% of basal control)			
	60 min incubation		120 min incubation	
	Mean ± SEM	n	Mean ± SEM	n
Control (HBSS)	100 ± 0.5	8	100 ± 1.3	8
β-Alanine 300 µM	115.4 ± 1.2***	4	144.9 ± 2.6***	4
Alamandine 0,001 nM	104.9 ± 0.1	4	99.28 ± 1.4	4
Alamandine 0,01 nM	96.6 ± 4.4	4	102.9 ± 2.1	4
Alamandine 0,1 nM	104.9 ± 2	4	98 ± 1.9	4
Alamandine 1 nM	95.9 ± 0.9	4	99.5 ± 1.3	4
Alamandine 3 nM	95.9 ± 2.2	4	103.1 ± 1.8	4
Alamandine 10 nM	96.1 ± 3.4	4	99 ± 1.9	4
Alamandine 30 nM	96.6 ± 0.4	4	94 ± 0.8	4
Alamandine 100 nM	93.4 ± 3.6	4	96.2 ± 2.5	4
Alamandine 1 µM	89.4 ± 2.4	4	93.4 ± 1.3	4

Table 16: Effect of β-alanine and alamandine on β-arrestin-activation and recruitment following 60 min and 120 min of incubation with CHO-K1 cells stably co-expressing the hMrgD and β-arrestin-2. The RLU values are presented as % of basal control (HBSS). Shown are mean ± standard errors of n experiments. ***$p<0.001$, significant differences from respective control (HBSS). ANOVA followed by Bonferroni post-hoc test.

Incubation time	RLU levels		
	HBSS	β-Alanine [300 µM]	Fold change
60 min	4389 ± 22.3 (8)	5064 ± 52.6*** (4)	1.2
90 min	954 ± 45.8 (38)	2397 ± 92.6*** (24)	2.5
120 min	3556 ± 44.7 (8)	5153 ± 93.5*** (4)	1.4

Table 17: Basal and β-alanine-induced increases in RLU levels in CHO-K1 cells stably co-expressing the hMrgD and β-arrestin-2 following 60 min, 90 min, and 120 min of incubation. Data are given as absolute RLU values. Shown are means ± SEM for (n) experiments. ***p<0.001, significant differences from respective controls (HBSS). Unpaired two-tailed t-test.

4.3.3. Study of angiotensin 1-7-induced activation and recruitment of β-arrestin.

The peptide angiotensin 1-7 was examined in the present work using this assay. Following 90 min of incubation with CHO-K1 cells stably co-expressing the hMrgD and β-arrestin-2, angiotensin 1-7 [0,001 nM to 1 µM] was not able to stimulate any response different from control **(Figure 20).** β-alanine [300 µM] was examined in parallel as a positive control and strongly induced a 2.8-fold signal increase **(Figure 20).**

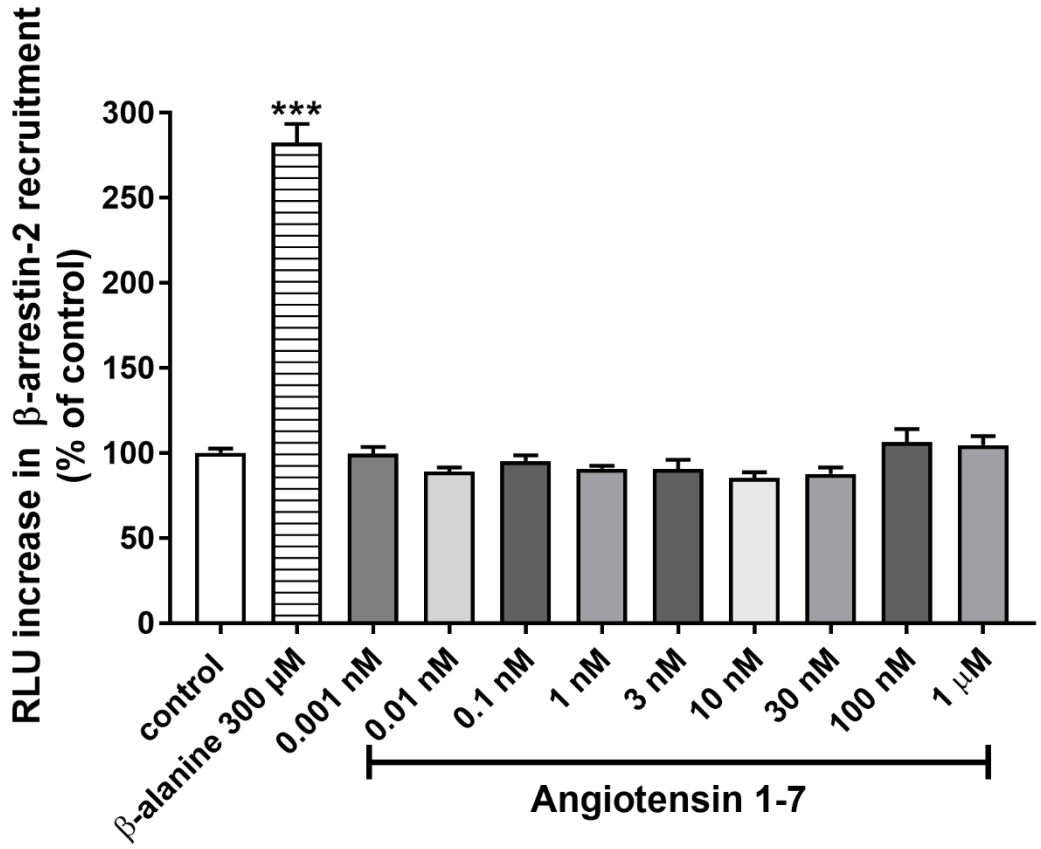

Figure 20: β-Arrestin activation and recruitment in response to angiotensin 1-7 in CHO-K1 cells stably co-expressing the hMrgD and β-arrestin-2. CHO cells were seeded in 96-well plates. After 48 h, agonists or solvent were added and incubated at 37°C for 90 min. A PathHunter detection mixture was then added and incubated at R.T. for 1 h followed by measuring RLUs using a luminometer. The data are presented as % of respective control (HBSS). Means ± SEM of 10-22 experiments. ***p<0.001, significant difference from respective control (HBSS). ANOVA followed by Bonferroni post-hoc test.

4.3.4. Study of small molecules-induced activation and recruitment of β-arrestin

Structural analogues of β-alanine which showed potential agonistic activity at the hMrgD receptor according to Müller (2014), were further investigated in this work for their β-arrestin recruitment potential in CHO-K1 cells stably co-expressing the hMrgD and β-arrestin-2. The concentration-response curves of DL-3-aminoisobutyric acid [1 µM to 3 mM], DL-3-aminobutyric acid [10 µM to 3 mM] and GABA [3 µM to 3 mM] are presented in **(Figure 21).** All tested molecules showed concentration-dependent increases in β-arrestin activation and recruitment**.** Compared to β-alanine, the concentration-response curve of DL-3-

aminoisobutyric acid was slightly shifted to the right with a statistically indistinguishable maximal response at [3 mM] (**p<0.01, F-test). The concentration-response curves of 3-aminobutyric acid and GABA were markedly shifted to the right with the maximal effect could not be reached, therefore, EC_{50} values could not be estimated. While β-alanine has doubled the basal response at [79.4 µM], 3-aminoisobutyric acid, 3-aminobutyric acid, and GABA induced a similar response at [234.4 µM], [724.4 µM], and [1.2 mM], respectively.

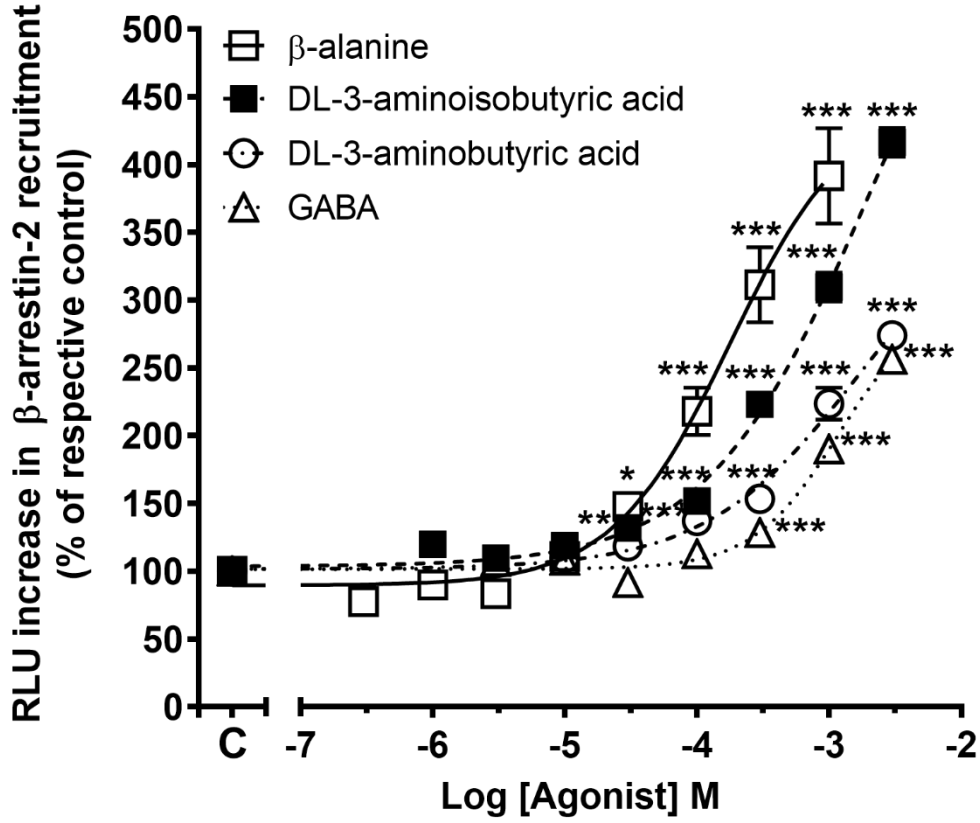

Figure 21: Concentration-response curves of β-alanine and structural analogues-induced activation and recruitment of β-arrestin in CHO-K1 cells stably co-expressing the hMrgD and β-arrestin-2. CHO cells were seeded in 96-well plates. After 48 h, agonists or solvent were added and incubated at 37°C for 90 min. A PathHunter detection mixture was then added and incubated at R.T. for 1 h followed by measuring RLUs using a luminometer. The data are presented as % of respective control (C, HBSS). Means ± SEM of 10-22 (β-alanine), 5-22 (DL-3-aminoisobutyric acid), 10-22 (DL-3-aminobutyric acid), 10-22 (GABA) experiments. *p<0.05; **p<0.01; ***p<0.001, significant differences from respective control (C, HBSS). ANOVA followed by Bonferroni post-hoc test.

The small dipeptide "L-carnosine" was tested for its β-arrestin recruitment potential in this work at concentrations of [10 µM, 100 µM, and 1 mM]. Unlike β-alanine [300 µM] which

activated the receptor and recruited β-arrestin, none of the tested concentrations of L-carnosine induced a response **(Figure 22).**

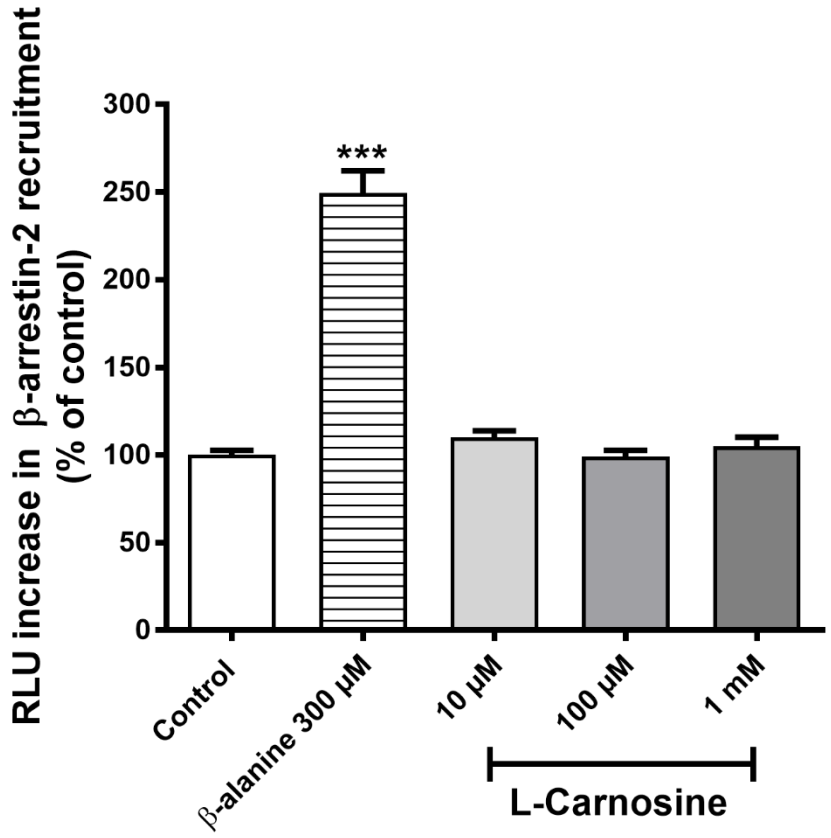

Figure 22: β-Arrestin activation and recruitment in response to L-carnosine in CHO-K1 cells stably co-expressing the hMrgD and β-arrestin-2. CHO cells were seeded in 96-well plates. After 48 h, Agonist or solvent was added and incubated at 37°C for 90 min. A PathHunter detection mixture was then added and incubated at R.T. for 1 h followed by measuring RLUs using a luminometer. The data are presented as % of basal control (HBSS). Means ± SEM of 10-22 experiments. ***p<0.001, significant difference from respective control (HBSS). ANOVA followed by Bonferroni post-hoc test.

4.4. Investigation of 5-Oxo-ETE activity at the hMrgD receptor

4.4.1. Experiments using NFAT-luciferase reporter gene assay

In cloned CHO cells stably expressing a short variant of the hMrgD receptor, the polyunsaturated keto acid "5-Oxo-ETE" [0.1 µM, 0.3 µM, and 1 µM] stimulated a weak response of 1.2-fold (*p<0.05) signal increase over respective basal control at [1 µM] concentration **(Figure 23 A)**. In these cells, β-alanine [300 µM] highly accelerated luciferase expression resulting in a 2.8-fold (***p<0.001) signal increase over respective basal control **(Figure 23 A)**. In non-transfected CHO cells, neither β-alanine nor 5-Oxo-ETE elicited a

response **(Figure 23 B)**. Effects of higher concentrations of 5-Oxo-ETE could not be estimated due to the toxic effects of the solvent EtOH on the cells. Increasing the percentage of EtOH above 0.33 % resulted in death of cells as visually observed under the microscope. In the presence of 3.3 % EtOH, the basal RLU values were decreased by 1.4-fold (***p<0.001), and 1.2-fold over basal HBSS levels in hMrgD-transfected and in non-transfected CHO cells, respectively **(Table 18).**

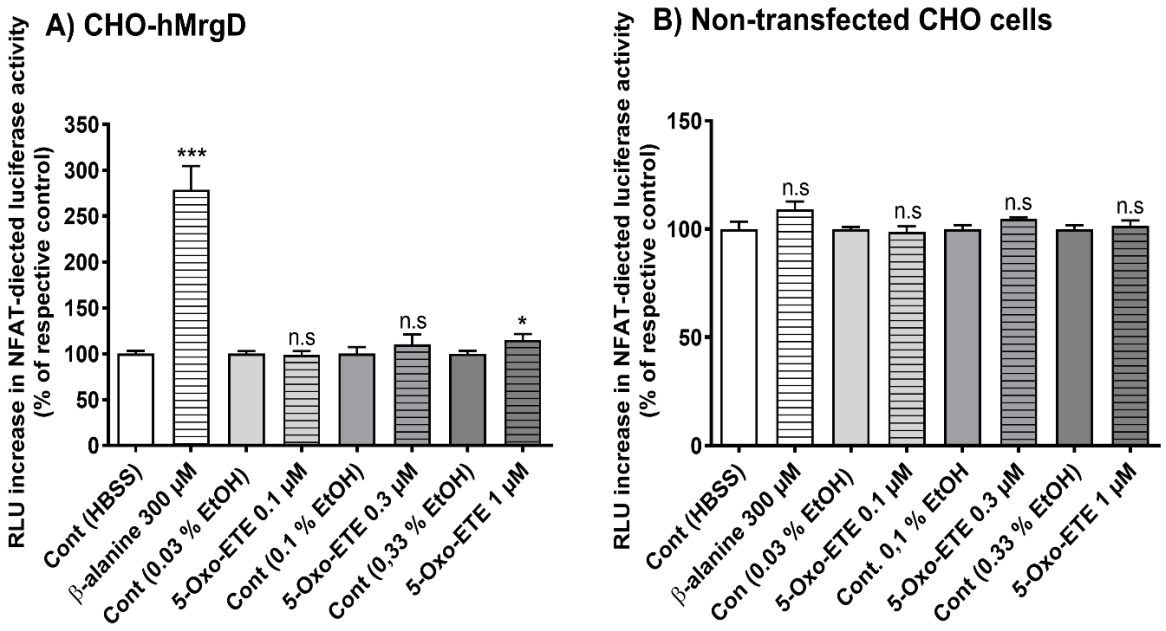

Figure 23: NFAT-directed luciferase activity of 5-Oxo-ETE tested in cloned CHO cells stably expressing a short variant of the hMrgD (A) and in non-transfected CHO cells (B). CHO cells were incubated with agonists or solvents for 3.5 h. The RLU values are presented as % of the increase in basal luciferase activity (% of respective controls; HBSS for β-alanine or 0.03 %, 0.1 %, and 0.33 % of EtOH in HBSS for [0.1 µM], [0.3 µM], and [1 µM] of 5-oxoETE, respectively). Means ± SEM of 3-10 experiments each. *p<0.05, ***p<0.001, significant differences from respective control (HBSS for β-alanine or 0.03 %, 0.1 %, and 0.33 % of EtOH in HBSS for [0.1 µM], [0.3 µM], and [1 µM] of 5-Oxo-ETE, respectively). Unpaired two-tailed t-test.

Treatment	RLU levels (% of basal HBSS)	
	CHO-hMrgD	**Non-transfected CHO cells**
Control (HBSS)	100 ± 3 (9)	100 ± 3.4 (9)
Control (0.03 % ETOH)	104.3 ± 3.1 (6)	100 ± 5.6 (6)
Control (0.1 % ETOH)	97.7 ± 6.9 (3)	87.9 ± 1.7 (3)
Control (0.33 % ETOH)	104.2 ± 4 (9)	106 ± 6.1 (9)
Control (1 % ETOH)	109.6 ± 7.7 (3)	93.6 ± 4.1 (3)
Control (3.3 % ETOH)	70.5 ± 3*** (6)	81 ± 5.1 (6)

Table 18: Basal RLU levels of different controls in NFAT-luciferase experiments where 5-Oxo-ETE was tested. Data are given as RLU values in % of basal HBSS. Shown are means ± SEM for (n) experiments. ***p<0.001, significant difference from respective control (HBSS). ANOVA followed by Bonferroni post-hoc test.

4.4.2. Experiments using PathHunter β-arrestin recruitment assay

After observing a small response in the NFAT-luciferase assay at [1 µM] in CHO cells stably expressing a short variant of the hMrgD receptor, 5-Oxo-ETE was further tested using the β-arrestin assay at similar concentrations of [0,1 µM, 0,3 µM, and 1 µM]. As compared to respective controls, none of the tested concentrations caused a significant response **(Figure 24).** In parallel wells, β-alanine [300 µM] caused a 2.5-fold (***p<0.001) signal increase **(Figure 24).** No lowering in basal control levels was observed in well having up to 0.33 % EtOH as compared to HBSS wells **(Table 19).**

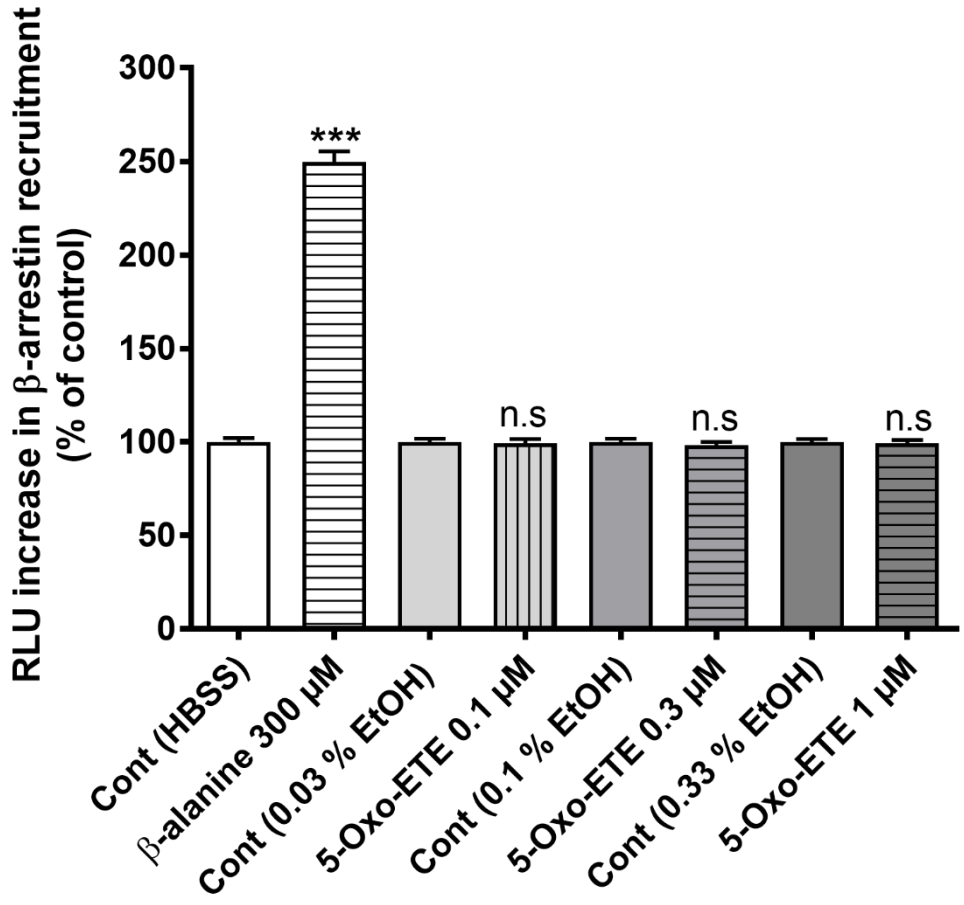

Figure 24: β-Arrestin activation and recruitment in response to 5-Oxo-ETE in CHO-K1 cells stably co-expressing the hMrgD and β-arrestin-2. CHO cells were seeded in 96-well plates. After 48 h, agonist or solvent was added and incubated at 37°C for 90 min. A PathHunter detection mixture was then added and incubated at R.T. for 1 h followed by measuring RLUs using a luminometer. The data are presented as % of basal control (HBSS for β-alanine or 0.03 %, 0.1 %, and 0.33 % EtOH in HBSS for [0.1 µM], [0.3 µM], and [1 µM] of 5-Oxo-ETE, respectively). Means ± SEM of 12 experiments. n.s. means no significance. ***$p<0.001$, significant difference from respective control (HBSS for β-alanine or 0.03 %, 0.1 %, and 0.33 % of EtOH in HBSS for [0.1 µM], [0.3 µM], and [1 µM] of 5-Oxo-ETE, respectively). Unpaired two-tailed t-test.

Treatment	RLU levels (% of basal HBSS)
	CHO-hMrgD-β-arrestin-2 cells
Control (HBSS)	100 ± 2 (12)
Control (0.03 % ETOH)	108.9 ± 1.9** (12)
Control (0.1 % ETOH)	102 ± 1.7 (12)
Control (0.33 % ETOH)	103.5 ± 1.6 (12)

Table 19: Basal RLU levels of different controls in β-arrestin recruitment experiments where 5-Oxo-ETE was tested. Data are given as RLU values in % of respective basal HBSS. Shown are means ± SEM for (n) experiments. **p<0.01, significant difference from respective control (HBSS). ANOVA followed by Bonferroni post-hoc test.

4.5. Investigation of potential antagonists at the hMrgD receptor

4.5.1. Interactions using NFAT-luciferase reporter gene assay

The NFAT-directed luciferase activities of four amino acids "L-lysine, D-(+)-3-phenyllactic acid, D-phenylalanine and D-tryptophan" at [1 mM] concentrations were tested in cloned CHO cells stably expressing a short variant of the hMrgD receptor. Compared to basal control, β-alanine [1 mM] significantly increased the NFAT-directed luciferase expression by 1.5-fold (***p<0.001) **(Figure 25 A)**. Among tested amino acids, D-(+)-3-phenyllactic acid and D-phenylalanine significantly lowered the RLU signal each by 1.3-fold (**p<0.01; *p<0.05, respectively) over basal **(Figure 25 A).** These two amino acids were then chosen for testing their inhibitory actions on β-alanine's stimulatory signal. In antagonism experiments, D-(+)-3-phenyllactic acid [1 mM] significantly inhibited the RLU signal by 1.3-fold (**p<0.01) over the β-alanine induced signal **(Figure 25 B).** Basal RLU values of the amino acids are shown in **(Table 20).**

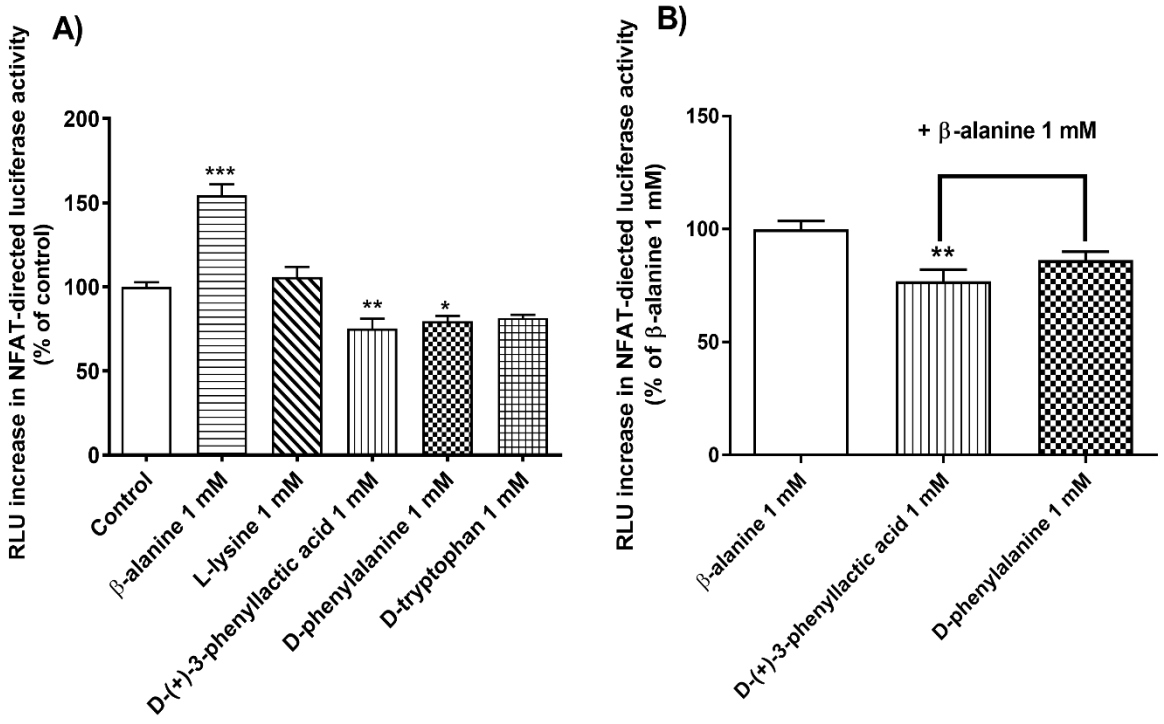

Figure 25: (A) The NFAT-directed luciferase activity of β-alanine, and other amino acids (L-lysine, D-(+)-3-phenyllactic acid, D-phenylalanine, and D-tryptophan) in cloned CHO cells stably expressing a short variant of the hMrgD. (B) Inhibition of NFAT-directed luciferase activity induced by β-alanine upon pre-treatment with D-(+)-3-phenyllactic acid. CHO cells were incubated with β-alanine or amino acids for 3.5 h. In antagonism experiment, cells were pre-incubated for 20 min with the amino acid followed by β-alanine addition. The RLU values are presented as % of basal control (Control, solvent, A; β-alanine [1 mM], B). Mean ± SEM of 4 (A), 4 (B) experiments. *p<0,05; **p<0,01; ***p<0.001, significant differences from respective control (Control, solvent, A; β-alanine [1 mM], B). ANOVA followed by Bonferroni post-hoc test.

Treatment	RLU levels
	CHO-hMrgD
Control (HBSS)	5436 ± 150.6 (4)
β-alanine [1 mM]	8403 ± 350.6***(4)
L-lysine [1 mM]	5752 ± 331.3 (4)
D-(+)-3-phenyllactic acid [1 mM]	4089 ± 314.5**(4)
D-phenylalanine [1 mM]	4324 ± 169.3*(4)
D-tryptophan [1 mM]	4432 ± 101.4 (4)

Table 20: Basal RLU levels of amino acids tested in NFAT-luciferase reporter gene assays. Data are given as absolute RLU values. Shown are means ± SEM for (n) experiments. *p<0,05; **p<0,01; ***p<0.001, significant differences from respective control (HBSS). ANOVA followed by Bonferroni post-hoc test.

4.5.2. Interactions using β-arrestin recruitment assay

In this section we present the results of some previously identified MrgD antagonists on their potential to inhibit β-alanine-induced activation of hMrgD and recruitment of β-arrestin.

4.5.2.1. Interaction with rimcazole

In CHO cells co-expressing the hMrgD and β-arrestin-2, β-alanine [0.3 µM to 1 mM] caused concentration-dependent recruitment of β-arrestin-2 with a maximal signal increase of 2.2-fold (***p<0.001) **(Figure 26)**. Interestingly, addition of the σ-receptor antagonist "rimcazole [20 µM]" showed a concentration-response curve that is not different (F-test) from that of β-alanine alone with undistinguishable maximal effect **(Figure 26)**. Signal increase of 100% over basal was achieved by β-alanine at [524.8 µM] and [436.5 µM] in absence and in

presence of rimcazole, respectively **(Figure 26).** Rimcazole [20 µM] alone has no significant influence on basal RLU levels **(Table 21).**

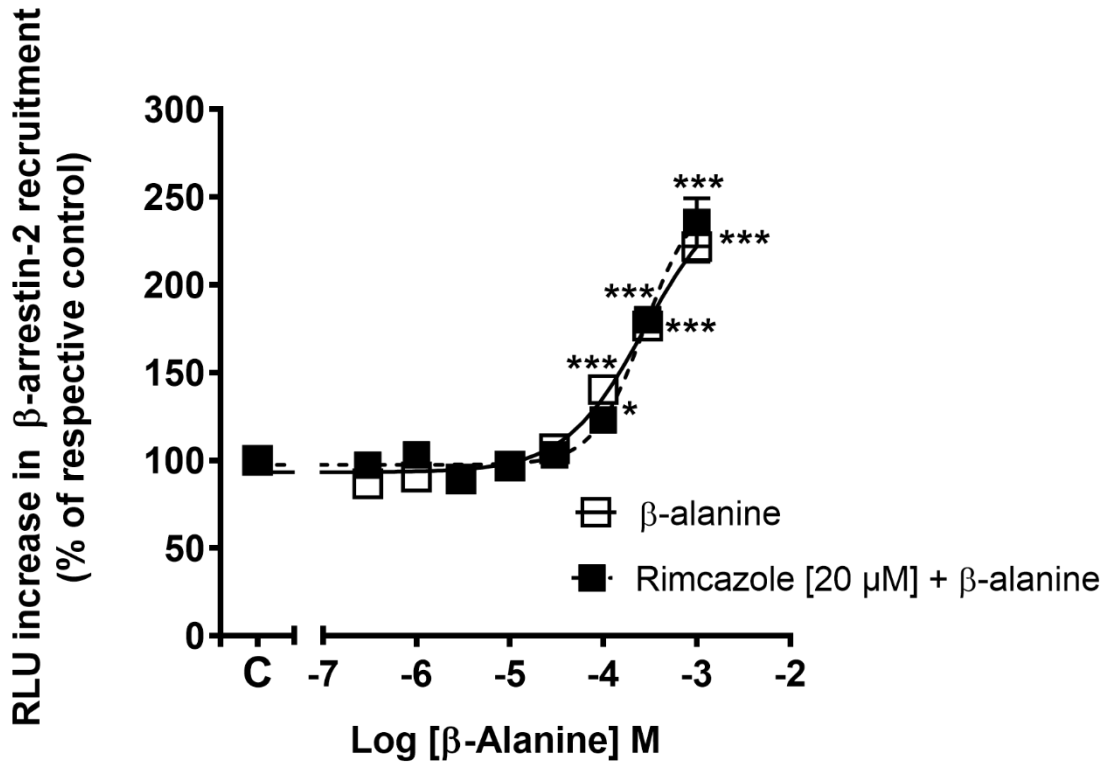

Figure 26: Concentration-response curves of β-alanine-induced activation and recruitment of β-arrestin in the presence and absence of rimcazole in CHO cells co-expressing the hMrgD and β-arrestin-2. CHO cells were seeded in 96-well plates. After 48 h, rimcazole [20 µM] or solvent was added and incubated at 37°C for 30 min. β-alanine or solvent was then given and further incubated at 37°C for 90 min. A PathHunter detection mixture was then added and incubated at R.T. for 1 h followed by measuring RLUs using a luminometer. The data are presented as % of basal control (C, HBSS for solid curve or rimcazole for dashed curve). Means ± SEM of 10-24 experiments. *$p<0.05$; ***$p<0.001$, significant differences from respective control (C, HBSS for solid curve or rimcazole for dashed curve). ANOVA followed by Bonferroni post-hoc test.

4.5.2.2. Interaction with chlorpromazine

In these set of experiments, β-alanine [0.3 µM to 1 mM] caused concentration-dependent increases in the activation and recruitment of β-arrestin-2 with a 2.3-fold maximal signal increase above basal **(Figure 27).** As with rimcazole, addition of the antipsychotic chlorpromazine [10 µM] did not inhibit β-alanine's stimulatory response. The concentration-response was not significantly different (F-test) from that of β-alanine with a statistically

indistinguishable maximal effect **(Figure 27)**. β-Alanine in absence and in presence of chlorpromazine, caused signal increase over basal by 100% at [501.2 µM] and [537 µM], respectively **(Figure 27).** Chlorpromazine [10 µM] alone did not cause significant changes in the basal RLU levels **(Table 21).**

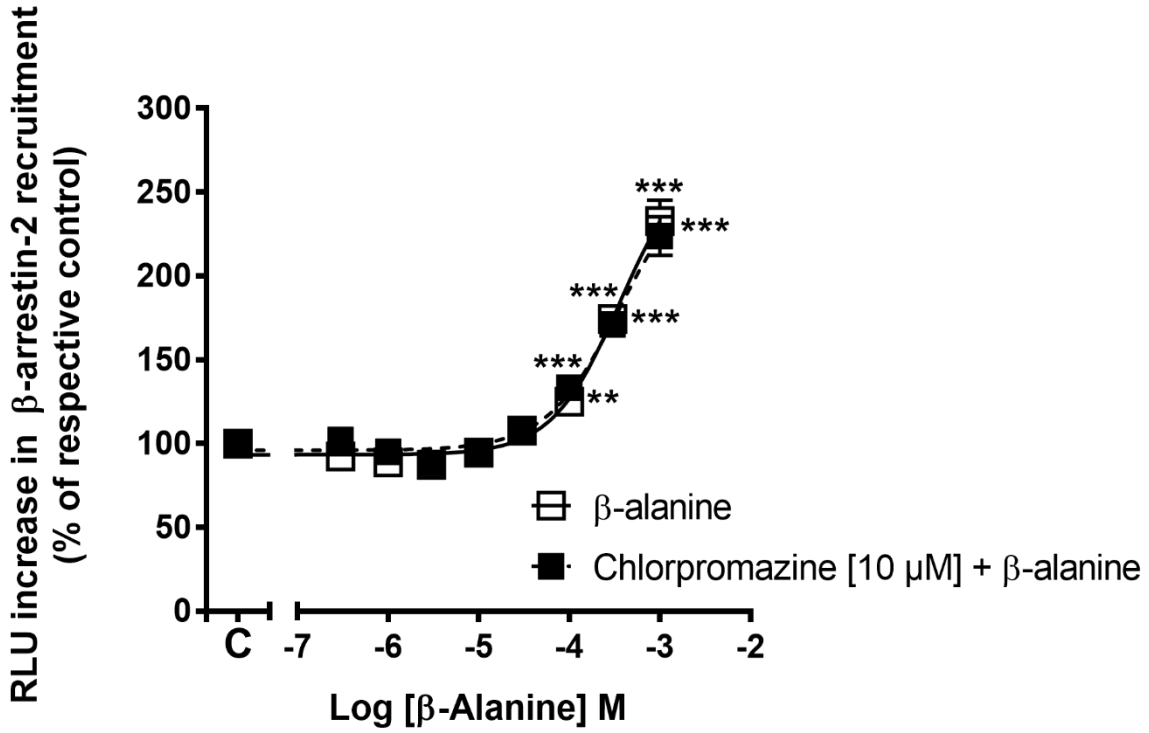

Figure 27: Concentration-response curves of β-alanine-induced activation and recruitment of β-arrestin in the presence and absence of chlorpromazine in CHO cells co-expressing the hMrgD and β-arrestin-2. CHO cells were seeded in 96-well plates. After 48 h, chlorpromazine [10 µM] or solvent was added and incubated at 37°C for 30 min. β-alanine or solvent was then given and further incubated at 37°C for 90 min. A PathHunter detection mixture was then added and incubated at R.T. for 1 h followed by measuring RLUs using a luminometer. The data are presented as % of basal control (C, HBSS for solid curve or chlorpromazine for dashed curve). Means ± SEM of 10-16 experiments. **p<0.01; ***p<0.001, significant differences from respective control (C, HBSS for solid curve or chlorpromazine for dashed curve). ANOVA followed by Bonferroni post-hoc test.

4.5.2.3. Interaction with thioridazine

In these analyses, β-alanine [0.3 µM to 1 mM] caused concentration-dependent increases in the activation and recruitment of β-arrestin-2 with a 2.4-fold maximal signal increase above basal **(Figure 28).** Addition of the antipsychotic thioridazine [10 µM] did not show antagonizing potential. However, intriguingly, thioridazine [10 µM] significantly shifted

(*p<0.05, F-test) the concentration-response curve of β-alanine to the left with a non-statistically different maximal response **(Figure 28).** In these set of experiments, β-alanine in absence and in presence of thioridazine induced doubling of the basal signal at [446.7 µM] and [251.2 µM], respectively **(Figure 28)**. Thioridazine [10 µM] alone caused no significant changes in the basal RLU levels **(Table 21).**

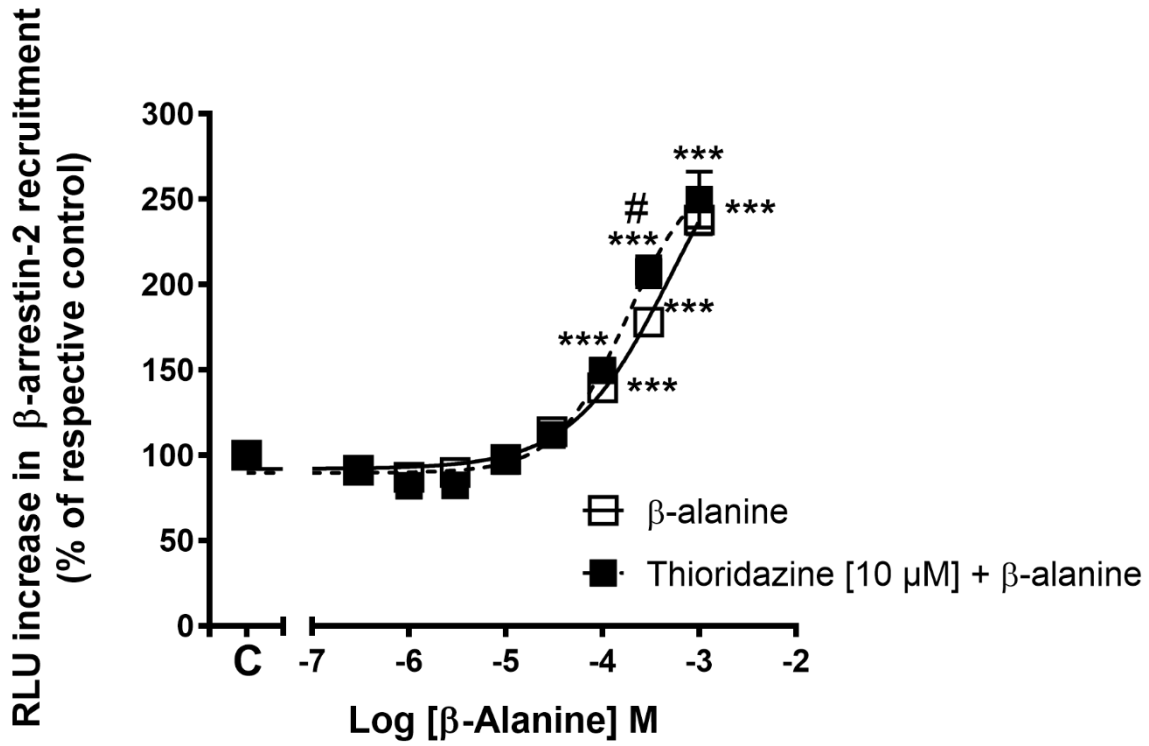

Figure 28: Concentration-response curves of β-alanine-induced activation and recruitment of β-arrestin in the presence and absence of thioridazine in CHO cells co-expressing the hMrgD and β-arrestin-2. CHO cells were seeded in 96-well plates. After 48 h, thioridazine [10 µM] or solvent was added and incubated at 37°C for 30 min. β-alanine or solvent was then given and further incubated at 37°C for 90 min. A PathHunter detection mixture was then added and incubated at R.T. for 1 h followed by measuring RLUs using a luminometer. The data are presented as % of basal control (C, HBSS for solid curve or thioridazine for dashed curve). Means ± SEM of 10-14 experiments. ***p<0.001, significant differences from respective control (C, HBSS for solid curve or thioridazine for dashed curve). #p<0.05, significant difference between values in the presence and absence of thioridazine. ANOVA followed by Bonferroni post-hoc test.

Antagonist	Basal RLU levels	
	Absence of antagonist	Presence of antagonist
Rimcazole 20 µM	1613 ± 44.3 (24)	1609 ± 42.6 (13)
Chlorpromazine 10 µM	1571 ± 34.5 (16)	1486 ± 34.7 (16)
Thioridazine 10 µM	1833 ± 36.9 (14)	2074 ± 81.2 (13)

Table 21: Basal RLU levels in the presence and absence of antagonists tested using the β-arrestin recruitment assays in CHO cells stably co-expressing the hMrgD and β-arrestin-2. Data are given as absolute RLU values. Shown are means ± SEM for (n) experiments. No significant differences between the values in the presence and absence of antagonists. ANOVA followed by Bonferroni post-hoc test.

5. Discussion

The GPCR MrgD receptor has been proposed to play role in nociception owing to its high expression in DRG (Dong et al., 2001; Crozier et al., 2007). MrgD is also reported to control cardiovascular function owing to its active contribution in the RAS (Lautner et al., 2013). Agonists include: amino acids as "β-alanine (Shinohara et al., 2004) and 3-aminoisobutyric acid (Müller et al., 2012)", and peptides as "alamandine (Lautner et al., 2013) and angiotensin 1-7 (Tetzner et al., 2016)". In the current work, we aimed to further characterize the hMrgD receptor by examining potential agonists and antagonists. Functional investigations of the hMrgD receptor were accomplished using Fluo-4 fluorescence measurements, AlphaScreen cAMP experiments, and NFAT reporter gene assays. Additionally, and for the first time, data on the coupling of the hMrgD to β-arrestin pathway using pathhunter eXpress β-arrestin assays are provided.

5.1. Overview of the applied expression system

In the present work, CHO Flp-In cells were used as the expression system for the hMrgD receptor. The Flp-In system involves the insertion of a Flp recombination target (FRT) site into the genome of the mammalian cell of choice. An expression vector having the gene of interest can be then integrated into the genome through a Flp-recombinase mediated DNA recombination at the FRT site (O'Gorman et al., 1991). The Flp-In recombinase system allows the rapid and efficient integration and expression of the gene of interest in mammalian cells at a specific genomic location, resulting in stable isogenic cell lines (Invitrogen; Sauer, 1994). Five different variants of the human receptor were previously produced in our lab which coded for a either a receptor with a short N-terminus, or two receptors with long N-terminus, or other two receptors with deleted N-terminus (Müller, 2014). The variants were all expressed in CHO Flp-In cells using the pcDNA5 / FRT / V5-His-TOPO vector, which contained the sequences of interest. Functionally, variants with either long N-terminus or deleted N-terminus showed no receptor function (Müller, 2014). Intriguingly, the short variant of the hMrgD caused, in both the NFAT luciferase assay, and in the [^{3}H] cAMP radioaffinity assay, the only significant and concentration-dependent response to β-alanine with the best signal-to noise ratio (Müller, 2014). In the same work, CHO Flp-In cells stably expressing a short variant of the hMrgD were cloned due to non-homogenous receptor distribution. The

cloned cells showed a weak, but significant left shift in the concentration-response curve of β-alanine in the NFAT luciferase assay with a reduction of the half maximal-concentration from [90 µM] to [47 µM] (Müller, 2014). Furthermore, expression analysis revealed a reduction in receptor expression in cloned cells as compared to non-cloned ones which was attributed to the high basal activity of the hMrgD receptor (Müller, 2014).

Therefore, cloned CHO Flp-In cells stably expressing a short variant of the hMrgD were chosen for further Gα-protein-dependent functional investigations in this work. Non-transfected CHO Flp-In cells served as a control to ensure the specificity of response we observe. For β-arrestin recruitment experiments, CHO Flp-In cells readily co-expressing the hMrgD and β-arrestin-2 supplied by the manufacturer "DiscoverX" were used.

5.2. Methodology of functional experiments

5.2.1. Fluo-4 Ca^{2+} mobilization assay

Fluorescent Ca^{2+} sensitive dyes have been successfully developed as reliable and convenient indicators of intracellular Ca^{2+} levels. In 2000, an analogue dye of Fluo-3 (Fluo-4) was developed for measuring cellular Ca^{2+} concentrations in the [100 nM to 1 µM] range (Gee et al., 2000). Fluo-4 has shown distinct advantages over the widely used fluo-3. One characteristic benefit is the greater absorption at 488 nm, thereby generating brighter fluorescence emission intensities when used with 488 excitation sources (Gee et al., 2000). Owing to the higher absorption efficiency of Fluo-4 compared to Fluo-3, lower Fluo-4 dye concentrations can be used to achieve a similar intensity of the fluorescent signal. Reducing used dye concentrations offer some benefits which include lowering of Ca^{2+} buffering effects and minimizing the levels of toxic by-products (as formaldehyde and acetic acid) which are produced from the hydrolysis of acetoxy-methyl (AM) ester used for loading. Even if the dye is used in the same concentration as Fluo-3, it can be excited with lower intensity illumination and yet still producing a similar fluorescence signal as Fluo-3. Decreasing illumination of the exciting light has the advantage of lowered photobleaching of the dye and decreased cell phototoxicity (Gee et al., 2000). Fluo-4 has shown quite good resistance to photobleaching with a decay half-life of 339 s upon continuous 20 µW laser illumination (Thomas et al., 2000). In the current work, the fluo-4 loading dye in a ready to use solution was ten times diluted in HBSS. Moreover, only a 2% 488 nm laser power was used to excite the dye. A time-dependent loss in fluorescence was observed but with no complete bleaching up to 600 s.

Other advantages of Fluo-4 include: a high rate of cell permeation, no impairment in normal physiological signaling, and a large dynamic range for reporting Ca^{2+} ($K_d[Ca^{2+}]$ of [345 nM] which produce good contrast pictures (Gee et al., 2000; Thomas et al., 2000). All together makes Fluo-4 the preferred indicator for a variety of applications including microplate screening, confocal microscopy, and flow cytometry.

Nevertheless, esterified Ca^{2+} indicators can cross other cellular membranes as those of intracellular organelles, where indicators can compartmentalize upon de-esterification with esterases. Beside passive compartmentalization, the acid form of the indicators can be actively compartmentalized by the cells from the cytosol into subcellular compartments (Al-Mohanna et al., 1994). Generally, the sub-cellular distribution of signal is not homogenous. Fluo-4-loaded HeLa cells showed uniform cytoplasmic fluorescence, minor mitochondrial / endoplasmic reticulum fluorescence signals and high nuclear fluorescence (Thomas et al., 2000). This would be of importance to consider when detecting Ca^{2+} increases in specific subcellular regions. However, that was a minor concern in our investigations. In most of HTS applications, the quantitation of stimulus-induced Ca^{2+} increments is generally performed without giving attention to localization of downstream signaling components (Coward et al., 1999). Furthermore, in cells loaded with Fluo-4, total cells measurements of fluorescence emission were shown to closely reflect the cytoplasmic responses (Gee et al., 2000).

The applicability of this assay in our cell system was firstly described by Sargheini, (2017). In the current research, we complete previous work and investigate the new peptide alamandine.

5.2.2. NFAT-luciferase reporter gene assay

Luciferase reporter gene assay is an efficient approach in monitoring gene activity and studying major GPCR pathways. Sensitivity, lack of endogenous luciferase expression, low background interference, broad dynamic range, convenience, reliability, and reproducibility makes firefly luciferase a valuable tool (Naylor, 1999; Cheng et al., 2010; de Almeida et al., 2011). Transcription factors of the NFAT family exist in many cell types and found to regulate various (patho) physiological processes. In the vascular endothelium, NFAT signaling has been proposed to play role in vascular development during embryogenesis, angiogenesis, proliferation of valve endothelial cells and in inflammatory processes as well (see Nilsson et al., 2008; Rinne et al., 2009). Intracellular Ca^{2+} increases activate the phosphatase calcineurin which in turn induces dephosphorylation, nuclear translocation and

transcriptional activity of NFAT (see Crabtree and Olson, 2002; Wu et al., 2007). Ca^{2+}-induced NFAT activation have been investigated in non-excitable T-cells (Macian, 2005) and vascular endothelial cells (Rinne et al., 2009), in excitable sympathetic ganglion neurons (Hernandez-Ochoa et al., 2007) and cardiac myocytes (Rinne et al., 2010) and in living cells (Rinne and Blatter, 2010).

The NFAT reporter gene assay was successfully used to assess the ligand-independent constitutive activity of the hMrgD receptor (Uno et al., 2012). In our lab, the applicability of the luciferase reporter gene assay in investigating GPCRs stably expressed in CHO Flp-In cells was proved and standardized (Hoffmann, 2010; Müller et al., 2012; Müller, 2014). In CHO Flp-In cells stably expressing a short variant of the hMrgD, β-alanine [3 µM – 1 mM] optimally accelerated NFAT luciferase expression following an incubation period of 3 h to 4 h (Müller, 2014). Therefore, this assay was of choice in investigating potential compounds. A 3.5 h incubation period of agonists was applied for all luciferase experiments in the current work. Long assay duration as needed for expression of the reporter gene is one limitation of the assay. Another drawback is the short half-life of the luciferase due to susceptibility to proteolysis (Bronstein, 1994). According to the established assay protocol, the firefly luciferase was incubated with the cells for 3 min in the dark followed by immediate measuring of the luminescence. This short time was found quite enough to lyse the cells, while avoiding any sharp decrease in luminescence. To rule out non-specific signals, control experiments in non-transfected CHO Flp-In cells were performed as well where neither β-alanine nor HBSS showed any disturbing effect.

5.2.3. AlphaScreen cAMP assay

To study the receptor coupling to Gαi/αs signaling pathway, the inhibition or augmentation of forskolin-induced increases in cAMP were investigated using AlphaScreen cAMP assay. AlphaScreen is a bead-based chemistry approach which was originally developed as a channeling immunoassay under the name of LOCI "luminescent oxygen channeling immunoassay" (Ullman et al., 1994). This approach was based on the non-enzymatic channeling of singlet oxygen species, produced by a photo excitable latex bead, to another latex bead which is in proximity with subsequent generation of a chemiluminescent signal. Likewise, the AlphaScreen technology accounts on the proximity of "donor" and "acceptor" beads as induced by the presence of analyte of interest. It is a non-radioactive, rapid, robust, and a highly sensitive amplified luminescent homogenous proximity assay that is appropriate

for HTS applications (see Eglen et al., 2008; Yasgar et al., 2016). AlphaScreen cAMP assay could provide comparable assay pharmacology to other assays with reproducible rank order of agonist and antagonist potency (Elster et al., 2007). Main disadvantage of the assay is the sensitivity to intense light or long exposure to ambient light. Another limitation is the liability of donor beads to bleaching which makes it effective for only single read. To avoid any loss of luminescence signal, the whole procedure from preparing the beads till addition to the plate and measuring were performed under conditions of minimal light exposure. Control experiments in non-transfected CHO cells showed that there are no unspecific signals caused by β-alanine or HBSS in this assay.

5.2.4. PathHunter β-arrestin recruitment assay

β-Arrestins are ubiquitously expressed in all cell types, where they are responsible for desensitizing GPCRs, regulating of GPCR intracellular trafficking and activating GPCRs to multiple signaling pathways (see Shenoy and Lefkowitz, 2011; Smith and Rajagopal, 2016). In the aspect of discovering ligands for orphan GPCRs, and biased GPCRs ligands, the β-arrestin recruitment assay has found of valuable use in drug discovery. Despite this fact, some GPCRs have very low affinity or even do not bind β-arrestins such as β3-adrenoreceptor (Nantel et al., 1993), α_{2A}-adrenoreceptor (DeGraff et al., 1999; DeGraff et al., 2002), the human-gonadotropin-releasing hormone receptor (Hislop et al., 2005), and the gastric inhibitory peptide receptor (Al-Sabah et al., 2014). It was questioned in this work to investigate the possible coupling of the hMrgD to the β-arrestin pathway and to compare the pharmacology of different ligands when using this assay to other G protein-cell-based assays. To achieve this, the highly specific PathHunter express β-arrestin assay was chosen. It is a homogenous β-galactosidase enzyme fragment complementation technology-based assay, where cells are engineered to co-express the ProLink (PK) tagged GPCR and the Enzyme Acceptor (EA) tagged β-arrestin-2 isoform. β-arrestin recruitment measured by the reconstituted β-galactosidase activity is directly downstream of receptor activation. This assay is superior to other cell-based assays regarding specificity of ligand-dependent receptor activation, elimination of endogenous receptor signal contamination and indirect-readout. Furthermore, since it examines the activation of β-arrestin and not G-protein-downstream signaling, the assay is suitable for all receptors which couples to different G-proteins (especially orphan GPCRs). High sensitivity, robustness and easy quantitation of luminescent signal readout are also in favor of the assay which makes it amenable for HTS. Using this

assay, novel ligands were identified for GPR92, GPR55, cannabinoid "CB_1 and CB_2" receptors (Yin et al., 2009), MrgX2, GPR88, GPR97 (Southern et al., 2013), and GPR27 (Dupuis et al., 2017) orphan GPCRs. A limitation of the assay when establishing the cell line, is that it requires the construction of fusion proteins for both the GPCR and β-arrestin.

5.3. Investigation of specificity of β-alanine-induced increments in Fluo-4 fluorescence to hMrgD-stably expressing CHO cells.

Discovered as the first endogenous ligand activating the MrgD in micromolar concentrations, β-alanine has revealed the coupling potential of the receptor to Gαq and Gαi proteins in CHO cells (Shinohara et al., 2004). Different working groups studied β-alanine-induced intracellular Ca^{2+} increases in CHO and HEK cells using Ca^{2+} sensitive fluorescent dyes (Shinohara et al., 2004; Milasta et al., 2006; Ajit et al., 2010). These findings were confirmed and reproduced in our lab, where β-alanine [3 µM to 1 mM] caused concentration-dependent increases in Fura-2 fluorescence and in NFAT-directed luciferase expression in CHO cells stably expressing a short variant of the hMrgD with a half-maximal concentration of [49 µM] and [90 µM], respectively (Müller et al., 2012, Müller, 2014). In these experiments, β-alanine could not stimulate a response in MOCK-transfected CHO cells which confirms the specificity of response to hMrgD-stably transfected cells and lack of endogenous expression of MrgD in CHO cells. As a more photostable derivative of Fluo-3 that is widely used and recommended, we were interested to establish the protocol for using Fluo-4 in our lab. Indeed, we could show that β-alanine [300 µM, 1 mM, and 3 mM] caused concentration-dependent, strong, and extended signal increases in fluo-4 fluorescence (Sargheini, 2017). That was further approved in the current work by analyses of pixel values in hMrgD-transfected cells. Moreover, control Fluo-4 experiments were performed to rule out any disturbing effects and emphasize the specificity of response **(Section 4.2.1.1).** In non-transfected CHO cells, despite estimation of small fluorescence signal increases by β-alanine [300 µM] as compared to HBSS, it is unlikely that β-alanine is the mediator of such response. First, no visual response could be observed from photomicrographs. Second, the increases were 2.8-fold lower than estimated for a similar concentration of β-alanine in hMrgD-transfected cells. Last, despite keeping always same conditions of cell culture and treatment, it is difficult to rule out the effect of environmental variables. For example, low temperatures can lead to prolonged fluorescent lifetimes (Oliver et al., 2000). Overall, this conforms to previous findings and

confirm the appropriateness of Fluo-4 Ca^{2+} mobilization assay in investigating effects of potential agonists at the hMrgD receptor.

5.4. Investigation of alamandine-induced Ca^{2+} increases via the hMrgD receptor

There are few literature reports on whether alamandine mediates Ca^{2+} signaling. One research article mentioned that alamandine could not increase Ca^{2+} levels in cardiomyocytes (Villela et al., 2014). They suggested that at least part of action of alamandine would differ from that known for β-alanine (Villela et al., 2014). Another research paper postulated that alamandine is regulating cardiac contractility not by direct Ca^{2+} increases but possibly by sensitizing the myofilament to Ca^{2+} via activation of protein kinase C (Soltani Hekmat et al., 2017). Recently, short-term (10 min) exposure of Fluo-4 AM-loaded cardiomyocytes of hypertensive rats to alamandine [100 nM] resulted in increases of the peak Ca^{2+} transient amplitude, an effect attributed to activation of the MrgD receptor (Jesus et al., 2020).

In the current work, alamandine was investigated for its potential to stimulate Ca^{2+} increments in our cell system **(Section 4.2.1.2).** Unlike the small fluorescence increases induced by alamandine [10 µM] both in hMrgD-stably transfected and non-transfected CHO cells, β-alanine [600 µM] caused strong fluorescence increments only in hMrgD-stably transfected cells. The signal elicited by alamandine beside being much weaker, but also rapidly disappeared unlike β-alanine-extended fluorescence. This may suggest different ligand-receptor binding kinetics (Strasser et al., 2017; Sykes et al., 2019). One factor responsible for different binding kinetics is the ligand structure (Strasser et al., 2017). This does not exclude the interaction of alamandine with the hMrgD receptor as β-alanine. Another factor affecting binding kinetics is the ligand size where larger ligands will have slower association rates. Alamandine (molecular weight of 855) caused a fluorescent signal as fast as that induced by β-alanine (molecular weight of 89.09). This could suggest that alamandine is activating MrgD receptor by binding to an allosteric active site or is activating another endogenous receptor in CHO cells. From this we conclude that there are at best only small Ca^{2+} responses to alamandine and a probable expression of endogenous receptors for alamandine in CHO cells.

5.5. Investigation of alamandine-induced activation of the hMrgD/Gαs/cAMP

Next, changes of cAMP levels were considered. Some research groups studied and suggested the importance of PKA-dependent molecular signaling pathway as downstream of cardiovascular regulation by alamandine (Qaradakhi et al., 2017; Liu et al., 2018; Shen et al., 2018). Tetzner and co-workers, (2016, and 2018) reported the AC/cAMP/PKA pathway as a primary intracellular pathway for both angiotensin 1-7 and alamandine signaling at the MrgD receptor (Tetzner et al., 2016; Tetzner et al., 2018). These reports assumed the coupling of the MrgD receptor to the Gαs-protein. In HEK293 cells expressing the MrgD receptor, alamandine [0.001 fM to 1 µM] caused a bell-shaped concentration- response curve, suggesting specific pharmacodynamic properties of alamandine compared to Ang 1-7. A maximal cAMP increase of 1.3-fold was reached at [0.01 nM] alamandine and the curve had an EC_{50} of [0.0004 nM] and IC_{50} of [0.3 nM]. They further showed that in the presence of the Gαi inhibitor (pertussis toxin; PTX), the concentration- response curve was no longer bell-shaped but sigmoidal. Thus, suggested the activation of Gαi pathway at higher alamandine concentrations which reduces the initial Gαs-mediated increase in cAMP (Tetzner et al., 2018). In the current work, we have reproduced a similar bell-shaped concentration response curve, however, both in hMrgD-transfected and in non-transfected CHO cells. Of notice is that alamandine induced 2.1-fold more cAMP increases above basal forskolin in non-transfected than in hMrgD-transfected cells. This might be attributed to the 2.3-fold increase in cAMP induced by forskolin [1 µM] above basal HBSS in hMrgD-transfected CHO cells than in non-transfected CHO cells **(Section 4.2.2.1, Table 15).** In contrast to alamandine signaling in both cell lines, β-alanine [300 µM] significantly inhibited forskolin-induced increments in cAMP only in hMrgD expressing CHO cells **(Section 4.2.2.1).** Findings support the Fluo-4 observations and conclude the likely expression of endogenous receptors for alamandine in CHO cells.

5.6. Investigation of the coupling of hMrgD to the β-arrestin pathway

β-arrestin-1 and β-arrestin-2 are two highly homologous ubiquitously expressed multifunctional adapter members of the arrestin family of proteins. They were identified through their sequence homology to the firstly recognized retinal member; so, named visual arrestin (Wilden et al., 1986). Beside arresting G protein coupling to and signaling through

GPCRs, β-arrestins also regulate trafficking of GPCRs. Independent of G protein activation, β-arrestins trigger physiological responses by scaffolding of many intracellular signaling networks through various types of signaling pathways. These involves the Hedgehog, Wnt, Notch, and transforming growth factor beta pathways, and downstream kinases such as MAPK and PI3K (see Benovic et al., 1987; Ritter and Hall, 2009; Shenoy and Lefkowitz, 2011; Chapman et al., 2014; Ghosh et al., 2015; Gu et al., 2015; Zhao et al., 2016 and Peterson and Lutrell, 2017). The β-arrestin-mediated signaling is as important as its G protein counterpart in regulating a lot of essential cellular responses. These include cell development, growth and survival, immune cell function, protein translation, and neuronal signaling. Upregulation of β-arrestins expression was found associated with the pathogenesis of cancer and several inflammatory disorders (see reviews Sharma and Paramesvaran, 2015; Bond et al., 2019).

Evidence on MAS-1 receptor trafficking and signaling in a β-arrestin-2 dependent manner was firstly reported by Cerniello and co-workers (2017). They showed that an activated MAS-1 receptor, once internalized mediates ERK activation by β-arrestin-2 (Cerniello et al., 2017). Furthermore, another research group evaluated the G protein independent signaling properties of MAS-1 and reported the recruitment and signaling of the activated receptor via β-arrestin (Gaidarov et al., 2018). Among the MAS related gene family of receptors, one report described the β-arrestin recruitment potential of MrgX2 (Southern et al., 2013). Stimulation of the MrgD receptor with saturating concentrations of β-alanine revealed receptor protein translocation from the plasma membrane to intracellular vesicles which indicate ligand-induced receptor internalization (Shinohara et al., 2004). However, up to date no research groups have studied coupling of the MrgD to the β-arrestin pathway. Since β-arrestin recruitment triggers major signaling cascades downstream of the GPCRs, we studied in this work the recruitment potential of the hMrgD to β-arrestin-2 using the highly sensitive PathHunter eXpress β-arrestin recruitment assay. That was aimed to provide a better understanding of the hMrgD receptor signaling.

5.6.1. Study of β-alanine-induced activation and recruitment of β-arrestin

In CHO cells readily co-expressing the hMrgD and β-arrestin-2 purchased from Discover X, β-alanine [0.3 µM to 1 mM] caused concentration dependent increases in β-arrestin-2 recruitment following 90 min incubation with the cells **(Section 4.3.1)**. The potency of β-alanine in recruiting β-arrestin-2 is lower compared to its potency in accelerating NFAT-

luciferase expression (Hanna et al., 2020). This could be explained due to the amplified response elicited by β-alanine when targeting signaling pathways which are more distal to the receptor than β-arrestin recruitment. Downstream of the Gαq signaling pathway and MAS-1 mediated PLCβ activation, the MAS-1 agonist "AR234958" has stimulated inositol phosphate accumulation and showed an EC_{50} of [96 nM]. Meanwhile, AR234958 has recruited β-arrestin and showed a higher EC_{50} of [340 nM] (Gaidarov et al., 2018).

Efficacy of ligands at their receptor targets is measured by their duration of action which is a function of the residence time of the ligand-receptor complex. A long residence time of the drug-receptor complex will prolong the duration of pharmacodynamic activity and hence improve the drug efficacy (see Cusack et al., 2015; Strasser et al., 2017). Out of this concept we additionally tested shorter (60 min) and longer (120 min) incubation periods of β-alanine with the hMrgD receptor. As reported by the kit manufacturer (DiscoverX), incubation of β-alanine for 90 min with hMrgD gave the optimal response with 2.5-fold increase in signal above basal **(Section 4.3.2, Table 17).** The findings here conclude that both the hMrgD receptor and β-alanine have non biasing tendency to either Gα protein-dependent or Gα protein-independent pathways. While providing a base for this statement, more experiments targeting signaling pathways downstream of β-arrestin like MAPK/ERK pathway would be needed for better understanding of the impact of this pathway.

5.6.2. Study of alamandine-induced activation and recruitment of β-arrestin

After establishment of the coupling of the hMrgD receptor to the β-arrestin pathway using β-alanine, assessing alamandine's potential to activate the hMrgD receptor and to recruit β-arrestin-2 was required. A wide concentration range [0,00001 nM to 100 µM] of alamandine was tested. Following 90 min of incubation with CHO cells co-expressing the hMrgD and β-arrestin-2, alamandine stimulated a weak response at the [0,1 nM] concentration in contrast to the strong signals elicited by β-alanine [100 µM and 300 µM] **(Section 4.3.2).** Studying the binding kinetics of some peptide agonists at class A Gonadotropin releasing hormone (GnRH) receptor, revealed a peptide-receptor residence time widely ranging from 5.6 min to 125 min (Nederpelt et al., 2016). To exclude the interaction kinetics as a factor responsible for the weak signaling output at the hMrgD receptor, alamandine [0,001 nM to 1 µM] was also incubated with the cells for 60 min and 120 min. While β-alanine's strong signal was greatly reduced, alamandine's weak response was completely lost **(Section 4.3.2, Table 16).**

The identification of MrgD as a receptor for alamandine does not rule out the possibility of existence of other binding sites for this novel angiotensin analogue. In line with this hypothesis and supporting to our findings, Jesus, and co-workers (2018), have reported binding of alamandine to cardiomyocytes isolated from transgenic mice lacking either the MrgD or MAS genes (Jesus et al., 2018). This propose the existence of another receptor in cardiomyocytes to which alamandine is binding and possibly activating. Receptors other than MrgD to which alamandine has been reported in literature to signal through are discussed below.

- **MAS receptor**

Alamandine signaling through the MAS receptor is questioned. Some research articles have reported the lack of alamandine binding and/or signaling via the MAS receptor. Lautner and co-workers (2013), have shown that MAS is not a putative receptor for alamandine action based on three findings. First, unlike binding to MrgD-expressing CHO cells, alamandine could not bind to MAS-expressing CHO cells. They also showed that pre-treatment of aortic rings from FVB/N mice with the potent and selective MAS-antagonist; D-Ala^{7}-Ang-1–7 (A-779), did not block alamandine-induced vasodilatory actions. Furthermore, incubation with alamandine caused nitric oxide release in MrgD-transfected but not in MAS-transfected CHO cells (Lautner et al., 2013). Recently, another research group supported the same hypothesis (Jesus et al., 2018). In freshly isolated cardiomyocytes from transgenic mice lacking the MAS gene, activation of the AMPK/NO pathway by alamandine was found preserved. Moreover, they showed the binding of fluorescently labelled alamandine to cardiomyocytes lacking the MAS gene (Jesus et al., 2018). More recently, blocking the MAS receptor did not affect the positive inotropic actions of alamandine in diseased cardiomyocytes (Jesus et al., 2020). In addition, anti-fibrotic effects mediated by alamadine were not MAS-dependent (Huang et al., 2020). Conversely, alamandine was recently reported to induce cAMP increases via the MAS receptor. Hence, MAS was described as a functional receptor for alamandine (Letzner et al., 2018).

- **AT-1 receptor**

In only one research article, alamandine was reported to signal via angiotensin AT-1 receptor activation under normal conditions of blood pressure (normotensive rats). However, in pathological condition as hypertension (renovascular hypertensive 2K1C rats), alamandine

mediated a biphasic response. A vasoconstrictive response via AT-1 receptor and a parallel vasodilatory response via PD123319-sensitive receptors (angiotensin AT-2 or MrgD or MAS receptors). The vasodilatory effect was found long lasting and could mask AT-1 receptor-mediated effects (Soltani-Hekmat et al., 2017). Authors explained the agonistic effect of alamandine at the AT-1 receptor due to alamandine's structural similarity to Ang1-7 which was reported as an AT-1 receptor agonist (Galandrin et al., 2016). Another research group studied the vasodilatory mechanism behind AT-1 receptor blockage. They showed that *in* vitro blockage of the AT-1 receptor of rabbit interlobar arteries using candesartan exerts vasodilatory/hypotensive effects that are mediated by alamandine (Michalatou et al., 2018). However, alamandine caused neither vasoconstrictive nor vasodilatory effects in rabbit aorta (Michalatou et al., 2018), yet enhanced acetylcholine mediated vasodilation (Habiyakare et al., 2014). That was explained as each vascular bed respond variably to peptides. Extensive simulation and modeling studies on angiotensin analogues, revealed the importance of the aromatic Phe residue at position 8 in triggering agonist activities. Such depressor activity of alamandine was explained to be due to the deletion of the Phe aromatic residue, thus rendering antagonist vasodilatory effects (Michalatou et al., 2018). On the other hand, in cardiomyocytes from hypertensive rats, blocking AT-1 receptor did not affect alamandine's contractile actions (Jesus et al., 2020).

Peptides typically bind to their targets with high affinity and target specificity. In scope of our findings from Gα protein-dependent and Gα protein-independent functional assays together with the contradictory reports on the binding sites for alamandine signaling, the hypothesis that alamandine is activating and mediating its effects via a so far unknown receptor has to be considered and further investigated.

5.6.3. Study of angiotensin 1-7-induced activation and recruitment of β-arrestin

Few research studies reported the possible activity of angiotensin 1-7 at the MrgD receptor. In 2008, Gembardt and colleagues, firstly reported the weak action of the peptide at MrgD where it stimulated arachidonic acid release via the receptor (Gembardt et al., 2008). Recently, another study claimed the same hypothesis that MrgD is an additional receptor for angiotensin 1–7 beside the MAS receptor (Tetzner et al., 2016). In their analyses using the cAMP read out assay, angiotensin 1–7 stimulated cAMP increases in primary HUVEC cells and in MrgD transfected HEK293 cells. They also showed that Ang 1-7 failed to increase cAMP levels in primary mesangial cells obtained from MAS and MrgD double knockout (KO) mice. More

recently, angiotensin 1-7 was reported to upregulate the expression of the MrgD receptor through which it mediates antifibrotic actions (Huang et al., 2020).

In this work we investigated the potential of angiotensin 1-7 to activate the hMrgD and to recruit β-arrestin-2. In CHO cells co-expressing the hMrgD and β-arrestin-2, a similar concentration range [0,001 nM to 1 µM] as described in literature for angiotensin 1-7 action was tested. Angiotensin 1-7 used at these concentrations failed to induce even a weak response following 90 min of incubation with the cells **(Section 4.3.3).**

Likewise, its metabolite, angiotensin 1-7 has other binding sites through which it was shown to signal. The MAS receptor was firstly identified by Santos and co-workers (2003) as the functional receptor for angiotensin 1-7. In that study, angiotensin 1-7 induced antidiuretic effect was abolished in MAS-KO mice. Moreover, in cells expressing the MAS receptor, angiotensin 1-7 promoted the release of arachidonic acid, an effect which was blocked when using A-779. In MAS-deficient aortic rings, the dose-dependent relaxation of angiotensin 1-7 was abolished without interfering with endothelium-dependent relaxation by acetylcholine (Santos et al., 2003). Since that, it became well accepted that ACE2 / angiotensin 1–7 / MAS represent an alternative axis, once activated counteracts many of the effects of ACE / angiotensin II / AT-1 axis including anti-inflammatory, antiproliferative, antifibrotic, antihypertrophic, and vasodilatory mechanisms of action (see reviews Santos et al., 2008; Gomes et al., 2012; Bader, 2013; Santos et al., 2013; de Souza-Neto et al., 2018). On the other hand, lack of evidence for direct Ang 1-7 binding and/or signaling through the MAS receptor has been reported by independent laboratories (Bikkavilli et al., 2006; Shemesh et al., 2008; Zhang et al., 2012b; Tirupula et al., 2014; Gaidarov et al., 2018). Based on the lack of classical G-protein signaling and failure of desensitization of MAS-1 in response to angiotensin 1-7, the International Union of Basic and Clinical Pharmacology (IUPHAR) nomenclature committee has refrained from designating the MAS-1 as an angiotensin 1-7 receptor (Karnik et al., 2017). Other than MAS and MrgD, early cell culture studies have reported some actions of angiotensin 1-7 at AT-1 and AT-2 receptors (Muthalif et al., 1998; Heitsch et al., 2001). Reports have proposed the interaction of MAS with AT-1 and AT-2 receptors and the tendency of MAS to heterodimerize with AT-1 receptor, which subsequently inhibit Ang II activity and promote Ang 1-7 activity (Castro et al., 2005; Kostenis et al., 2005). On the other side, other research groups have reported low binding affinity of Ang 1-7 at AT-1 and AT-2 receptors (Rowe et al., 1995; Tallant et al., 1997).

Under our experimental conditions, our findings suggest that angiotensin 1-7 is not activating the hMrgD receptor. It is possible that Ang 1-7 is mediating its effects via the previously mentioned receptors, but also the likeliness that it is activating another receptor exists. Angiotensin 1-7, together with alamandine, angiotensin A, and angiotensin IV, are currently proposed as natural candidates which belong to the counter-regulatory RAS that may contribute to the treatment of COVID-19 associated cardiovascular disorders in SARS-CoV-2 infected patients (Annweiler et al., 2020). However, in terms of our findings and the controversial reports, further investigations are needed to identify receptors primarily mediating these peptides actions.

5.6.4. Study of small molecules-induced activation and recruitment of β-arrestin

In our lab, small molecules with structures closely related to that of β-alanine were screened and functionally tested for their activity at the hMrgD receptor and a structure-activity relationship has been characterized (Müller, 2014). Among tested molecules, four have been chosen in the present work for further investigation at the hMrgD using the β-arrestin recruitment assay.

5.6.4.1. DL-3-aminoisobutyric acid

3-Aminoisobutyric acid is a non-proteinogenic amino acid that originates from the catabolism of the pyrimidine base thymine. Laterally, β-alanine is produced from the degradation of uracil (Manning and Pollitt, 1985; van Kuilenburg et al., 2004). Two enantiomers of 3-aminoisobutyric acid exist. While the urine predominant D-enantiomer is produced from thymine, the plasma predominant L-enantiomer is produced from valine (Armstrong et al., 1963; van Gennip et al., 1981; van Kuilenburg et al., 2004). The plasma concentration of 3-aminoisibutyric acid in humans is about [2.3 µM] (van Kuilenburg et al., 2004). Beside stimulating glycine receptors (Schmieden and Betz, 1995), 3-aminoisobutyric acid was reported to activate the MrgD receptor (Müller et al., 2012; Müller, 2014; Uno et al., 2012). In CHO cells expressing the hMrgD receptor, the amino acid showed activity with EC_{50} ranging from [53.4 µM to 821.7 µM], which is higher compared to that of β-alanine [22.6 µM to 219.8 µM] (Uno et al., 2012). In that study the correlation between 3-aminoisobutyric acid, MrgD and cancer development was described (Uno et al., 2012).

Our group has formerly reported concentration-dependent increases in NFAT-directed luciferase expression upon addition of a stereoisomeric mixture (DL) of 3-aminoisobutyric acid in CHO cells stably expressing a short variant of the hMrgD receptor (Müller et al., 2012; Müller, 2014). The concentration-response curve had an EC_{50} of [165 µM] and showed a maximal effect that is indistinguishable from that of β-alanine. Activity of DL-3-aminoisobutyric acid at the hMrgD receptor was further confirmed using [^{3}H] cAMP radioaffinity and Fura-2 assays (Müller et al., 2012; Müller, 2014). In the present work, in CHO cells co-expressing the hMrgD and β-arrestin-2, DL-3-aminoisobutyric acid caused concentration-dependent signal increases. Compared to β-alanine, the concentration-response curve of 3-aminoisobutyric acid was slightly shifted to the right **(Section 4.3.4).** The findings here provide additional evidence on the activity of 3-aminoisobutyric acid at the hMrgD receptor with similar efficacy and lower potency to that of β-alanine. Recently, Kitase and colleagues (2018) have also reported the signaling of 3-aminoisobutyric acid via the MrgD receptor in preventing mitochondrial breakdown due to reactive oxygen species which makes the amino acid an osteocyte protective factor (Kitase et al., 2018). In that study, the protective effect of 3-aminoisobutyric acid was assumed to be lost with age owing to the lower expression of MrgD in older murine cells. Furthermore, the inhibition and knockdown of MrgD receptor prevented the protective actions of L-form at murine osteocytes against oxidative stress (Kitase et al., 2018). Other literature reports have described biological actions of 3-aminoisobutyric acid related to cell metabolism (see review Tanianskii et al., 2019). 3-Aminoisobutyric acid was shown to regulate lipid and carbohydrate metabolism in fat tissue, liver, and skeletal muscles, and to induce fat tissue browning with subsequent increase in fatty acid oxidation, and prevention of diet-induced obesity (Maisonneuve et al., 2004; Begriche et al., 2008; Roberts et al., 2014). The amino acid was also shown to play role in the improvement of insulin resistance and inflammation in skeletal muscles (Jung et al., 2015). Others involve reduction of hepatic endoplasmic reticulum stress and glucose/lipid metabolic disturbance in type-2 diabetes (Shi et al., 2016), and amelioration of renal fibrosis (Wang et al., 2017). However, the signaling mechanisms through which 3-aminoisobutyric acid regulate cell metabolism are still not clear. A possible relation of these actions to the hMrgD receptor is not yet studied and further investigations are required.

5.6.4.2. DL-3-aminobutyric acid

3-Aminobutyric acid is a natural non-proteinogenic β-amino acid known to protect the plants against pathogens (Jakab et al., 2001; Cohen, 2002). There are no reports in literature on its action in humans. Its structure is closely related to that of GABA, β-alanine, and 3-aminoisobutyric acid. Activation of glycine receptors by 3-aminobutyric acid was reported (Schmieden and Betz, 1995). For the first time, we have previously shown using NFAT-luciferase assay that 3-aminobutyric acid is an agonist at the hMrgD which activates the receptor at high micromolar concentrations comparable to that of GABA (Müller et al., 2012; Müller, 2014). In the present work, 3-aminobutyric acid caused concentration-dependent increases in β-arrestin-2 recruitment. Compared to β-alanine, the concentration-response curve was markedly right-shifted **(Section 4.3.4).** The EC_{50} could not be estimated as the maximal effect could not be reached up to [3 mM]. However, if we assume that the maximal effect was reached, the EC_{50} would have been much higher than that of β-alanine. The findings here support previous investigations and provides an evidence that 3-aminobutyric acid is a weak agonist at the hMrgD receptor.

5.6.4.3. GABA

GABA is the major inhibitory neurotransmitter in the mammalian nervous system which mediates its actions mainly via anion selective ionotropic $GABA_A$ receptors. In healthy people the plasma concentration of GABA is around [2 µM] (Küçükibrahimoğlu et al., 2009). β-alanine was found to activate the $GABA_A$ receptor with less potency than native GABA (Wu et al., 1993). Owing to this and to the structural similarity between GABA and β-alanine, it is expected that GABA can also act at the MrgD receptor. Indeed, several research groups have reported the activation of the MrgD receptor by GABA (Shinohara et al., 2004; Ajit et al., 2010; Uno et al., 2012). In these studies, GABA showed EC_{50} ranging from [53 µM to 4.4 mM] at the hMrgD, which is much higher as compared to that of β-alanine [3.76 µM to 219.8 µM]. It was reported that low affinity $GABA_A$ receptors are activated by concentrations of GABA in the millimolar range (Mody et al., 1994), while the high affinity receptors are activated by concentrations of GABA in the low micromolar range (Farrant and Nusser, 2005; Lee et al., 2012).

We further confirmed this by our group using the NFAT-luciferase assay in CHO cells expressing a short variant of the hMrgD receptor (Müller et al., 2012; Müller, 2014).

Similarly, in the present work GABA could recruit β-arrestin-2 via the hMrgD receptor. Compared to β-alanine, the concentration-response curve was extremely shifted to the right **(Section 4.3.4).** Likewise, in the response curve of 3-aminobutyric acid, the maximal effect was not achieved up to [3 mM] and thus EC_{50} could not be estimated. Interestingly, the rank order potency of DL-3-aminobutyric acid and GABA was reversed (Hanna et al., 2020). In the NFAT luciferase assay, DL-3-aminobutyric acid was less potent than GABA and GABA was less than potent than DL-3-aminobutyric acid in the β-arrestin assay. This could argue for biased signaling of these two ligands where GABA preferentially activate the G protein-dependent pathway while DL-3-aminobutyric acid prefers the β-arrestin pathway.

5.6.4.4. L-Carnosine

L-Carnosine is a naturally occurring dipeptide composed of β-alanine and L-histidine (Hipkiss et al., 1998). Endogenously, carnosine is synthesized by carnosine synthase and metabolized to its precursors by carnosinase (Boldyrev et al., 2013). In the skeletal muscles and olfactory bulb of mammals, carnosine exists in concentrations as high as in the millimolar range (Kohen et al., 1988; Boldyrev et al., 2013). The relationship between carnosine and the MrgD receptor was studied by Shinohara and co-workers (2004) where L-carnosine displayed agonistic activity at the rat MrgD receptor but not at the human orthologue (Shinohara et al., 2004). Carnosine was further investigated by our group in CHO cells stably expressing a short variant of the hMrgD receptor (Müller, 2014). At [1 mM] concentration, the dipeptide was able to accelerate NFAT-luciferase expression, however, it was not able to inhibit forskolin induced increases in cAMP in the [^{3}H] cAMP radioaffinity assay (Müller, 2014). In the present work, L-carnosine was not able to show any signs of receptor activation where it failed to recruit β-arrestin-2 **(Section 4.3.4).** The previous explanation discussed by Müller (2014) can now be confirmed where it is more likely that the response observed in NFAT assay was due to β-alanine which resulted from the breakdown of carnosine during the 3 h incubation period.

5.7. Investigation of 5-Oxo-ETE activity at the hMrgD receptor

5-Oxo-ETE is an important pro-inflammatory mediator which mediates all its chemotactic actions via the selective Gαi-coupled GPCR oxoeicosanoid receptor 1 (OXER1) primarily through the βγ subunits (see reviews Grant et al., 2009; Powell and Rokach, 2013; Powell and Rokach, 2015). Bautzova and co-workers (2018), have recently reported the dependency of 5-

Oxo-ETE on MrgD in triggering nociception in constipation-predominant irritable bowel syndrome. In their investigations, 5-Oxo-ETE induced Ca^{2+} increments in MrgD expressing CHO cells (Bautzova et al., 2018). In our work, 5-Oxo-ETE caused a small increase in NFAT-directed luciferase expression at [1 µM] concentration in cloned CHO cells stably expressing a short variant of hMrgD **(Section 4.4.1).** Both β-alanine and 5-Oxo-ETE signals were abolished in non-transfected CHO cells. Effects of concentrations higher than [1 µM] of 5-Oxo-ETE could not be estimated due to the toxic effect of the solvent EtOH on the cells **(Section 4.4.1, Table 18)**. 5-Oxo-ETE was further addressed using the highly sensitive β-arrestin recruitment assay. Unlike β-alanine which strongly induced a response, 5-Oxo-ETE was unable to recruit β-arrestin-2 **(Section 4.4.2).** Under our experimental conditions and in scope of the limited concentration range, which was tested, the activity of 5-Oxo-ETE at the hMrgD receptor could not be decisively evaluated. Possibly if higher concentrations would have been examined, a response in the β-arrestin assay could have been measured. The OXER1 has no orthologue in rodents (Grant et al., 2009). So, the activity we see in CHO cells is either due to activation of MrgD receptor or another endogenous receptor other than OXER1 or an artifact. Nevertheless, we could show that 5-Oxo-ETE even if activating the hMrgD receptor, but it is less potent than β-alanine.

5.8. Investigation of potential antagonists at the hMrgD receptor

With the aim of further characterization of the hMrgD receptor, screening, and investigation of compounds with inhibitory potential at the receptor was required. Ajit and co-workers (2010) were the first to report the antagonistic potential of the psychotropic drugs, chlorpromazine and thioridazine, at the MrgD receptor (Ajit et al., 2010). These compounds and other structurally related ones were further studied by our group using NFAT reporter gene and [^{3}H] cAMP radioaffinity assays (Müller, 2014). In the present work, we searched also for antagonists among some amino acids using NFAT luciferase assay. Moreover, the compounds which were identified as promising inhibitory candidates in previous work were further examined for their blocking potential of β-arrestin recruitment.

5.8.1. Interactions using NFAT-reporter gene assay

The amino acids L-lysine [100 µM, and 1 mM], D-phenylalanine [1 µM, and 100 µM] and D-tryptophan [10 nM, 1 µM, and 100 µM], were screened in previous work among β-alanine structurally related compounds and displayed no agonist potentials at the hMrgD receptor

(Müller, 2014). In the present work, these amino acids together with D-(+)-3-phenyllactic acid were examined at [1 mM] concentration in the NFAT luciferase assay **(Section 4.5.1)**. Again, no signs of activation were observed as compared to β-alanine, however, on the other way round, D-(+)-3-phenyllactic acid and D-phenylalanine caused significant decreases in NFAT-luciferase directed expression as compared to control. This may suggest their inverse agonist actions by lowering signals below the constitutive activity levels of the receptor. These two compounds were further examined for inhibiting the signal of β-alanine. Only, D-(+)-3-phenyllactic acid could significantly lower β-alanine-induced increases, but to levels which are still higher than basal levels. This may suggest that D-(+)-3-phenyllactic acid is a weak inverse agonist at the hMrgD receptor. Further investigations are needed to establish a concentration-activity curves for D-(+)-3-phenyllactic acid and for β-alanine in the presence and absence of D-(+)-3-phenyllactic acid. In addition, different experimental assays are required to validate the effect.

5.8.2. Interactions using β-arrestin recruitment assay

5.8.2.1. Interaction with rimcazole

Rimcazole was originally developed as an antipsychotic drug by acting as a σ-receptor antagonist with higher affinity to the σ2 subtype (Ferris et al., 1982; Gilmore et al., 2004). Beside σ-receptors, rimcazole has poor binding affinity for dopamine, NMDA, serotonin, and opioid receptors (Gilmore et al., 2004). Research studies have supported the much higher binding affinity of rimcazole for dopamine transporters than for σ-receptors, but with low potency in inhibiting dopamine uptake (Izenwasser et al., 1993; Husbands et al., 1997; Husbands et al., 1999; Gilmore et al., 2004). Owing to limited efficacy and incidence of grand mal seizure, EEG abnormality, muscle fasciculations, and tremors at high doses, further clinical trials were terminated (Davidson et al., 1982; Chouinard and Annable, 1988; Gilmore et al., 2004). Nevertheless, *in vitro* research keeps studying rimcazole as an experimental tool for its effectiveness and specificity. With its help, recent studies have described the dual targeting of σ-receptor and dopamine transporter as a promising approach for the discovery of drugs that could be beneficial in the clinical management of stimulant abuse (Zanettini et al., 2018; Job and Katz, 2019).

In CHO cells stably expressing a short variant of the hMrgD receptor, rimcazole [20 µM] showed antagonistic potential at the hMrgD receptor. That was demonstrated by the

significant parallel shifting of the concentration-response curve of β-alanine to the right with an apparent pK_B value of 5.2 both in NFAT-luciferase and in [^{3}H] cAMP radioaffinity assays (Müller et al., 2012; Müller, 2014). According to these analyses, rimcazole was described as a weakly potent, and probably competitive antagonist at the hMrgD receptor (Müller, 2014).

In the present study, interestingly, rimcazole [20 μM] did not show any tendency to inhibit β-alanine-induced activation of the hMrgD receptor and recruitment of β-arrestin-2 **(Section 4.5.2.1).** Findings could suggest that rimcazole is a weak biased antagonist at the hMrgD receptor with selective preference of blocking the G protein-dependent signaling pathways.

On its own, rimcazole did not show nociceptive or antinociceptive properties. However, it was believed to be involved in pain regulation by blocking the action of other compounds. By blocking the σ-receptors, rimcazole decreased the pain threshold (Kest et al., 1995). On the other side, rimcazole promoted antinociception by antagonizing nociceptin action at the nociceptin receptor (Kobayashi et al., 1997). Furthermore, rimcazole was shown to enhance resiniferatoxin binding to vanilloid receptor with subsequent receptor desensitization and decreased perception of neuropathic pain (Szallasi et al., 1996). Future *in vitro* experiments addressing rimcazole potential to block β-alanine induced nociceptive effects via the hMrgD receptor would be interesting.

5.8.2.2. Interaction with chlorpromazine

Chlorpromazine is a first-generation antipsychotic phenothiazine derivative which was originally developed as an antihistaminic to be used in anesthesia (Adams et al., 2005; Dudley et al., 2017). Chlorpromazine is a benchmark for treatment of schizophrenia and has been listed by the World Health Organization (WHO) as one of five essential medications used in the management of psychotic disorders (WHO, 2013; Dudley et al., 2017). As a typical antipsychotic, chlorpromazine causes irreversible inhibition of dopamine D2 receptors which subsequently results in unwanted extrapyramidal side effects as tardive dyskinesia, tremors, and akinesia (Seeman, 2002). Other adverse effects result as well from the non-specific inhibition of different molecular targets. Beside dopamine D2 and D4 and histamine H1 receptors, chlorpromazine has affinity to α-adrenergic, muscarinic, and 5-HT2A serotonin receptors (Peroutka and Snyder, 1980; Richelson, 1988; Roth et al., 1995; Suzuki et al., 2013).

A possible interaction of chlorpromazine with the MrgD receptor was first described by Ajit and co-workers (2010). In their investigations, chlorpromazine blocked the MrgD receptor and showed an IC_{50} of [2,7 µM], however, no affinities were determined in that work (Ajit et al., 2010). In our lab, the affinity of chlorpromazine at the hMrgD receptor was determined using NFAT luciferase assay. In CHO stably expressing hMrgD cells, chlorpromazine [10 µM] caused a significant parallel shift of the concentration-response curve of β-alanine to the righ with statistically undistinguishable maximal effect and an apparent pK_B of 5.1 (Müller et al., 2012; Müller, 2014). These finding described chlorpromazine as a weak, possibly competitive antagonist at the hMrgD receptor (Müller et al., 2012; Müller, 2014).

In the current research, similar to what was observed with rimcazole, chlorpromazine [10 µM] could not antagonize β-alanine-induced recruitment of β-arrestin-2 to the activated hMrgD receptor **(Section 4.5.2.2).** Together that would suggest that chlorpromazine is a weakly potent G-protein biased antagonist of the hMrgD receptor.

Chlorpromazine is well established among commonly prescribed drugs for management of acute migraine pain in emergency settings (Cameron et al., 1995; Gelfand and Goadsby, 2012; Khazaei et al., 2019). It is not well understood how dopamine and chlorpromazine contribute to pain relief (Charbit et al., 2010; Gelfand and Goadsby, 2012). It is unlikely that chlorpromazine-induced blocking of the MrgD receptor is relevant to any clinical outcome, where the plasma concentrations achieved would be too low to block the receptor (Mackay et al., 1974). Chlorpromazine may serve as a template for developing more potent biased antagonists.

5.8.2.3. Interaction with thioridazine

Thioridazine is a long-established neuroleptic drug from the phenothiazine group, which has been lately used as a third line anti-tubercular drug (Thanacoody et al., 2011; Amaral and Molnar, 2012; Scalacci et al., 2017). Thioridazine cardiac toxic effects are the most serious among phenothiazine members owing to inhibition of human cardiac K^+ human ether-go-go-related gene "hERG" channel (Kim and Kim, 2005). Similarly, to other members, thioridazine interact non-specifically with different receptors including dopamine D2, and D4, serotonin 5-HT2A, histamine H1, α-adrenergic and muscarinic receptors (Peroutka and Snyder, 1980; Richelson, 1988; Roth et al., 1995). Furthermore, structurally related thioridazine and chlorpromazine have displayed anticancer effects through inhibition of the histamine

releasing factor TCTP (Tuynder et al., 2004; Amson et al., 2017) or via blocking of the dopamine D2 receptor (Yong et al., 2017).

Likewise, for chlorpromazine, Ajit and co-workers (2010) have reported for the first time that thioridazine is an antagonist at the MrgD receptor and showed an IC_{50} of [1.5 µM] (Ajit et al., 2010). In our lab, we have determined different affinities for thioridazine interaction with the hMrgD receptor under different experimental conditions. Apparent affinity constants pK_B of 5.2 and 4.8 were determined for thioridazine [10 µM] in NFAT-luciferase, and in [^{3}H] cAMP radioaffinity assays, respectively (Müller et al., 2012; Müller, 2014). These findings suggested that thioridazine is a weak antagonist at the hMrgD receptor, however, the exact mode of antagonism could not be exactly determined without a schild plot analysis.

Despite showing affinities below the plasma levels needed for thioridazine to block the receptor (Cohen-Mansfield et al., 2000), we wanted in the present study to investigate it further using the β-arrestin recruitment assay **(Section 4.5.2.3).** Like previously investigated antagonists, thioridazine [10 µM] did not show antagonistic activity. On the other hand, it may potentiate β-alanine-induced recruitment of β-arrestin-2 by significantly increasing the response to β-alanine [300 µM].

5.9. Molecular determinants of MrgD receptor function

A predicted two-dimensional model of the hMrgD receptor was developed in our lab. Amino acids of the MrgD receptor which were found conserved among various species (with the exception of $T^{6.54}$ which is only found in humans and rhesus monkeys but not in mice or rats or wolves), and whose positions in other class A GPCRs has shown to play important role in receptor activation were studied by site-directed mutagenesis (Müller, 2014; Arbogast et al., 2018). Mutation of the residues R3.30, W6.55, R7.39 by alanine replacement completely abolished responses to β-alanine either in NFAT-luciferase assay or in the [^{3}H] cAMP radioaffinity assay. Furthermore, Y3.33A, Y3.36A, and Y6.59A mutant constructs obviously reduced responses to β-alanine. This emphasizes the crucial role these six amino acid residues in TMs 3, 6, and 7 play in the binding and/or activation process of the hMrgD receptor. The positively charged residue K3.29 was also mutated and showed no difference from the wildtype in regard to β-alanine-induced increases in NFAT luciferase activity (Arbogast et al., 2018). This indicate that K3.29 residue is not necessary for the interaction and activation of the MrgD by β-alanine. Furthermore, in our lab, establishing a structure-activity relationship

based on functional analysis of β-alanine related compounds has provided information on the binding site of the hMrgD receptor (Müller, 2014). The binding site for the agonist in the hMrgD receptor is spatially very limited. The amino and carboxylic acid function groups should have a defined distance to each other to interact effectively with the receptor. Moreover, substituents of the short carbon chain of β-alanine are only accepted to a very limited extent with the guarantee of the hydrophobic interactions of the carbon chain of β-alanine (Müller, 2014).

It has been postulated that both β-alanine and alamandine bind to the same orthosteric binding pocket of the MrgD receptor. This hypothesis was initially based on two reported findings by Lautner and co-workers (2013). First, when the binding of alamandine to MrgD-stably transfected CHO cells was competed by β-alanine. Second, when alamandine-induced vasorelaxation of the aortic rings from FVB/N mice was inhibited upon pre-treatment with β-alanine (Lautner et al., 2013). Another research group studied the possible molecular interactions within the MrgD/ alamandine complex (Qaradakhi et al., 2017). A homology model was built based on the crystal structure of the angiotensin AT1-receptor. The model together with molecular dynamic simulations displayed an interaction and stable proximity between the C-terminus of alamandine and the 2-positively charged residues K3.29 and R7.39 located in the orthosteric site of MrgD. These together with T2.60, H3.25, M3.26, M3.32, W6.55, L6.58, V7.32, and F7.35 residues were found to constitute the main interface for MrgD interaction with alamandine (Qaradakhi et al., 2017). The interaction pattern of MrgD with alamandine (Qaradakhi et al., 2017) is interestingly similar to what expected for β-alanine as revealed from site-directed mutagenesis studies (Arbogast et al., 2018) with TMs 3, 6, and 7 constituting the active binding site. Together with findings from the present work, alamandine is likely a partial agonist at the MrgD receptor which occupies the orthosteric binding site of the receptor with only partial efficacy. Partial agonists act as competing antagonists in the presence of full agonists, inhibiting the latter maximal response. As a proof of concept, functional experiments targeting G protein-dependent and G protein-independent pathways in recombinant cell systems using β-alanine and alamandine, each alone and together should be performed.

Polar interactions are the primary driving forces for peptide recognition and binding. Alignment of binding site residues from different GPCRs-peptide crystal structures together with SAR and mutagenesis studies, have classified class A peptide GPCRs into three major groups (see review Tikhonova et al., 2019). In one group where the receptors bind the free C-

terminal carboxyl group of peptides, conserved positively charged residues at positions 4.64, 5.42, and 6.55 in the receptor helical bundle were found essential in forming polar interactions with either the C-terminus of the peptide or peptide backbone (Tikhonova et al., 2019). That could also mean that the primary receptor at which alamandine acts as a full agonist is another receptor than the MrgD receptor. Directed mutagenesis studies followed by functional characterization of MrgD using alamandine are needed to examine all these residues and to validate the reported interactions.

6. Summary and Conclusion

The GPCR MrgD is mainly expressed in small diameter DRG sensory neurons and has been implicated to play role in nociception. Receptor involvement in cardiovascular, and retinal functions and contribution to lung tumors development have been reported. In the present work, the hMrgD receptor was further characterized. That was achieved using the first recognized endogenous ligand "β-alanine", the newly discovered RAS peptide "alamandine", and other compounds which were reported to activate the receptor. Looking for new antagonists and further investigating known ones was also addressed in this work. Beside the Gα protein-dependent receptor signaling, for the first time we provide evidence on the Gα protein-independent signaling of the hMrgD receptor through coupling to the β-arrestin pathway. Interestingly, evidence for biased signaling of the hMrgD receptor could also be revealed in this work.

CHO Flp-In cells stably expressing a short variant of the hMrgD receptor formerly studied by our group were further used as the expression system in the current research. In previous findings, β-alanine caused increases in Fluo-4 fluorescence in CHO-hMrgD cells as microscopically observed. In the present work, quantitation of such concentration-dependent increments was done. Moreover, control experiments were performed where β-alanine failed to stimulate a similar response in non-transfected control cells, thus ensuring specificity of response and approving lack of expression of MrgD in CHO cells. Alamandine-induced Ca^{2+} increases via the hMrgD receptor were also studied. Interestingly, alamandine stimulated similar small, and short increments in Fluo-4 fluorescence, both in hMrgD-transfected and in non-transfected CHO cells. However, later stimulation with β-alanine caused strong, and extended signal rises only in hMrgD transfected cells. Targeting the Gαi or Gαs/cAMP pathway using the AlphaScreen cAMP assay was the next step. As reported in primary and HEK293 cells, in our cell system, alamandine showed a bell-shaped concentration response curve with cAMP increases at low concentrations and decreases at higher ones. Such pattern of response was again similar in both hMrgD-transfected and non-transfected cell lines. On the other hand, β-alanine inhibited forskolin-induced cAMP increments only in hMrgD-CHO cells. Together, findings suggest the likely expression of an endogenous receptor in CHO cells through which alamandine is mediating its G protein-dependent responses.

For better understanding of the hMrgD receptor signaling, we studied the receptor coupling to the β-arrestin pathway using the highly sensitive PathHunter β-arrestin assay. First, the assay was established and validated using β-alanine which caused concentration-dependent activation and recruitment of β-arrestin-2 following 90 min of incubation. Then, a wide concentration range of alamandine was tested. In contrast to the strong signal elicited by β-alanine, alamandine stimulated a weak response. To exclude the interaction kinetics factor, shorter (60 min) and longer (120 min) incubation periods were additionally investigated, where β-alanine signal was greatly reduced and alamandine response was completely abolished. These data complement previous findings, suggesting that alamandine is likely a partial agonist at the MrgD receptor, and that the primary receptor mediating its actions is another one. Reported as a weak MrgD agonist in few studies, the precursor of alamandine, the heptapeptide "angiotensin 1-7" was a candidate to examine its action. Angiotensin 1-7 failed to activate the hMrgD receptor and recruit β-arrestin-2 at any of the tested concentrations. In previous work by our group, small molecules structural analogues of β-alanine experienced agonist potentials as revealed by NFAT-luciferase and [^{3}H] radioaffinity cAMP assays. In the present work, these compounds were further investigated using the β-arrestin assay. All of DL-3-aminoisobutyric acid, DL-3-aminobutyric acid, and GABA caused concentration-dependent increases in β-arrestin-2 recruitment, however with different potencies. DL-3-aminoisobutyric acid showed similar efficacy as β-alanine but with slightly lower potency. DL-3-aminobutyric acid and GABA had a markedly right-shifted concentration-response curves as compared to that of β-alanine, confirming their low affinity, and weak agonist activities at the hMrgD receptor. Interestingly, the rank order potency of DL-3-aminobutyric acid and GABA in the β-arrestin assay was the reverse to that previously observed in the NFAT-luciferase assay. This could suggest a biased signaling potential of these two ligands, where GABA preferentially activate the G protein-dependent pathway, while DL-3-aminobutyric acid prefers the β-arrestin pathway. The dipeptide L-carnosine was also investigated based on previous observations that it accelerated NFAT luciferase expression, while could not inhibit cAMP levels. In the current work, L-carnosine could not induce β-arrestin-2 recruitment, suggesting a lack of activity at the hMrgD receptor and supporting the hypothesis that the observed response in NFAT assay was due to the dipeptide breakdown to β-alanine. Signaling of the polyunsaturated fatty acid "5-Oxo-ETE" via the hMrgD receptor was studied in this work. 5-Oxo-ETE could stimulate a weak signal in NFAT-luciferase reporter gene assay, however, lacked any response in the β-arrestin assay.

Owing to the cytotoxic effects of EtOH and subsequently the limited concentration-range tested, the activity of 5-Oxo-ETE at the hMrgD receptor remain questioned.

Among some screened amino acids, interestingly, D-(+)-3-phenyllactic acid lowered the NFAT-luciferase signal below the constitutive activity level of the receptor. In further examinations, D-(+)-3-phenyllactic acid could inhibit β-alanine-induced signal increases. These findings may suggest a weak inverse agonist activity of D-(+)-3-phenyllactic acid at the hMrgD receptor. Antipsychotic compounds like rimacazole, chlorpromazine, and thioridazine which were characterized as weak antagonists in former research as shown in NFAT-luciferase and [^{3}H] radioaffinity cAMP assays, were further studied in the current work using the β-arrestin recruitment assay. Interestingly, none of them could inhibit β-alanine potential to recruit β-arrestin-2 as observed from the failed right-shifting of β-alanine concentration-response curve in their presence. These findings indicate that these compounds act as weak G protein biased antagonists of the hMrgD receptor.

Under our experimental conditions and in scope of the studied hMrgD signaling, the data provided conclude that β-alanine is the most potent endogenous agonist of the hMrgD receptor so far identified. The peptide alamandine is likely to act as a high affinity, but weak partial agonist at the hMrgD receptor. For the first time, our research present evidence on the coupling of the hMrgD receptor to the β-arrestin pathway. Moreover, our data could reveal biased signaling of some agonists and antagonists at the hMrgD receptor which could serve as templates for developing more potent biased alternatives. It would be important to perform more detailed investigation of the signaling cascade downstream of the β-arrestin pathway using β-alanine, and to study the functional consequence in disease models.

7. References

Adams C, Rathbone J, Thornley B, Clarke M, Borrill J, Wahlbeck K and and Awad AG (2005) Chlor-promazine for schizophrenia: a Cochrane systematic review of 50 years of randomised controlled trials. *BMC Med* 3:15.

Ajit SK, Pausch MH, Kennedy JD and Kaftan EJ (2010) Development of a FLIPR assay for the simultaneous identification of MrgD agonists and antagonists from a single screen. *J Biomed Biotechnol* 2010:326020.

Alkanfari I, Gupta K, Jahan T, Ali H (2018) Naturally Occurring Missense MRGPRX2 Variants Display Loss of Function Phenotype for Mast Cell Degranulation in Response to Substance P, Hemokinin-1, Human β-Defensin-3, and Icatibant. *J Immunol* 201:343-349.

Allen JA, and Roth BL (2011) Strategies to discover unexpected targets for drugs active at G protein–coupled receptors. *Annu Rev Pharmacol Toxicol* 51:117–144.

Al-Mohanna FA, Caddy KW, and Bolsover SR (1994) The nucleus is insulated from large cytosolic calcium ion changes. *Nature* 367:745–750.

Al-Sabah S, Al-Fulaij M, Shaaban G, Ahmed HA, Mann RJ, Donnelly D, Bünemann M, and Krasel C (2014) The GIP receptor displays higher basal activity than the GLP-1 receptor but does not recruit GRK2 or arrestin3 effectively. *PLoS One* 9:e106890.

Alvarez-Curto E, Inoue A, Jenkins L, Raihan SZ, Prihandoko R, Tobin AB, and Milligan G (2016) Targeted elimination of G proteins and arrestins defines their specific contributions to both intensity and duration of G-protein-coupled signaling. J Biol Chem 291: 27147-27159.

Amaral L, and Molnar J (2012) Potential therapy of multidrug-resistant and extremely drug-resistant tuberculosis with thioridazine. *In Vivo* 26:231-236.

Ambroz C, Clark AJL, and Catt KJ (1991) The mas oncogene enhances angiotensin induced [Ca2+]i responses in cells with pre-existing angiotensin II receptors. *Biochim Biophys Acta* 1133:107–111.

Amson R, Auclair C, André F, Karp J, and Telerman A (2017) Targeting TCTP with Sertraline and Thioridazine in Cancer Treatment. *Results Probl Cell Differ.* 64:283-290.

Annweiler C, Cao Z, Wu Y, Faucon E, Mouhat S, Kovacic H, and Sabatier J-Met (2020) Counter-regulatory 'Renin-Angiotensin' System-based Candidate Drugs to Treat COVID-19 Diseases in SARS-CoV-2-infected patients. *Infect Disord Drug Targets* 20:407-408.

Arbogast M, Hanna DMF, Müller S, Sargheini N, Hoffmann K, and von Kügelgen I (2018) Analysis of the ligand binding site of the human Mas-related G protein-coupled receptor D by site-directed mutagenesis. *Naunyn-Schmiedebergs Arch Pharmacol* 391 Supp 1: S32.

Armstrong MD, Yates K, Kakimoto Y, Taniguchi K, and Kappe T (1963) Excretion of *β*-aminoisobutyric acid by man. *J Biol Chem* 238:1447–1455.

Artoli GG, Gualano B, Smith A, Stout J, and Lancha AH (2009) Role of β-alanine supplementation on muscle carnosine and exercise performance. *Med Sci Sports Exerc* 42:1162–1173.

Attramadal H, Arriza JL, Aoki C, Dawson TM, Codina J, Kwatra MM, Snyder SH, Caron MG, and Lefkowitz RJ (1992) Beta-arrestin2, a novel member of the arrestin/beta-arrestin gene family. *J Biol Chem* 267:17882–17890.

Bader M (2013) ACE2, angiotensin-(1-7), and Mas: the other side of the coin. *Pflugers Arch* 465:79–85.

Bader M, Alenina N, Andrade-Navarro MA, and Santos RA (2014) MAS and its related G protein-coupled receptors, Mrgprs. *Pharmacol Rev* 66:1080-1105.

Bader M, Peters J, Baltatu O, Müller DN, Luft FC, and Ganten D (2001) Tissue renin-angiotensin systems: new insights from experimental animal models in hypertension research. *J Mol Med (Berl).* 79:76–102.

Baguet A, Koppo K, Pottier A, and Derave W (2010) Beta-alanine supplementation reduces acidosis but not oxygen uptake response during high-intensity cycling exercise. *Eur J Appl Physiol* 108:495– 503.

Ballesteros J, and Weinstein H (1995) Integrated methods for the construction of three-dimensional models and computational probing of structure-function relations in G protein-coupled receptors. *Methods Neurosci* 25:366-428.

Ballesteros JA, Jensen AD, Liapakis G, Rasmussen SGF, Shi L, Gether U, and Javitch JA (2001) Activation of the beta(2)- adrenergic receptor involves disruption of an ionic lock between the cytoplasmic ends of transmembrane segments 3 and 6. *J Biol Chem* 276:29171–29177.

Bang I, and Choi HJ (2015) Structural Features of β2 Adrenergic Receptor: Crystal Structures and Beyond. *Mol Cells* 38:105–111.

Bartuzi D, Kaczor AA, Targowska-Duda KM, and Matosiuk D (2017) Recent Advances and Applications of Molecular Docking to G Protein-Coupled Receptors. *Molecules* 2017 22:340.

Bautzova T, Hockley JRF, Perez-Berezo T, Pujo J, Tranter MM, Desormeaux C, Barbaro MR, Basso L, Le Faouder P, Rolland C, Malapert P, Moqrich A, Eutamene H, Denadai-Souza A, Vergnolle N, Smith ESJ, Hughes DI, Barbara G, Dietrich G, Bulmer DC, Cenac N (2018) 5-oxoETE triggers nociception in constipation-predominant irritable bowel syndrome through MAS-related G protein-coupled receptor D. *Sci Signal* 11:eaal2171.

Begriche K, Massart J, Abbey-toby A, Igoudjil A, Lettéron P, and Fromenty (2008) β-Aminoisobutyric Acid Prevents Diet-induced Obesity in Mice with Partial Leptin Deficiency. *Obesity* 16:2053–2067.

Beitz E (2000) TEXtopo: shaded membrane protein topology plots in LATEX2ε. *Bioinformatics* 16:1050–1051.

Benovic JL, Kühn H, Weyand I, Codina J, Caron MG, and Lefkowitz RJ (1987) Functional desensitization of the isolated beta-adrenergic receptor by the beta-adrenergic receptor kinase: potential role of an analog of the retinal protein arrestin (48-kDa protein). *Proc Natl Acad Sci* 84: 8879–8882.

Biebermann H, Schöneberg T, Schulz A, Krause G, Grüters A, Schultz G, and Gudermann T (1998) A conserved tyrosine residue (Y601) in transmembrane domain 5 of the human

thyrotropin receptor serves as a molecular switch to determine G-protein coupling. *FASEB J* 12:1461–1471.

Bikkavilli RK, Tsang SY, Tang WM, Sun JX, Ngai SM, Lee SS, Ko WH, Wise H, and Cheung WT (2006) Identification and characterization of surrogate peptide ligand for orphan G protein-coupled receptor mas using phage displayed peptide library. *Biochem Pharmacol* 71:319–337.

Blackburn-Munro G, and Jensen BS (2003) The anticonvulsant retigabine attenuates nociceptive behaviours in rat models of persistent and neuropathic pain. *Eur J Pharmacol* 460:109 –116.

Boldyrev AA, Aldini G, and Derave W (2013) Physiology and pathophysiology of carnosine. *Physiol Rev* 93:1803–1845.

Bond RA, Lucero Garcia-Rojas EY, Hegde A, and Walker JKL (2019) Therapeutic Potential of Targeting ß-Arrestin. *Front Pharmacol* 10:124.

Bronstein I, Fortin J, Stanley PE, Stewart GS, and Kricka LJ (1994) Chemiluminescent and bioluminescent reporter gene assays. *Anal Biochem* 219:169-181.

Burstein ES, Ott TR, Feddock M, Ma JN, Fuhs S, Wong S, Schiffer HH, Brann MR, and Nash NR (2006) Characterization of the Mas-related gene family: structural and functional conservation of human and rhesus MrgX receptors. *Br J Pharmacol* 147:73–82.

Cahill TJ 3rd, Thomsen AR, Tarrasch JT, Plouffe B, Nguyen AH, Yang F, Huang L-Y, Kahsai AW, Bassoni DL, Gavino BJ, Lamerdin JE, Triest S, Shukla AK, Berger B, Little J 4th, Antar A, Blanc A, Qu C-X, Chen X, Kawakami K, Inoue A, Aoki J, Steyaert J, Sun J-P, Bouvier M, Skiniotis G, and Lefkowitz RJ (2017) Distinct conformations of GPCR–-arrestin complexes mediate desensitization, signaling, and endocytosis. *Proc Natl Acad Sci U S A* 114:2562–2567.

Cai K, Itoh Y, and Khorana HG (2001) Mapping of contact sites in complex formation between transducin and light-activated rhodopsin by covalent crosslinking: use of a photoactivatable reagent. *Proc Natl Acad Sci U S A* 98:4877–4882.

Cameron JD, Lane PL, and Speechley M (1995) Intravenous chlorpromazine vs intravenous metoclopramide in acute migraine headache. *Acad Emerg Med* 2:597–602.

Campbell AP, and Smrcka AV (2018) Targeting G protein-coupled receptor signalling by blocking G proteins. Nat Rev Drug Discov 17:789-803.

Carpenter B, Nehme´ R, Warne T, Leslie AG, and Tate CG (2016) Structure of the adenosine A(2A) receptor bound to an engineered G protein. *Nature* 536:104–107.

Carr R 3rd, Schilling J, Song J, Carter RL, Du Y, Yoo SM, Traynham CJ, Koch WJ, Cheung JY, Tilley DG, and Benovic JL (2016) β-arrestin-biased signaling through the β2-adrenergic receptor promotes cardiomyocyte contraction. *Proc Natl Acad Sci U S A* 113:E4107-4116.

Castro CH, Santos RA, Ferreira AJ, Bader M, Alenina N, and Almeida AP (2005) Evidence for a functional interaction of the angiotensin-(1-7) receptor Mas with AT1 and AT2 receptors in the mouse heart. *Hypertension* 46:937–942.

Caterina MJ, and Julius D (1999) Sense and specificity: a molecular identity for nociceptors. *Curr. Opin. Neurobiol* 9:525–530.

Cavanaugh DJ, Lee H, Lo L, Shields SD, Zylka MJ, Basbaum AI, and Anderson DJ (2009) Distinct subsets of unmyelinated primary sensory fibers mediate behavioral responses to noxious thermal and mechanical stimuli. *Proc Natl Acad Sci U S A* 106: 9075–9080.

Cerniello FM, Carretero OA, Longo Carbajosa NA, Cerrato BD, Santos RA, Grecco HE, and Gironacci MM (2017) MAS1 Receptor Trafficking Involves ERK1/2 Activation Through a β-Arrestin2-Dependent Pathway. *Hypertension* 70:982-989.

Chapman NA, Dupré DJ, Rainey JK (2014) The apelin receptor: physiology, pathology, cell signalling, and ligand modulation of a peptide-activated class A GPCR. *Biochem Cell Biol* 92:431-440.

Charbit AR, Akerman S, and Goadsby PJ (2010). Dopamine: what's new in migraine? *Curr Opin Neurol*. 23:275–281.

Chen CC, Akopian AN, Sivilotti L, Colquhoun D, Burnstock G, and Wood JN (1995) A P2X purinoceptor expressed by a subset of sensory neurons. *Nature* 377:428–431.

Cheng Z, Garvin D, Paguio A, Stecha P, Wood K and Fan F (2010) Luciferase reporter assay system for deciphering GPCR pathways. *Curr Chem Genomics* 4: 84-91.

Cherezov V, Rosenbaum DM, Hanson MA, Rasmussen SGF, Thian FS, Kobilka TS, Choi HJ, Kuhn P, Weis WI, Kobilka BK, and Stevens RC (2007) High-resolution crystal structure of an engineered human β2–adrenergic G protein–coupled receptor. *Science* 318:1258–1265.

Chini B, and Parenti M (2009) G-protein-coupled receptors, cholesterol and palmitoylation: facts about fats. *J. Mol. Endocrinol 42*:371-379.

Choe HW, Park JH, Kim YJ, and Ernst OP (2011) Transmembrane signaling by GPCRs: insight from rhodopsin and opsin structures. *Neuropharmacology* 60:52–57.

Chouinard G, and Annable L (1984) An early phase II clinical trial of BW234U in the treatment of acute schizophrenia in newly admitted patients. *Psychopharmacology* 84:282–284.

Christianson JA, Traub RJ, and Davis BM (2006) Differences in spinal distribution andneurochemical phenotype of colonic afferents in mouse and rat. *J. Comp. Neurol.* 494:246–259.

Chung S, Funakoshi T, and Civelli O (2008) Orphan GPCR research. *Br J Pharmacol* 153:339–346.

Civelli O (2005) GPCR deorphanizations: the novel, the known and the unexpected transmitters. *Trends Pharmacol Sci* 26:15–19.

Civelli O, Reinscheid RK, Zhang Y, Wang Z, Fredriksson R, and Schioth HB (2013) G protein-coupled receptor deorphanizations. *Annu Rev Pharmacol Toxicol* 53:127–146.

Civelli O, Saito Y, Wang Z, Nothacker H, and Reinscheid RK (2006) Orphan GPCRs and their ligands. *Pharmacol Ther* 110:525–532.

Cohen YR (2002) b-Aminobutyric Acid-Induced Resistance Against Plant Pathogens. *Plant Dis* 86:448–457.

Cohen-Mansfield J, Taylor L, Woosley R, Lipson S, Werner P and Billig N (2000) Relationships be-tween psychotropic drug dosage, plasma drug concentration, and prolactin levels in nursing home residents. *Ther Drug Monit* 22:688–694.

Coleman DE, Berghuis AM, Lee E, Linder ME, Gilman AG, and Sprang SR (1994) Structures of active conformations of Gi alpha 1 and the mechanism of GTP hydrolysis. *Science* 1265:1405-1412.

Coward P, Chan SD, Wada HG, Humphries GM, and Conklin BR (1999) Chimeric G proteins allow a high-throughput signaling assay of Gi-coupled receptors. *Anal Biochem* 270:242–248.

Cox PJ, Pitcher T, Trim SA, Bell CH, Qin W, and Kinloch RA (2008) The effect of deletion of the orphan G - protein coupled receptor (GPCR) gene MrgE on pain-like behaviours in mice. *Mol Pain* 4:2.

Crabtree GR, and Olson EN (2002) NFAT signaling: choreographing the social lives of cells. *Cell* 109:S67–79.

Crozier RA, Ajit SK, Kaftan EJ, and Pausch MH (2007) MrgD activation inhibits KCNQ/M-currents and contributes to enhanced neuronal excitability. *J Neurosci* 27:4492-4496.

Cusack KP, Wang Y, Hoemann MZ, Marjanovic J, Heym RG, and Vasudevan A (2015) Design strategies to address kinetics of drug binding and residence time. *Bioorg Med Chem Lett* 25:2019-2027.

Davidson J, Miller R, Wingfield M, Zung W, and Dren AT (1982). The first clinical study of BW-234U in schizophrenia. *Psychopharmacol Bull* 18:173–176.

de Almeida PE, van Rappard JR, and Wu JC (2011) In vivo bioluminescence for tracking cell fate and function. *Am J Physiol Heart Circ Physio*l 301:H663-H671.

de Souza-Neto FP, Carvalho Santuchi M, de Morais E Silva M, Campagnole-Santos MJ, and da Silva RF (2018) Angiotensin-(1-7) and Alamandine on Experimental Models of Hypertension and Atherosclerosis. *Curr Hypertens Rep* 20:17.

de Souza-Neto FP, Silva MME, Santuchi MC, de Alcântara-Leonídio TC, Motta-Santos D, Oliveira AC, Melo MB, Canta GN, de Souza LE, Irigoyen MCC, Campagnole-Santos MJ,

Guatimosim S, Santos RAS, and da Silva RF (2019) Alamandine attenuates arterial remodelling induced by transverse aortic constriction in mice. *Clin Sci (Lond).* 133:629-643.

DeGraff JL, Gagnon AW, Benovic JL, and Orsini MJ (1999) Role of arrestins in endocytosis and signaling of alpha2-adrenergic receptor subtypes. *J Biol Chem* 274:11253–11259.

DeGraff JL, Gurevich VV, and Benovic JL (2002) The third intracellular loop of alpha 2-adrenergic receptors determines subtype specificity of arrestin interaction. *J Biol Chem* 277:43247–43252.

Derave W, Everaert I, Beckman S, and Baguet A (2010) Muscle carnosine metabolism and β-alanine supplementation in relation to exercise and training. *Sports Med* 40:247–263.

Diaz C, Angelloz-Nicoud P, and Pihan E (2018) Modeling and Deorphanization of Orphan GPCRs. *Methods Mol Biol* 1705:413-429.

Dong X, Han S, Zylka MJ, Simon MI, and Anderson DJ (2001) A diverse family of GPCRs expressed in specific subsets of nociceptive sensory neurons. *Cell* 106:619–632.

Draper-Joyce CJ, Khoshouei M, Thal DM, Liang Y-L, Nguyen ATN, Furness SGB, Venugopal H, Baltos J-A, Plitzko JM, Danev R, Baumeister W, May LT, Wootten D, Sexton PM, Glikhova A, and Christopoulos A (2018) Structure of the adenosine-bound human adenosine A1 receptor-Gi complex. *Nature* 558:559–563.

Dror RO, Mildorf TJ, Hilger D, Manglik A, Borhani DW, Arlow DH, Philippsen A, Villanueva N, Yang Z, Lerch MT, Hubbell WL, Kobilka BK, Sunahara RK, and Shaw DE (2015) Signal transduction. Structural basis for nucleotide exchange in heterotrimeric G proteins. Science 348:1361–1365.

Du Y, Duc NM, Rasmussen SGF, Hilger D, Kubiak X, Wang L, Bohon J, Kim HR, Wegrecki M, Asuru A, Jeong KM, Lee J, Chance MR, Lodowski DT, Kobilka BK, and Chung KY (2019) Assembly of a GPCR-G Protein Complex. *Cell* 177:1232-1242.

Duan Y, Beli E, Li Calzi S, Quigley JL, Miller RC, Moldovan L, Feng D, Salazar TE, Hazra S, Al-Sabah J, Chalam KV, Phuong Trinh TL, Meroueh M, Markel TA, Murray MC, Vyas RJ, Boulton ME, Parsons-Wingerter P, Oudit GY, Obukhov AG, and Grant MB (2018) Loss

of Angiotensin-Converting Enzyme 2 Exacerbates Diabetic Retinopathy by Promoting Bone Marrow Dysfunction. *Stem Cells* 36:1430-1440.

Dudley K, Liu X, and De Haan S. (2017) Chlorpromazine dose for people with schizophrenia. *Cochrane Database Syst Rev 4*, CD007778.

Dupuis N, Laschet C, Franssen D, Szpakowska M, Gilissen J, Geubelle P, Soni A, Parent AS, Pirotte B, Chevigné A, Twizere JC, and Hanson J (2017) Activation of the Orphan G Protein-Coupled Receptor GPR27 by Surrogate Ligands Promotes *β*-Arrestin 2 Recruitment. *Mol Pharmacol*. 91:595-608.

Eason MG, Jacinto MT, and Liggett SB (1994) Contribution of ligand structure to activation of alpha 2-adrenergic receptor subtype coupling to Gs. *Mol Pharmacol* 45:696 –702.

Eglen RM, Reisine T, Roby P, Rouleau N, Illy C, Bosse R, and Bielefeld M (2008) The use of AlphaScreen technology in HTS: current status. *Curr Chem Genomics* 1:2–10.

Eichel K, Jullie D, Barsi-Rhyne B, Latorraca N. R, Masureel M, Sibarita JB, Dror RO, and von Zastrow M (2018) Catalytic activation of beta-arrestin by GPCRs. *Nature* 557:381–386.

Elster L, Elling C, and Heding A (2007) Bioluminescence Resonance Energy Transfer as a Screening Assay: Focus on Partial and Agonism. *J Biomol Screen* 12: 41-49.

Erlandson SC, McMahon C, and Kruse AC (2018) Structural Basis for G Protein-Coupled Receptor Signaling. *Annu Rev Biophys* 47:1-18.

Etelvino GM, Peluso AA, and Santos RA (2014) New components of the renin-angiotensin system: alamandine and the MAS-related G protein-coupled receptor D. *Curr Hypertens Rep* 16:433.

Farrant M, and Nusser Z (2005) Variations on an inhibitory theme: phasic and tonic activation of GABA(A) receptors. *Nat Rev Neurosci* 6:215–229.

Farrens DL, Altenbach C, Yang K, Hubbell WL, and Khorana HG (1996) Requirement of rigid-body motion of transmembrane helices for light activation of rhodopsin. *Science* 274:768–770.

Fenalti G, Giguere PM, Katritch V, Huang XP, Thompson AA, Cherezov V, Roth BL, and Stevens RC (2014) Molecular control of delta-opioid receptor signalling. *Nature* 506:191−196.

Ferrario CM (1990) Importance of the renin-angiotensin aldosterone system (RAS) in the physiology and pathology of hypertension. *Drugs* 39:l-8.

Ferris RM, Harfenist M, McKenzie GM, Cooper B, Soroko FE, and Mazwell RA (1982) BW 234U, (cis-9-[3-(3,5-dimethyl-1-piperazinyl) propyl] carbazole dihydrochloride): A novel antipsychotic agent. *J Pharm Pharmacol* 34:388–390.

Flock T, Hauser, AS, Lund N, Gloriam DE, Balaji S, and Babu MM (2017) Selectivity determinants of GPCR-G-protein binding. *Nature* 545:317–322.

Flower DR (1999) Modelling G-protein-coupled receptors for drug design. *Biochim Biophys Acta* 1422: 207-234.

Foord SM, Bonner TI, Neubig RR, Rosser EM, Pin J-P, Davenport AP, Spedding M, and Harmar AJ (2005) International Union of Pharmacology. XLVI. G protein-coupled receptor list. *Pharmacol Rev* 57:279-288.

Fraga-Silva RA, Ferreira AJ, and Dos Santos RA (2013) Opportunities for targeting the angiotensin-converting enzyme 2/angiotensin-(1-7)/ mas receptor pathway in hypertension. *Curr Hypertens Rep* 15:31–38.

Fredriksson R, Lagerström MC, Lundin L-G, and SchioÈth HB (2003) The G-protein-coupled receptors in the human genome form five main families. Phylogenetic analysis, paralogon groups, and fingerprints. *Mol Pharmacol* 63:1256-1272.

Frielle T, Collins S, Daniel KW, Carom MG, Lefkowitz RJ, Kobilka BK (1987) Cloning of the cDNA for the human beta 1-adrenergic receptor. *Proc Natl Acad Sci U S A* 84:7920–7924.

Gaidarov I, Adams J, Frazer J, Anthony T, Chen X, Gatlin J, Semple G, and Unett DJ (2018) Angiotensin (1-7) does not interact directly with MAS1, but can potently antagonize signaling from the AT1 receptor. *Cell Signal* 50:9-24.

Galandrin S, Denis C, Boularan C, Marie J, M'Kadmi C, Pilette C, Dubroca C, Nicaise Y, Seguelas M-H, N'Guyen D, Banères J-L, Pathak A, Sénard J-M, and Galés C (2016) Cardioprotective angiotensin-(1-7) peptide acts as a natural-biased ligand at the angiotensin II type 1 receptor. *Hypertension* 68:1365–1374.

García-Nafría J, Nehme´ R, Edwards PC, and Tate CG (2018) Cryo-EM structure of the serotonin 5-HT1B receptor coupled to heterotrimeric Go. *Nature* 558:620–623.

Gee KR, Brown KA, Chen WN, Bishop-Stewart J, Gray D, and Johnson I (2000) Chemical and physiological characterization of fluo-4 Ca(2+)-indicator dyes. *Cell Calcium* 27:97-106.

Gelfand AA, and Goadsby PJ (2012) A Neurologist's Guide to Acute Migraine Therapy in the Emergency Room. *Neurohospitalist* 2:51-59.

Gembardt F, Grajewski S, Vahl M, Schultheiss HP, and Walther T (2008) Angiotensin metabolites can stimulate receptors of the Mas related genes family. *Mol Cell Biochem* 319:115–123.

Ghosh E, Kumari P, Jaiman D, and Shukla AK (2015) Methodological advances: the unsung heroes of the GPCR structural revolution. *Nat Rev Mol Cell Biol* 16:69-81.

Gilmore DL, Liu Y, and Matsumoto RR (2004) Review of the pharmacological and clinical profile of rimcazole. *CNS Drug Rev* 10:1-22.

Gojkovic Z, Sandrini MP, and Piskur J (2001) Eukaryotic β-alanine synthases are functionally related but have a high degree of structural diversity. *Genetics* 158:999–1011.

Gomes ER, Santos RA, and Guatimosim S (2012) Angiotensin-(1-7)-mediated signaling in cardiomyocytes. *Int J Hypertens* 2012:493129.

Goncalves JA, South K, Ahuja S, Zaitseva E, Opefi CA, Eilers M, Vogel R, Reeves PJ, and Smith SO (2010) Highly conserved tyrosine stabilizes the active state of rhodopsin. *PNAS* 107:19861–19866.

Goodman OB Jr, Krupnick JG, Santini F, Gurevich VV, Penn RB, Gagnon AW, Keen JH, and Benovic JL (1996) β-arrestin acts as a clathrin adaptor in endocytosis of the β2-adrenergic receptor. *Nature* 383:447–450.

Goudet C, Gaven F, Kniazeff J, Vol C, Liu J, Cohen-Gonsaud M, Acher F, Prézeau L, and Pin JP (2004) Heptahelical domain of metabotropic glutamate receptor 5 behaves like rhodopsin-like receptors. *Proc Natl Acad Sci U S A* 101:378-383.

Grant GE, Rokach J, and Powell WS (2009) 5-Oxo-ETE and the OXE receptor. *Prostaglandins Other Lipid Mediat* 89:98–104.

Grisanti LA, Thomas TP, Carter RL, de Lucia C, Gao E, Koch WJ, Benovic JL, Tilley DG (2018) Pepducin-mediated cardioprotection via β-arrestin-biased β2-adrenergic receptor-specific signaling. *Theranostics* 8:4664-4678.

Grundmann M, Merten N, Malfacini D, Inoue A, Preis P, Simon K, Rüttiger N, Ziegler N, Benkel T, Schmitt NK, Ishida S, Müller I, Reher R, Kawakami K, Inoue Am Rick U, Kühl T, Imhof D, Aoki J, König GM, Hoffmann C, Gomeza J, Wess J, and Kostenis E (2018) Lack of beta-arrestin signaling in the absence of active G proteins. *Nat Commun* 9:341.

Grynkiewicz G, Poenie M, and Tsien RY (1985) A new generation of Ca2+ indicators with greatly improved fluorescence properties. *J Biol Chem* 260:3440-3450.

Gu YJ, Sun WY, Zhang S, Wu JJ, and Wei W (2015) The emerging roles of β-arrestins in fibrotic diseases. *Acta Pharmacol Sin* 36:1277-1287.

Gurevich VV, and Gurevich EV (2019) GPCR Signaling Regulation: The Role of GRKs and Arrestins. *Front Pharmacol* 10:125.

Gurwitz D, Haring R, Heldman E, Fraser CM, Manor D, and Fisher A (1994). Discrete activation of transduction pathways associated with acetylcholine m1 receptor by several muscarinic ligands. *Eur J Pharmacol* 267:21–31.

Gutierrez-de-Teran H, Massink A, Rodriguez D, Liu W, Han GW, Joseph JS, Katritch I, Heitman LH, Xia L, Ijzerman AP, Cherezov V, Katritch V, and Stevens RC (2013) The role of a sodium ion binding site in the allosteric modulation of the A(2A) adenosine G protein-coupled receptor. *Structure* 21:2175-2185.

Habiyakare B, Alsaadon H, Mathai ML, Hayes A, and Zulli A (2014) Reduction of angiotensin A and alamandine vasoactivity in the rabbit model of atherogenesis: differential effects of alamandine and Ang(1-7). *Int J Exp Pathol* 95:290–295.

Han SK, Dong X, Hwang JI, Zylka MJ, Anderson DJ, and Simon MI (2002) Orphan G protein-coupled receptors MrgA1 and MrgC11 are distinctively activated by RFamide- related peptides through the Galpha q/11 pathway. *Proc Natl Acad Sci U S A* 99:14740–14745.

Hanna DMF, Arbogast M, Müller S, and von Kügelgen I (2020) Coupling of the human Mas-related G protein coupled receptor D to the β-arrestin pathway. *Naunyn-Schmiedebergs Arch Pharmacol* 393 Supp 1: S33.

Hanson MA, Cherezov V, Griffith MT, Roth CB, Jaakola VP, Chien YET, Velasquez J, Kuhn P, and Stevens RCA (2008) specific cholesterol binding site is established by the 2.8 angstrom structure of the human beta2-adrenergic receptor. *Structure* 16:897−905.

Hanson MA, Roth CB, Jo E, Griffith MT, Scott FL, Reinhart G, Desale H, Clemons B, Cahalan SM, Schuerer SC, Sanna MG, Han GW, Kuhn P, Rosen H, and Stevens RC (2012) Crystal structure of a lipid G protein-coupled receptor. *Science* 335:851-855.

Hao JJ , Shi ZZ , Zhao ZX , Zhang Y, Gong T , Li CX , Zhan T , Cai Y , Dong JT, Fu SB , Zhan QM and Wan GMR (2012) Characterization of genetic rearrangements in esophageal squamous carcinoma cell lines by a combination of M-FISH and array-CGH: further confirmation of some split genomic regions in primary tumors. *BMC Cancer* 12: 367.

Hayaishi O, Nishizuka Y, Tatibana M, Takeshita M, and Kuno S (1961) Enzymatic studies on the metabolism of β-alanine. *J Biol Chem* 236:781–790.

Heitsch H, Brovkovych S, Malinski T, and Wiemer G (2001) Angiotensin- (1-7)-stimulated nitric oxide and superoxide release from endothelial cells. *Hypertension* 37:72–76.

Hekmat AS, Zare N, Moravej A, Meshkibaf MH, Javanmardi K (2019) Effect of Prolonged Infusion of Alamandine on Cardiovascular Parameters and Cardiac ACE2 Expression in a Rat Model of Renovascular Hypertension. *Biol Pharm Bull.* 42:960-967.

Hernandez-Ochoa EO, Contreras M, Cseresnyes Z, and Schneider MF (2007) Ca^{2+} signal summation and NFATc1 nuclear translocation in sympathetic ganglion neurons during repetitive action potentials. *Cell Calcium* 41:559–571.

Hipkiss A, Preston J, Himsworth D, Worthington V, Keown M, Michaelis J, Lawrence J, Mateen A, Allende L, and Eagles P (1998) Pluripotent protective effects of carnosine, a naturally occurring dipeptidea. *Ann N Y Acad Sci* 854:37–53.

Hislop JN, Caunt CJ, Sedgley KR, Kelly E, Mundell S, Green LD, and McArdle CA (2005) Internalization of gonadotropin-releasing hormone receptors (GnRHRs): does arrestin binding to the C-terminal tail target GnRHRs for dynamindependent internalization? *J Mol Endocrinol* 35:177–189.

Hockley JRF, Boundouki G, Cibert-Goton V, McGuire C, Yip PK, Chan C, Tranter M, Wood JN, Nassar MA, Blackshaw AL, Aziz Q, Michael GI, Baker MD, Winchester WJ, Knowles CH, and Bulmer DC (2014) Multiple roles for NaV1.9 in the activation of visceral afferents by noxious inflammatory, mechanical, and human disease-derived stimuli. *Pain* 155:1962–1975.

Hockley RF, Taylor TS, Callejo G, Wilbrey AL, Gutteridge A, Bach K, Winchester WJ, Bulmer DC, McMurray G, and Smith ESJ (2019) Single-cell RNAseq reveals seven classes of colonic sensory neuron. *Gut* 68: 633-644.

Hoffmann K (2010) Identifizierung der molekularen Interaktionstelle von Agonisten und neuen, hochpotenten Antagonisten am humanen P2Y12-Rezeptor (Dissertation).

Huang Y, Li Y, Lou A, Wang GZ, Hu Y, Zhang Y, Huang W, Wang J, Li Y, Zhu X, Chen T, Lin J, Meng Y, and Li X (2020) Alamandine attenuates hepatic fibrosis by regulating autophagy induced by NOX4 dependent ROS. *Clin Sci (lond)* 134:853-869.

Hunt SP, and Mantyh PW (2001) The molecular dynamics of pain control. *Nat Rev Neurosci* 2:83–91.

Hurley JB (1992) Signal transduction enzymes of vertebrate photoreceptors. *J Bioenerg Biomembr* 24:219-26.

Hurowitz EH, Melnyk JM, Chen YJ, Kouros-Mehr H, Simon MI, and Shizuya H (2000) Genomic characterization of the human heterotrimeric G protein alpha, beta, and gamma subunit genes. *DNA Res* 7:111-120.

Husbands SM, Izenwasser S, Kopajtic T, , Bowen WD, Vilner BJ, Katz JL, and Newman AH (1999) Structure-activity relationships at the monoamine transporters and ó receptors for a novel series of 9-[3-(cis-3,5-dimethyl-1-piperazinyl) propyl] carbazole (rimcazole) analogues. *J Med Chem* 42:4446–4455.

Husbands SM, Izenwasser S, Loeloff RJ, Katz JL, Bowen WD, Vilner BJ, and Newman AH (1997) Isothiocyanate derivatives of 9-[3-(cis-3,5-dimethyl-1-piperazinyl) propyl] carbazole (rimcazole): Irreversible ligands for the dopamine transporter. *J Med Chem* 40:4340–4346.

Ishihara T, Nakamura S, Kaziro Y, Takahashi T, Takahashi K, and Nagata S (1991) Molecular cloning and expression of a cDNA encoding the secretin receptor. *Embo J* 10:1635–1641.

Itoh Y, Cai K, and Khorana HG (2001) Mapping of contact sites in complex formation between light-activated rhodopsin and transducin by covalent crosslinking: use of a chemically preactivated reagent. *Proc Natl Acad Sci U S A* 98:4883–4887.

Izenwasser S, Newman AH, and Katz JL (1993) Cocaine and several ó receptor ligands inhibit dopamine uptake in rat caudate-putamen. *Eur J Pharmacol* 243:201–205.

Jackson TR and Hanley MR (1989) Tumor promoter 12-O-tetradecanoylphorbol 13-acetate inhibits mas/angiotensin receptor-stimulated inositol phosphate production and intracellular Ca2+ elevation in the 401L-C3 neuronal cell line. *FEBS Lett* 251:27–30.

Jackson TR, Blair LA, Marshall J, Goedert M, and Hanley MR (1988) The mas oncogene encodes an angiotensin receptor. *Nature* 335:437–440.

Jakab G, Rigoli G, and Zimmerli L (2001) b- Aminobutyric acid induced resistance in plants. *Eur J Plant Pathol* 107:29–37.

Janssen JWG, Steenvoorden ACM, Schmidtberger M, and Bartram CR (1988) Activation of the Mas oncogene during transfection of monoblastic cell line DNA. *Leukemia* 2:318–320.

Jastrzebska B (2013) GPCR: G protein complexes--the fundamental signaling assembly. *Amino Acids* 45:1303-1314.

Jesus ICG, Scalzo S, Alves F, Marques K, Rocha-Resende C, Bader M, Santos RAS, Guatimosim S (2018) Alamandine acts via MrgD to induce AMPK/NO activation against ANG II hypertrophy in cardiomyocytes. *Am J Physiol Cell Physiol*. 314:C702-C711.

Jesus ICG, Mesquita TRR, Monteiro ALL, Parreira AB, Santos AK, Coelho ELX, Silva MM, Souza LAC, Campagnole-Santos MJ, Santos RS, and Guatimosim S (2020) Alamandine enhances cardiomyocyte contractility in hypertensive rats through a nitric oxide-dependent activation of CaMKII. *Am J Physiol Cell Physiol* 318:C740-C750.

Ji TH., Grossmann M, and Ji I (1998) G protein-coupled receptors. I. Diversity of receptor–ligand interactions. *J. Biol. Chem* 273:17299–17302.

Job MO, and Katz JL (2019) A behavioral economic analysis of the effects of rimcazole on reinforcing effects of coca injection and food presentation in rats. *Psychopharmacology (Berl)* 236:3601-3612.

Jung TW, Hwang HJ, Hong HC, Yoo HJ, Baik SH, and Choi KM (2015) BAIBA attenuates insulin resistance and inflammation induced by palmitate or a high fat diet via an AMPK–PPAR_-dependent pathway in mice. *Diabetologia* 58:2096–2105.

Kang Y, Kuybeda O, de Waal P.W, Mukherjee S, Van Eps N, Dutka P, Zhou XE, Bartesaghi A, Erramilli S, Morizumi T, Gu X, Yin Y, Liu P, Jiang Y, Meng X, Zhao G, Melcher K, Ernst OP, Kossiakoff AA, Subramaniam M, and Xu HE (2018) Cryo-EM structure of human rhodopsin bound to an inhibitory G protein. *Nature* 558:553–558.

Kang Y, Zhou XE, Gao X, He Y, Liu W, Ishchenko A, Barty A, White TA, Yefanov O, Han GW, Xu Q, de Waal PW, Ke J, Tan MH, Zhang C, Moeller A, West GM, Pascal BD, Van Eps N, Caro LN[1], Vishnivetskiy SA, Lee RJ, Suino-Powell KM, Gu X, Pal K, Ma J, Zhi X, Boutet S, Williams GJ, Messerschmidt M, Gati C, Zatsepin NA, Wang D, James D, Basu S, Roy-Chowdhury S, Conrad CE, Coe J, Liu H, Lisova S, Kupitz C, Grotjohann I, Fromme R, Jiang Y, Tan M, Yang H, Li J, Wang M, Zheng Z, Li D, Howe N, Zhao Y, Standfuss J, Diederichs K, Dong Y, Potter CS, Carragher B, Caffrey M, Jiang H, Chapman HN, Spence JC, Fromme P, Weierstall U, Ernst OP, Katritch V, Gurevich VV, Griffin PR, Hubbell WL, Stevens RC, Cherezov V, Melcher K, and Xu H (2015) Crystal structure of rhodopsin bound to arrestin by femtosecond X-ray laser. *Nature* 523:561–567.

Kao JP, Harootunian AT, and Tsien RY (1989) Photochemically generated cytosolic calcium pulses and their detection by fluo-3. *J Biol Chem* 264: 8179–8184.

Karnik SS, Singh KD, Tirupula K, and Unal H (2017) Significance of angiotensin 1-7 coupling with MAS1 receptor and other GPCRs to the renin-angiotensin system: IUPHAR Review 22. *Br J Pharmacol* 174:737-753.

Katritch V, Cherezov V, and Stevens RC (2013) Structure-function of the G protein-coupled receptor superfamily. *Annu Rev Pharmacol Toxicol* 53:531-556.

Katritch V, Fenalti G, Abola EE, Roth BL, Cherezov V, and Stevens RC (2014) Allosteric sodium in class A GPCR signaling. *Trends Biochem Sci* 39:233–244.

Kenakin T (2007) Collateral efficacy in drug discovery: taking advantage of the good (allosteric) nature of 7TM receptors. *Trends Pharmacol Sci* 28:407–415.

Kest B, Mogil JS, SternbergWF, Pechnick RN, and Liebeskind JC (1995). Antinociception following 1,3-di-*o*-tolylguanidine, a selective ó receptor ligand. *Pharmacol Biochem Behav* 1995 50:587–592.

Khazaei M, Hosseini Nejad Mir N, Yadranji Aghdam F, Taheri M, and Ghafouri-Fard S (2019) Effectiveness of intravenous dexamethasone, metoclopramide, ketorolac, and chlorpromazine for pain relief and prevention of recurrence in the migraine headache: a prospective double-blind randomized clinical trial. *Neurol Sci* 2019 40:1029-1033.

Kim K, and Kim E (2005) The phenothiazine drugs inhibit hERG potassium channels. *Drug Chem Toxicol* 28:303-313.

Kim YJ, Hofmann KP, Ernst OP, Scheerer P, Choe H-W, and Sommer ME (2013) Crystal structure of pre-activated arrestin p44. *Nature* 497:142–146.

Kisselev OG, and Downs MA (2006) Rhodopsin-interacting surface of the transducin gamma subunit. *Biochemistry* 45:9386–9392.

Kitase Y, Vallejo JA, Gutheil W, Vemula H, Jähn K, Yi J, Zhou J, Brotto M, Bonewald and LF (2018) β-aminoisobutyric Acid, L-BAIBA, Is a Muscle-Derived Osteocyte Survival Factor. *Cell Rep* 22:1531–1544.

Kobayashi T, Ikeda K, Togashi S, Itoh N, and Kumanishi T (1997) Effects of ó ligands on the nociceptin_orphanin FQ receptor co-expressed with the G-protein-activated K+ channel in *Xenopus* oocytes. *Br J Pharmacol* 120:986–987.

Kobilka BK, and Deupi X (2007) Conformational complexity of G-protein-coupled receptors. *Trends Pharmacol Sci* 28:397- 406.

Koehl A, Hu H, Maeda S, Zhang Y, Qu Q, Paggi JM, Latorraca NR, Hilger D, Dawson R, Matile H, Schertler GFX, Granier S, Weis WI, Dror RO, Manglik A, Skiniotis G, and Kobilka BA (2018) Structure of the μ-opioid receptor-Gi protein complex. *Nature* 558:547–552.

Kohen R, Yamamoto Y, Cundy KC, and Ames BN (1988) Antioxidant activity of carnosine, homocarnosine, and anserine present in muscle and brain. *Proc Natl Acad Sci U S A* 85:3175–3179.

Kolakowski LF Jr (1994) GCRDb: A G-protein-coupled receptor database. *Receptors Channels* 2:1–7.

Kostenis E, Milligan G, Christopoulos A, Sanchez-Ferrer CF, Heringer-Walther S, Sexton PM, Gembardt F, Kellett E, Martini L, and Vanderheyden P, Schultheiss HP, and Walther T (2005) G-protein-coupled receptor Mas is a physiological antagonist of the angiotensin II type 1 receptor. *Circulation* 111:1806–1813.

Küçükibrahimoğlu E, Saygın M Z, Çalışkan M, Kaplan O K, Ünsal C and Gören M Z (2009) The change in plasma GABA, glutamine, and glutamate levels in fluoxetine- or S-citalopram-treated female patients with major depression. *Eur J Clin Pharmacol* 65:571–577.

Kumari P, Srivastava A, Ghosh E, Ranjan R, Dogra S, Yadav PN, and Shukla AK (2017) Core engagement with -arrestin is dispensable for agonist-induced vasopressin receptor endocytosis and ERK activation. *Mol Biol Cell* 28:1003–1010.

Lagerström MC, and Schiöth HB (2008) Structural diversity of G protein-coupled receptors and significance for drug discovery. *Nat Rev Drug Discov* 7:339-357.

Lally CC, Bauer B, Selent J, and Sommer ME (2017) C-edge loops of arrestin function as a membrane anchor. *Nat Commun* 8:14258.

Lambright DG, Noel JP, Hamm HE, and Sigler PB (1994) Structural determinants for activation of the alpha-subunit of a heterotrimeric G protein. *Nature* 369:621-628.

Lambright DG, Sondek J, Bohm A, Skiba NP, Hamm HE, and Sigler PB (1996) The 2.0 A crystal structure of a heterotrimeric G protein. *Nature* 379:311-319.

Laporte SA, Oakley RH, Zhang J, Holt JA, Ferguson SSG, Caron MG., and Barak LS (1999) The β2-adrenergic receptor/βarrestin complex recruits the clathrin adaptor AP-2 during endocytosis. *Proc Natl Acad Sci* 96:3712–3717.

Lappano R, and Maggiolini M. (2011) Gprotein-coupled receptors: novel targets for drug discovery in cancer. *Nat Rev Drug Discov* 10:47–60.

Latorraca NR, Wang JK, Bauer B, Townshend RJL, Hollingsworth SA, Olivieri JE, Xu HE, Sommer ME, and Dror RO (2018) Molecular mechanism of GPCR-mediated arrestin activation. *Nature* 557:452-456.

Lautner RQ, Villela DC, Fraga-Silva RA, Silva N, Verano-Braga T, Costa- Fraga F, Jankowski J, Jankowski V, Sousa F, Alzamora A, Soares E, Barbosa C, Kjeldsen F, Oliveira A, Braga J, Savergnini S, Maia G, Peluso AB, Passos-Silva D, Ferreira A, Alves F, Martins A, Raizada M, Paula R, Motta-Santos D, Klempin F, Pimenta A, Alenina N, Sinisterra R, Bader M, Campagnole-Santos MJ, and Santos RAS (2013) Discovery and characterization of alamandine: a novel component of the renin-angiotensin system. *Circ Res* 112:1104–1111.

Lebon G, Warne T, Edwards PC, Bennett K, Langmead CJ, Leslie AGW, and Tate CG (2011) Agonist-bound adenosine A2A receptor structures reveal common features of GPCR activation. *Nature* 474:521–525.

Lee K, Charbonnet M, and Gold M (2012) Upregulation of high-affinity GABAA receptors in cultured rat dorsal root ganglion neurons. *Neuroscience* 208:133–142.

Lee Y, Basith S, and Choi S (2018) Recent Advances in Structure-Based Drug Design Targeting Class A G Protein-Coupled Receptors Utilizing Crystal Structures and Computational Simulations. *J Med Chem* 61:1-46.

Lembo PM, Grazzini E, Groblewski T, O'Donnell D, Roy MO, Zhang J, Hoffert C, Cao J, Schmidt R, and Pelletier M, Labarre M, Gosselin M, Fortin Y, Banville D, Shen SH, Ström P,

Payza K, Dray A, Walker P, and Ahmad S (2002) Proenkephalin A gene products activate a new family of sensory neuron—specific GPCRs. *Nat Neurosci* 5:201–209.

Li B, Nowak NM, Kim SK, Jacobson KA, Bagheri A, Schmidt C, and Vess J (2005) Random mutagenesis of the M3 muscarinic acetylcholine receptor expressed in yeast: identification of second-site mutations that restore function to a coupling-deficient mutant M3 receptor. *J Biol Chem* 280:5664–5675.

Li P, Chen XR, Xu F, Liu C, Li C, Liu H, Wang H, Sun W, Sheng Y-H, and Kong X-Q (2018) Alamandine attenuates sepsis-associated cardiac dysfunction via inhibiting MAPKs signaling pathways. *Life Sci* 206:106–116.

Liang YL, Khoshouei M, Radjainia M, Zhang Y, Glukhova A, Tarrasch J, Thal DM, Furness SGB, Christopoulos G, Coudrat T, Danev R, Baumeister W, Miller LJ, Christopoulos A, Kobilka BK, Wootten D, Skiniotis G, and Sexton PM (2017) Phase-plate cryo-EM structure of a class B GPCR-G-protein complex. *Nature* 546:118–123.

Liu C, Yang CX, Chen XR, Liu BX, Li Y, Wang XZ, Sun W, Li P, and Kong XQ (2018) Alamandine attenuates hypertension and cardiac hypertrophy in hypertensive rats. *Amino Acids* 50:1071-1081.

Liu Q, Sikand P,Ma C, Tang Z, Han L, Li Z, Sun S, LaMotte RH, and Dong X (2012b) Mechanisms of itch evoked by β-alanine. *J Neurosci* 32:14532–14537.

Liu Q, Tang Z, Surdenikova L, Kim S, Patel KN, Kim A, Ru F, Guan Y, Weng HJ, Geng Y, Undem BJ, Kollarik M, Chen ZF, Anderson DJ, and Dong X (2009) Sensory neuron-specific GPCR Mrgprs are itch receptors mediating chloroquine-induced pruritus. *Cell* 139:1353–1365.

Liu W, Chun E, Thompson AA, Chubukov P, Xu F, Katritch V, Han GW, Roth CB, Heitman L H, AP IJ, Cherezov V, and Stevens RC (2012a) Structural basis for allosteric regulation of GPCRs by sodium ions. *Science* 337:232−236.

Liu X, Xu X, Hilger D, Aschauer P, Tiemann JKS, Du Y, Liu H, Hirata K, Sun X, Guixà-González R, Mathiesen JM, Hildebrand PW, and Kobilka BK (2019) Structural Insights into the Process of GPCR-G Protein Complex Formation. *Cell* 177:1243-1251.

Lohse M, Benovic J, Codina J, Caron M, and Lefkowitz R (1990) Beta- Arrestin: a protein that regulates beta-adrenergic receptor function. *Science* 248:1547–1550.

lter M, Mansoor S, and Sensoy O (2019) Utilization of Biased G Protein-Coupled Receptor Signaling towards Development of Safer and Personalized Therapeutics. *Molecules* 24:2052.

Lu M, and Wu B (2016) Structural studies of G protein-coupled receptors. *IUBMB Life.* 68:894-903.

Macian F (2005) NFAT proteins: key regulators of T-cell development and function. *Nat Rev Immunol* 5:472–484.

Mackay AV, Healey AF, and Baker JG (1974) The relationship of plasma chlorpromazine to its 7-hydroxy and sulphoxide metabolites in a large population of chronic schizophrenics. *Br J Clin Pharmacol* 1:425–430.

Maisonneuve C, Igoudjil A, Begriche K, Lettéron P, Guimont MC, Bastin J, Laigneau JP, Pessayre D, and Fromenty B (2004) Effects of zidovudine, stavudine and beta-aminoisobutyric acid on lipid homeostasis in mice: Possible role in human fat wasting. *Antivir Ther* 9:801–810.

Manning NJ, and Pollitt RJ (1985) Tracer studies of the interconversion of R- and S-methylmalonic semialdehydes in man. *Biochem J* 231:481–484.

Mayer D, Damberger FF, Samarasimhareddy M, Feldmueller M, Vuckovic Z, Flock T, Bauer B, Mutt E, Zosel F, Allain FHT, Standfuss J, Schertler GFX, Deupi X, Sommer ME, Hurevich M, Friedler A, and Veprintsev DB (2019) Distinct G protein-coupled receptor phosphorylation motifs modulate arrestin affinity and activation and global conformation. *Nat Commun* 10:1261.

Meixiong J, and Dong X (2017) Mas-Related G Protein-Coupled Receptors and the Biology of Itch Sensation. *Annu Rev Genet* 51:103-121.

Mendoza-Torres E, Oyarzun A, Mondaca-Ruff D, Azocar A, Castro PF, Jalil JE, Chiong M, Lavandero S, and Ocaranza MP (2015) ACE2 and vasoactive peptides: novel players in cardiovascular/renal remodeling and hypertension. *Ther Adv Cardiovasc Dis* 9: 217–237.

MiaoY, Caliman AD, and McCammon JA (2015) Allosteric effects of sodium ion binding on activation of the m3 muscarinic G-protein-coupled receptor. *Biophys J* 108:1796−1806.

Michalatou M, Androutsou ME, Antonopoulos M, Vlahakos DV, Agelis G, Zulli A, Qaradakhi T, Mikkelsen K, Apostolopoulos V, and Matsoukas J (2018) Transdermal Delivery of AT1 Receptor Antagonists Reduce Blood Pressure and Reveal a Vasodilatory Effect on Kidney Blood Vessels. *Curr Mol Pharmacol* 11:226-236.

Milasta S, Pediani J, Appelbe S, Trim S, Wyatt M, Cox P, Fidock M, and Milligan G (2006) Interactions between the Mas-related receptors MrgD and MrgE alter signalling and trafficking of MrgD. *Mol Pharmacol* 69:479–491.

Miller DJ, and O'Dowd A (2000) Vascular smooth muscle actions of carnosine as its zinc complex are mediated by histamine H(1) and H(2) receptors. *Biochemistry (Mosc)* 65:798-806.

Miller-Gallacher JL, Nehme R, Warne T, Edwards PC, Schertler GF, Leslie AG, and Tate CG (2014) The 2.1 A resolution structure of cyanopindolol-bound beta1-adrenoceptor identifies an intramembrane Na+ ion that stabilises the ligand-free receptor. *PLoS One* 9:e92727.

Minta A, Kao JP, and Tsien RY (1989) Fluorescent indicators for cytosolic calcium based on rhodamine and fluorescein chromophores. *J Biol Chem* 264:8171-8178.

Mixon MB, Lee E, Coleman DE, Berghuis AM, Gilman AG, and Sprang SR (1995) Tertiary and quaternary structural changes in Gi alpha 1 induced by GTP hydrolysis. *Science* 270:954-960.

Mody I, De Koninck Y, Otis TS, and Soltesz I (1994) Bridging the cleft at GABA synapses in the brain. *Trends Neurosci* 17:517–525.

Molliver DC, Wright DE, Leitner ML, Parsadanian AS, Doster K, Wen D, Yan Q, and Snider WD (1997) IB4-binding DRG neurons switch from NGF to GDNF dependence in early postnatal life. *Neuron* 19:849–861.

Morishita R, Nakayama H, Isobe T, Matsuda T, Hashimoto Y, Okano T, Fukada Y, Mizuno K, Ohno S, Kozawa O, Kato K, and Asano T (1995) Primary structure of a gamma subunit of G protein, 7I2, and its phosphorylation by protein kinase C. *J Biol Chem* 270**:**29469-29475.

Müller S (2014) Molekularpharmakologische Charakterisierung des humanen MRGD-Rezeptors *(Doctoral dissertation)*.

Müller S, Hoffmann K and von Kügelgen I (2012) MRGPRD receptor endogenously expressed in dorsal root ganglia: evidence for an activation by 3-aminoisobutyric acid. *Naunyn-Schmiedeberg's Arch Pharmacol* 385 Suppl 1:61.

Murphy TJ, Alexander RW, Griendling KK, Runge MS, and Bernstein KE (1991) Isolation of a cDNA encoding the vascular type-1 angiotensin II receptor. *Nature* 351:233–236.

Muthalif MM, Benter IF, Uddin MR, Harper JL, and Malik KU (1998) Signal transduction mechanisms involved in angiotensin-(1-7)-stimulated arachidonic acid release and prostanoid synthesis in rabbit aortic smooth muscle cells. *J Pharmacol Exp Ther* 284:388-398.

Nantel F, Bonin H, Emorine LJ, Zilberfarb V, Strosberg AD, Bouvier M, and Marullo S (1993) The human beta 3-adrenergic receptor is resistant to short term agonistpromoted desensitization. *Mol Pharmacol* 43:548–555.

Naylor L H (1999) Reporter gene technology: the future looks bright. *Biochem Pharmacol* 58:749–757.

Nederpelt I, Georgi V, Schiele F, Nowak-Reppel K, Fernández-Montalván AE, IJzerman AP, and Heitman LH (2016) Characterization of 12 GnRH peptide agonists - a kinetic perspective. *Br J Pharmacol* 173:128-141.

Neer EJ, Schmidt CJ, Nambudripad R, and Smith TF (1994) The ancient regulatory-protein family of WD-repeat proteins. *Nature* 371:297-300.

Nestler EJ, and Duman RS (1998) Heterotrimeric G Proteins. Basic Neurochemistry: Molecular, Cellular and Medical Aspects. 6th edition.

Ngo T, Kufareva I, Coleman JLj, Graham RM, Abagyan R, and Smith NJ (2016) Identifying ligands at orphan GPCRs: current status using structure-based approaches. *Br J Pharmacol* 173:2934-2951.

Nilsson LM, Nilsson-Ohman J, Zetterqvist AV, and Gomez MF (2008) Nuclear factor of activated T-cells transcription factors in the vasculature: the good guys or the bad guys? Curr Opin Lipidol. 19:483–490.

Nishimura S, Uno M, Kaneta Y, Fukuchi K, Nishigohri H, Hasegawa J, Komori H, Takeda S, Enomoto K, Nara F, and Agatsuma T (2012). MRGD, a MAS-related G-protein coupled receptor, promotes tumorigenisis and is highly expressed in lung cancer. *PLoS One*. 7:e38618. doi: 10.1371/journal.pone.0038618.

Noel JP, Hamm HE, and Sigler PB (1993) The 2.2 A crystal structure of transducin-alpha complexed with GTP gamma S. *Nature* 366:654-663.

Nygaard R, Frimurer TM, Holst B, Rosenkilde MM, and Schwartz TW (2009). Ligand binding and micro-switches in 7TM receptor structures. *Trends Pharmacol Sci* 30:249-259.

O'Hara PJ, Sheppard PO, Thøgersen H, Venezia D, Haldeman BA, McGrane V, Houamed KM, Thomsen C, Gilbert TL, and Mulvihill ER (1993) The ligand-binding domain in metabotropic glutamate receptors is related to bacterial periplasmic binding proteins. *Neuron* 11:41–52.

O'Gorman S, Fox DT, and Wahl GM (1991) Recombinase-mediated gene activation and site-specific integration in mammalian cells. *Science* 251:1351-1355.

Oliveira AC, Melo MB, Motta-Santos D, Peluso AA, Souza-Neto F, da Silva RF, Almeida JFQ, Canta G, Reis AM, Goncalves G, Cerri G, Coutinho D, Couto I, de Jesus G, Guatimosim S, Linhares ND, Alenina N, Bader M, Campagnole-Santos MJ, and Santos RAS (2019) Genetic deletion of the alamandine receptor mrgd leads to dilated cardiomyopathy in mice. *Am J Physiol* 316:H123–133.

Oliver AE, Baker GA, Fugate RD, Tablin F, and Crowe JH (2000) Effects of temperature on calcium-sensitive fluorescent probes. *Biophys J* 78:2116-2126.

Overington JP, Al-Lazikani B, and Hopkins AL (2006) How many drug targets are there? *Nat Rev Drug Discov* 5:993–996.

Paguio A, Garvin D, Swanson B, Worzella T, Wood K and Fan F (2006) Using luciferase reporter assays to screen for GPCR modulators. *Cell Notes* 16:22–25.

Palczewski K, Kumasaka T, Hori T, Behnke CA, Motoshima H, Fox BA, Le Trong I, Teller DC, Okada T, Stenkamp RE, Yamamoto M, and Miyano M (2000) Crystal structure of rhodopsin: a G protein-coupled receptor. *Science* 289:739–745.

Pan AC, Borhani DW, Dror RO, and Shaw DE (2013) Molecular determinants of drug-receptor binding kinetics. *Drug Discov Today* 18:667-673.

Park BM, Phuong HTA, Yu L, and Kim SH (2018) Alamandine Protects the Heart Against Reperfusion Injury via the MrgD Receptor. *Circ J* 82:2584-2593.

Park JH, Scheerer P, Hofmann KP, Choe H-W, and Ernst OP (2008) Crystal structure of the ligand-free G-protein coupled receptor opsin. *Nature* 454:183-187.

Passmore GM, Selyanko AA, Mistry M, Al-Qatari M, Marsh SJ, Matthews EA, Dickenson AH, Brown TA, Burbidge SA, Main M, and Brown DA (2003) KCNQ/M currents in sensory neurons: significance for pain therapy. *J Neurosci* 23:7227–7236.

Peroutka SJ, and Snyder SH (1980) "Relationship of neuroleptic drug effects at brain dopamine, serotonin, α-adrenergic, and histamine receptors to clinical potency," *American Journal of Psychiatry* 137:1518–1522.

Peterson YK, and Luttrell LM (2017) The diverse roles of Arrestin scaffolds in G protein–coupled receptor signaling. *Pharmacol. Rev* 69:256–297.

Peterson YK, and Luttrell LM (2017) The diverse roles of Arrestin scaffolds in G protein–coupled receptor signaling. *Pharmacol. Rev* 69:256–297.

Pfister C, Bennett N, Bruckert F, Catty P, Clerc A, Pagès F, and Deterre P (1993) Interactions of a G-protein with its effector: transducin and cGMP phosphodiesterase in retinal rods. *Cell Signal* 5:235-241.

Pin JP, Galvez T, and Prezeau L (2003) Evolution, structure, and activation mechanism of family 3/C G-protein-coupled receptors. *Pharmacol Ther* 98:325–354.

Powell WS, and Rokach J (2013) The eosinophil chemoattractant 5-oxo-ETE and the OXE receptor. *Prog Lipid Res* 52:651-665.

Powell WS, and Rokach J (2015) Biosynthesis, biological effects, and receptors of hydroxyeicosatetraenoic acids (HETEs) and oxoeicosatetraenoic acids (oxo-ETEs) derived from arachidonic acid. *Biochim Biophys Acta* 1851:340-55.

Pulvermüller A, Maretzki D, Rudnicka-Nawrot M, Smith WC, Palczewski K, and Hofmann KP (1997) Functional differences in the interaction of arrestin and its splice variant, p44, with rhodopsin. *Biochemistry* 36:9253–9260.

Qaradakhi T, Matsoukas MT, Hayes A, Rybalka E, Caprnda M, Rimarova K, Sepsi M, Büsselberg D, Kruzliak P, Matsoukas J, Apostolopoulos V, and Zulli A (2017). Alamandine reverses hyperhomocysteinemia-induced vascular dysfunction via PKA-dependent mechanisms. *Cardiovasc Ther* 35 doi: 10.1111/1755-5922.12306.

Rajagopal S, Rajagopal K, and Lefkowitz RJ (2010) Teaching old receptors new tricks: biasing seven-transmembrane receptors. *Nat Rev Drug Discov* 9:373–386.

Rasmussen SG, Choi HJ, Fung JJ, Pardon E, Casarosa P, Chae PS, Devree BT, Rosenbaum DM, Thian FS, Kobilka TS, Schnapp A, Konetzki I, Sunahara RK, Gellman SH, Pautsch A, Steyaert J, Weis WI, and Kobilka BK (2011b). Structure of a nanobody-stabilized active state of the β2 adrenoceptor. *Nature* 469:175–180.

Rasmussen SG, Choi HJ, Rosenbaum DM, Kobilka TS, Thian FS, Edwards PC, Burghammer M, Ratnala VR, Sanishvili R, Fischetti RF, Schertler GF, Weis WI, and (2007) Crystal structure of the human beta2 adrenergic G-protein-coupled receptor. *Nature* 450:383-387.

Rasmussen SG, DeVree BT, Zou Y, Kruse AC, Chung KY, Kobilka TS, Thian FS, Chae PS, Pardon E, Calinski D, Mathiesen JM, Shah ST, Lyons JA, Caffrey M, Gellman SH, Steyaert J, Skiniotis G, Weis WI, Sunahara RK, and Kobilka BK (2011a) Crystal structure of the beta2 adrenergic receptor-Gs protein complex. *Nature* 477:549-555.

Richelson E (1988) Neuroleptic Binding to Human Brain Receptors: Relation to Clinical Effects. *Ann NY Acad Sci* 537:435–442.

Ring AM, Manglik A, Kruse AC, Enos MD, Weis WI, Garcia KC, and Kobilka BK (2013) Adrenaline-activated structure of β2-adrenoceptor stabilized by an engineered nanobody. *Nature* 502:575–79.

Rinne A, and Blatter LA (2010) Activation of NFATc1 is directly mediated by IP3 in adult cardiac myocytes. *Am J Physiol Heart Circ Physiol*. 299 :H1701-H1707.

Rinne A, Banach K, and Blatter LA (2009) Regulation of nuclear factor of activated T cells (NFAT) in vascular endothelial cells. *J Mol Cell Cardiol* 47:400–410.

Rinne A, Kapur N, Molkentin JD, Pogwizd SM, Bers DM, Banach K, and Blatter LA (2010) Isoform- and tissue-specific regulation of the Ca^{2+}-sensitive transcription factor NFAT in cardiac myocytes and in heart failure. *Am J Physiol Heart Circ Physiol* 298:H2001–2009.

Ririe DG, Roberts PR, Shouse MN, and Zaloga GP (2000) Vasodilatory actions of the dietary peptide carnosine. *Nutrition* 16:168–172.

Ritter SL, and Hall RA (2009) Fine-tuning of GPCR activity by receptor-interacting proteins. *Nat Rev Mol Cell Biol* 10:819–830.

Roberts LD, Boström P, O'Sullivan JF, Schinzel RT, Lewis GD, Dejam A, Lee YK, Palma MJ, Calhoun S, Georgiadi A, Chen M-H, Ramachandran VS, Larson MG, Bouchard C, Rankinen T, Souza AL, Clish CB, Wang TJ, Estall JL, Soukas AA, Cowan CA, Spiegelman BM, and Gerszten RE (2014) β-Aminoisobutyric acid induces browning of white fat and hepatic β-oxidation and is inversely correlated with cardiometabolic risk factors. *Cell Metab* 19:96–108.

Robinson, DR, McNaughton PA, Evans ML, and Hicks GA (2004) Characterization of the primary spinal afferent innervation of the mouse colon using retrograde labelling. *Neurogastroenterol. Motil.* 16:113–124.

Roth BL, Tandra S, Burgess LH, Sibley DR, and Meltzer HY (1995) D4 dopamine receptor binding affinity does not distinguish between typical and atypical antipsychotic drugs. *Psychopharmacol-ogy (Berl)* 120:365–368.

Rowe BP, Saylor DL, Speth RC, and Absher DR (1995) Angiotensin-(1-7) binding at angiotensin-ii receptors in the rat-brain. *Regul. Pept.* 56:139–146.

Ruat M, Traiffort E, Arrang JM, Tardivel-Lacombe J, Diaz J, Leurs R, and Schwartz JC (1993) A novel rat serotonin (5-HT6) receptor: molecular cloning, localization, and stimulation of cAMP accumulation. *Biochem Biophys Res Commun* 193:268–276.

Santos R, Ursu O, Gaulton A, Bento AP, Donadi RS, Bologa CG, Karlsson A, Al-Lazikani B, Hersey A, Oprea TI, and Overington JP (2017) A comprehensive map of molecular drug targets. *Nat Rev Drug Discov* 16:19-34.

Santos RA, Ferreira AJ, and Simoes ESAC (2008) Recent advances in the angiotensin-converting enzyme 2-angiotensin(1-7)-Mas axis. *Exp Physiol* 93:519–527.

Santos RA, Simoes e Silva AC, Maric C, Silva DM, Machado RP, de Buhr I, Heringer-Walther S, Pinheiro SV, Lopes MT, Bader M, Mendes EP, Lemos VS, Campagnole-Santos MJ, Schultheiss HP, Speth R, and Walther T (2003) Angiotensin-(1–7) is an endogenous ligand for the G protein-coupled receptor Mas. *Proc Natl Acad Sci U S A* 100:8258–8263.

Santos RA, Ferreira AJ, Verano-Braga T, and Bader M (2013) Angiotensin-converting enzyme 2, angiotensin-(1-7) and Mas: new players of the renin-angiotensin system. *J Endocrinol* 216:R1-R17.

Sargheini N (2017) The molecular characterization of human MrgD receptor *(Bachelor thesis).*

Sasaki K, Yamano Y, Bardhan S, Iwai N, Murray JJ, Hasegawa M, Matsuda Y, and Inagami T (1991) Cloning and expression of a complementary DNA encoding a bovine adrenal angiotensin II type-1 receptor. *Nature* 351:230–233.

Sauer B (1994) Site-specific recombination: developments and applications. *Curr Opin Biotechnol* 5:521–527.

Scalacci N, Brown AK, Pavan FR, Ribeiro CM, Manetti F, Bhakta S, Maitra A, Smith DL, Petricci E, and Castagnolo D (2017) Synthesis and SAR evaluation of novel thioridazine derivatives active against drug-resistant tuberculosis. *Eur J Med Chem* 127:147-158.

Scheerer P, and Sommer ME (2017) Structural mechanism of arrestin activation. *Curr Opin Struct Biol* 45:160-169.

Scheerer P, Park JH, Hildebrand PW, Kim YJ, Krauss N, Choe HW, Hofmann KP, and Ernst OP (2008) Crystal structure of opsin in its G-protein-interacting conformation. *Nature* 455:497-502.

Schmieden V, and Betz H (1995) Pharmacology of the inhibitory glycine receptor: Agonist and antagonist actions of amino acids and piperidine carboxylic acid compounds. *Mol Pharmacol* 48: 919–927.

Schöneberg T, Hofreiter M, Schulz A, and Rompler, H (2007) Learning from the past: evolution of GPCR functions. *Trends Pharmacol.Sci* 28:117−121.

Schröder K, Pulvermüller A, and Hofmann KP (2002) Arrestin and its splice variant Arr1-370A (p44). Mechanism and biological role of their interaction with rhodopsin. *J Biol Chem* 277:43987–43996.

Scott MG, Le Rouzic E, Perianin A, Pierotti V, Enslen H, Benichou S, Marullo S, and Benmerah A (2002) Differential nucleocytoplasmic shuttling of beta-arrestins. Characterization of a leucine-rich nuclear export signal in beta arrestin2. *J Biol Chem* 277:37693–37701.

Seeman P (2002) Atypical antipsychotics: mechanism of action. *Canadian Journal of Psychiatry* 47:27–38.

Seifert R, and Wenzel-Seifert K (2002) Constitutive activity of G-protein-coupled receptors: cause of disease and common property of wild-type receptors. *Naunyn Schmiedeberg's Arch. Pharmacol* 366:381–416.

Shapiro DA, Kristiansen K, Weiner DM, Kroeze WK, and Roth BL (2002) Evidence for a model of agonist-induced activation of 5-hydroxytryptamine 2A serotonin receptors that involves the disruption of a strong ionic interaction between helices 3 and 6. *J Biol Chem* 277:11441–11449.

Sharma D, and Parameswaran N (2015) Multifaceted role of β-arrestins in inflammation and disease. *Genes Immun* 16:499–513.

Shemesh R, Toporik A, Levine Z, Hecht I, Rotman G, Wool A, Dahary D, Gofer E, Kliger Y, Soffer MA, Rosenberg A, Eshel D, Cohen Y (2008) Discovery and validation of novel peptide agonists for G protein-coupled receptors. *J Biol Chem* 283:34643–34649.

Shen YH, Chen XR, Yang CX, Liu BX, and Li P (2018) Alamandine injected into the paraventricular nucleus increases blood pressure and sympathetic activation in spontaneously hypertensive rats. *Peptides* 103:98–102.

Shenoy SK (2007) Seven-transmembrane receptors and ubiquitination. *Circ Res* 100:1142–1154.

Shenoy SK, and Lefkowitz RJ (2011) β-Arrestin-mediated receptor trafficking and signal transduction. *Trends Pharmacol Sci* 32:521–533.

Shenoy SK, McDonald PH, Kohout TA, and Lefkowitz RJ (2001) Regulation of receptor fate by Ubiquitination of activated β2-adrenergic receptor and β-Arrestin. *Science* 294:1307–1313.

Shi C, Zhao M, Shu X, Xiong X, and Wang J (2016) β-aminoisobutyric acid attenuates hepatic endoplasmic reticulum stress and glucose / lipid metabolic disturbance in mice with type 2 diabetes. *Sci Rep* 6:21924.

Shinohara T, Harada M, Ogi K, Maruyama M, Fujii R, Tanaka H, Fukusumi S, Komatsu H, Hosoya M, Noguchi Y, Watanabe T, Moriya T, Itoh Y, and Hinuma S (2004) Identification of a G protein-coupled receptor specifically responsive to beta-alanine. *J Biol Chem* 279: 23559-23564.

Shukla AK, Manglik A, Kruse AC, Xiao K, Reis RI, Tseng W-C, Status DP, Hilger D, Uysal S, Huang L-Y, Paduch M, Tripathi-Shukla P, Koide A, Koide S, Weis WI, Kossiakoff AA, Kobilka BK, Lefkowitz RJ (2013) Structure of active -arrestin-1 bound to a G-protein-coupled receptor phosphopeptide. *Nature* 497:137–141.

Singh M, Yadav A, Ma X, and Amoah E (2010) Plasmid DNA Transformation in Escherichia Coli: Effect of Heat Shock Temperature, Duration, and Cold Incubation of CaCl2 Treated Cells. *Int J Biotech Biochem* 6:561-568.

Smith JS, and Rajagopal S (2016) The β-Arrestins: Multifunctional Regulators of G Protein-coupled Receptors. *J Biol Chem* 291:8969-8977.

Smith JS, Lefkowitz RJ, and Rajagopal S (2018) Biased Signalling: From Simple Switches to Allosteric Microprocessors. *Nat Rev Drug Discov* 17:243-260.

Smith WC, Gurevich EV, Dugger DR, Vishnivetskiy SA, Shelamer CL, McDowell JH, and Gurevich VV (2000) Cloning and functional characterization of salamander rod and cone Arrestins. *Invest Ophthalmol. Vis Sci* 41:2445–2455.

Smrcka AV (2008) G protein βγ subunits: Central mediators of G protein-coupled receptor signaling. *Cell Mol Life Sci* 65:2191–2214.

Soares ER, Barbosa CM, Campagnole-Santos MJ, Santos RAS, and Alzamora AC (2017) Hypotensive effect induced by microinjection of Alamandine, a derivative of angiotensin-(1-7), into caudal ventrolateral medulla of 2K1C hypertensive rats. *Peptides* 96:67–75.

Solinski HJ, Gudermann T, and Breit A (2014) Pharmacology and signaling of MAS-related G protein-coupled receptors. *Pharmacol Rev* 66:570-597.

Soltani Hekmat A, Javanmardi K, Kouhpayeh A, Baharamali E, and Farjam M (2017) Differences in cardiovascular responses to alamandine in two-kidney, one clip hypertensive and normotensive rats. *Circ J* 81:405–12.

Song XD, Feng JP, and Yang RX (2019) Alamandine protects rat from myocardial ischemia-reperfusion injury by activating JNK and inhibiting NF-κB. *Eur Rev Med Pharmacol Sci*. 23:6718-6726.

Southern C, Cook JM, Neetoo-Isseljee Z, Taylor DL, Kettleborough CA, Merritt A, Bassoni DL, Raab WJ, Quinn E, Wehrman TS, Davenport AP, Brown AJ, Green A, Wigglesworth MJ, and Rees S (2013) Screening beta-arrestin recruitment for the identification of natural ligands for orphan G-protein-coupled receptors. *J Biomol Screen* 18:599–609.

Stacey M, Lin HH, Gordon S, and McKnight AJ (2000) LNB-TM7, a group of seven-transmembrane proteins related to family-B G-protein-coupled receptors. *Trends Biochem Sci* 25:284–289.

Standfuss J, Edwards PC, D'Antona A, Fransen M, Xie G, Oprian DD, Schertler GFX (2011) The structural basis of agonist-induced activation in constitutively active rhodopsin. *Nature* 471:656–660.

Stellingwerff T, Decombaz J, Harris R C and Boesch C (2012) Optimizing human in vivo dosing and delivery of b-alanine supplements for muscle carnosine synthesis. *Amino Acids* 43: 57–65.

Strasser A, Wittmann HJ, and Seifert R (2017) Binding Kinetics and Pathways of Ligands to GPCRs. *Trends Pharmacol Sci* 38:717-732.

Subramanian H, Gupta K, and Ali H (2016) Roles of Mas-related G protein-coupled receptor X2 on mast cell-mediated host defense, pseudoallergic drug reactions, and chronic inflammatory diseases. *J Allergy Clin Immunol* 138:700-710.

Suzuki H, Gen K, and Inoue Y (2013) Comparison of the anti-dopamine D_2 and anti-serotonin 5-HT(2A) activities of chlorpromazine, bromperidol, haloperidol and second-generation antipsychotics parent compounds and metabolites thereof. *J Psychopharmacol* 27: 396–400.

Suzuki Y, Osamu I, Mukai N, Takahashi H, and Takamatsu K (2002). High level of skeletal muscle carnosine contributes to the letter half of exercise performance during 30-s maximal cycle ergometer sprinting. *Jpn J Physiol* 52: 199–205.

Sykes DA, Stoddart LA, Kilpatrick LE, and Hill SJ (2019) Binding kinetics of ligands acting at GPCRs. *Mol Cell Endocrinol* 485:9–19.

Szallasi A, Nilsson S, Blumberg PM, Hokfelt T, and Lundberg JM (1996). Binding of neuroleptic drugs (trifluoperazine and rimcazole) to vanilloid receptors in porcine dorsal horn. *Eur J Pharmacol* 298:321–327.

Takeda S, Kadowaki S, Haga T, Takaesu H, and Mitaku S (2002) Identification of G protein-coupled receptor genes from the human genome sequence. *FEBS Lett* 520: 97–101.

Tallant EA, Lu X, Weiss RB, Chappell MC, and Ferrario CM (1997) Bovine aortic endothelial cells contain an angiotensin-(1-7) receptor. *Hypertension* 29:388–393.

Tan Q, Zhu Y, Li J, Chen Z, Han GW, Kufareva I, Li T, Ma L, Fenalti G, Li J, Zhang W, Xie X, Yang H, Jiang H, Cherezov V, Liu H, Stevens RC, Zhao Q, and Wu B (2013) Structure of the CCR5 chemokine receptor-HIV entry inhibitor maraviroc complex. *Science* 341:1387-1390.

Tanianskii DA, Jarzebska N, Birkenfeld AL, O'Sullivan JF, and Rodionov RN (2019) Beta-Aminoisobutyric Acid as a Novel Regulator of Carbohydrate and Lipid Metabolism. *Nutrients* 11:524.

Tatemoto K, Nozaki Y, Tsuda R, Konno S, Tomura K, Furuno M, Ogasawara H, Edamura K, Takagi H, and Iwamura H, Noguchi M, Naito T (2006) Immunoglobulin E independent activation of mast cell is mediated by Mrg receptors. *Biochem Biophys Res Commun* 349:1322–1328.

Tetzner A, Gebolys K, Meinert C, Klein S, Uhlich A, Trebicka J, Villacañas Ó, and Walther T (2016) G-Protein-Coupled Receptor MrgD Is a Receptor for Angiotensin-(1-7) Involving Adenylyl Cyclase, cAMP, and Phosphokinase A. *Hypertension* 68:185-194.

Tetzner A, Naughton M, Gebolys K, Eichhorst J, Sala E, Villacañas Ó, and Walther T (2018) Decarboxylation of Ang-(1-7) to Ala^{1}-Ang-(1-7) leads to significant changes in pharmacodynamics. *Eur J Pharmacol* 833:116-123.

Thanacoody RH (2011) Thioridazine: the good and the bad. *Recent Pat Antiinfect Drug Discov* 6:92–98.

Thomas D, Tovey SC, Collins TJ, Bootman MD, Berridge MJ, and Lipp P (2000) A comparison of fluorescent Ca2+ indicator properties and their use in measuring elementary and global Ca2+ signals. *Cell Calcium* 28:213-223.

Tiedje KE, Stevens K, Barnes S, and Weaver DF (2010) β-Alanine as a small molecule neurotransmitter. *Neurochem. Int* 57:177–188.

Tikhonova IG, Gigoux V, and Fourmy D (2019) Understanding Peptide Binding in Class A G Protein-Coupled Receptors. *Mol Pharmacol* 96:550-561.

Tirupula KC, Desnoyer R, Speth RC, and Karnik SS (2014) Atypical signaling and functional desensitization response of MAS receptor to peptide ligands. *PLoS One* 9: e103520.

Tobin AB (2008) G-protein-coupled receptor phosphorylation: where, when and by whom. *Br J Pharmacol* 153 (Suppl. 1):S167–S176.

Trzaskowski B, Latek D,Yuan S, Ghoshdastider U, Debinski A, and Filipek S (2012) Action of Molecular Switches in GPCRs - Theoretical and Experimental Studies. *Curr Med Chem* 19: 1090–1109.

Tsien RY, Pozzan T, and Rink TJ (1982) Calcium homeostasis in intact lymphocytes: cytoplasmic free calcium monitored with a new, intracellularly trapped fluorescent indicator. *J Cell Biol* 94:325-334.

Tuynder M, Fiucci G, Prieur S, Lespagnol A, Geant A, Beaucourt S, Duflaut D, Besse S, Susini L, Cavarelli J, Moras D, Amson R, and Telerman A (2004) Translationally controlled tumor protein is a target of tumor reversion. *Proc Natl Acad Sci U S A* 101:15364–15369.

Tyndall JD, and Sandilya R (2005) GPCR agonists and antagonists in the clinic. *Med Chem* 1:405–421.

Uchiyama T, Okajima F, Mogi C, Tobo A, Tomono S, and Sato K (2017) Alamandine reduces leptin expression through the c-Src/p38 MAP kinase pathway in adipose tissue. PLoS ONE 12:e0178769.

Ullman EF, Kirakossian H, Singh S, Wu ZP, Irvin BR, Pease JS, Switchenko AC, Irvine JD, Dafforn A, Skold CN, and Wagner DB (1994) Luminescent oxygen channeling immunoassay: measurement of particle binding kinetics by chemiluminescence. *Proc Natl Acad Sci U S A* 91:5426–5430.

Unger VM, Hargrave PA, Baldwin JM, and Schertler GF (1997) Arrangement of rhodopsin transmembrane alpha-helices. *Nature* 389:203-206.

Uno M, Nishimura S, Fukuchi K, Kaneta Y, Oda Y, Komori H, Takeda S, Haga T, Agatsuma T and Nara F (2012) Identification of physiologically active substances as novel ligands for MRGPRD. *J Biomed Biotechnol* 2012:816159.

Vaidya ADB (2014) Reverse Pharmacology-A Paradigm Shift for Drug Discovery and Development. *Curr Res Drug Discov* 1:39-44.

Van Eps N, Altenbach C, Caro LN, Latorraca NR, Hollingsworth SA, Dror RO, Ernst OP, and Hubbell WL (2018) Gi- and Gs-coupled GPCRs show different modes of G-protein binding. Proc Natl Acad Sci U S A 115:2383–2388.

van Gennip AH, Kamerling JP, de Bree PK and Wadman SK (1981) Linear relationship between the R- and S -enantiomer of *β*-aminoisobutyric acid in human urine. *Clin Chim Acta* 116:261–267.

Van Kuilenburg AB, Stroomer AE, Van Lenthe H, Abeling NG, and Van Gennip AH (2004) New insights in dihydropyrimidine dehydrogenase deficiency: a pivotal role for beta-aminoisobutyric acid? *Biochem J* 379:119-124.

van't Veer LJ, van der Feltz MJM, van den Berg-Bakker CA, Cheng NC, Hermens RPMG, van Oorschot DAJ, Kievits T, and Schrier PI (1993) Activation of the mas oncogene involves coupling to human alphoid sequences. *Oncogene* 8:2673–2681.

Vanni S, Neri M,Tavernelli I, and Rothlisberger U (2009) Observation of "Ionic Lock" Formation in Molecular Dynamics Simulations of Wild-Type β1 and β2 Adrenergic Receptors†. *Biochemistry* 48:4789–4797.

Vass M, Kooistra AJ, Yang D, Stevens RC, Wang MW, and de Graaf C. Chemical Diversity in the G Protein-Coupled Receptor Superfamily (2018) *Trends Pharmacol Sci* 39:494-512.

Venkatakrishnan AJ, Deupi X, Lebon G, Tate CG, Schertler GF, and Babu MM (2013) Molecular signatures of G-protein-coupled receptors. *Nature* 494:185–194.

Villela DC, Passos-Silva DG, and Santos RA (2014) Alamandine: a new member of the angiotensin family. *Curr Opin Nephrol Hypertens* 23:130-134.

Vinson CR, Conover S, and Adler PN (1989) A *Drosophila* tissue polarity locus encodes a protein containing seven potential transmembrane domains. *Nature* 338:263–264.

Violin JD, and Lefkowitz RJ (2007) β-arrestin-biased ligands at seven-transmembrane receptors. *Trends Pharmacol Sci* 28:416–422.

Violin JD, Crombie AL, Soergel DG, and Lark MW (2014) Biased ligands at G-protein-coupled receptors: promise and progress. *Trends Pharmacol Sci* 35:308–316.

Vogel R, Mahalingam M, Ludeke S, Huber T, Siebert F, and Sakmar TP (2008) Functional role of the "ionic lock"—an interhelical hydrogen-bond network in family A heptahelical receptors. *J Mol Biol* 380:648–55.

Vogelstein B, and Gillespie D (1979) Preparative and analytical purification of DNA from agarose. *Proc Natl Acad Sci U S A* 76:615–619.

Wall MA, Coleman DE, Lee E, Iñiguez-Lluhi JA, Posner BA, Gilman AG, and Sprang SR (1995) The structure of the G protein heterotrimer Gi alpha 1 beta 1 gamma 2. *Cell* 83:1047-1058.

Wang H, Qian J, Zhao X, Xing C, and Sun B (2017) β-Aminoisobutyric acid ameliorates the renal fibrosis in mouse obstructed kidneys via inhibition of renal fibroblast activation and fibrosis. *J Pharmacol Sci* 133:203–213.

Wang H-S, Pan Z, Shi W, Brown BS, Wymore RS, Cohen IS, Dixon JE, and McKinnonD (1998) KCNQ2 and KCNQ3 potassium channel subunits: molecular correlates of the M-channel. *Science* 282:1890 –1893.

Wang L, Liu C, Chen X, and Li P (2019) Alamandine attenuates long-term hypertension-induced cardiac fibrosis independent of blood pressure. *Mol Med Rep* 19:4553-4560.

Warne T, Serrano-Vega MJ, Tate CG, and Schertler GF (2009) Development and crystallization of a minimal thermostabilised G protein-coupled receptor. *Protein Expr Purif* 65:204–213.

Wenzel-Seifert K, and Seifert R (2000) Molecular analysis of beta(2)-adrenoceptor coupling to G(s)-, G(i)-, and G(q)-proteins. *Mol Pharmacol* 58:954-966.

Wettschureck N, and Offermanns S (2005) Mammalian G proteins and their cell type specific functions. *Physiol Rev* 85:1159-1204.

Wilden U, Wüst E, Weyand I, and Kühn H (1986) Rapid affinity purification of retinal arrestin (48 kDa protein) via its light-dependent binding to phosphorylated rhodopsin. *FEBS Lett.* 207:292–295.

Wilfinger WW, Mackey K and Chomczynski P (1997) Effect of pH and ionic strength on the spec-trophotometric assessment of nucleic acid purity. *Biotechniques* 22:474–481.

Wilkie TM, Gilbert DJ, Olsen AS, Chen XN, Amatruda TT, Korenberg JR, Trask BJ, de Jong P, Reed RR, Simon MI, Jenkins NA, and Copeland NG (1992) Evolution of the mammalian G protein *a* subunit multigene family. *Nat Genet* 1:85-91.

Wilson BA, Cruz-Diaz N, Marshall AC, Pirro NT, Su Y, Gwathmey TM, Rose JC, Chappell MC (2015) An angiotensin-(1-7) peptidase in the kidney cortex, proximal tubules, and human HK-2 epithelial cells that is distinct from insulin-degrading enzyme. *Am J Physiol Renal Physiol*. 308:F594-601.

Wise A, Jupe SC, and Rees S (2004) The identification of ligands at orphan G-protein coupled receptors. *Annu Rev Pharmacol Toxicol* 44:43–66.

Wittenberger T, Schaller HC, and Hellebrand S (2001) An expressed sequence tag (EST) data mining strategy succeeding in the discovery of new G-protein coupled receptors. *J Mol Biol* 307:799–813.

Woolf CJ, and Ma Q (2007) Nociceptors--noxious stimulus detectors. *Neuron* 55:353–364.

World Health Organisation 18th (April 2013) WHO Model List of Essential Medicines. apps.who.int/iris/bitstream/10665/93142/1/ EML˙18˙eng.pdf?ua=1.

Wu B, Chien EY, Mol CD, Fenalti G, Liu W, Katritch V, Abagyan R, Brooun A, Wells P, Bi FC, Hamel DJ, Kuhn P, Handel TM, Cherezov V, and Stevens RC (2010) Structures of the CXCR4 Chemokine GPCR with Small- Molecule and Cyclic Peptide Antagonists. *Science* 330:1066-1071.

Wu FS, Gibbs TT, and Farb DH (1993) Dual activation of GABAA and glycine receptors by beta-alanine inverse modulation by progesterone and 5 alpha-pregnan-3 alpha-ol-20-one. *Eur J Pharmacol*. 246:239–246.

Wu H, Peisley A, Graef IA, and Crabtree GR (2007) NFAT signaling and the invention of vertebrates. *Trends Cell Biol* 17:251–260.

Xu F, Wu H, Katritch V, Han GW, Jacobson KA, Gao ZG, Cherezov V, and Stevens RC (2011) Structure of an agonist bound human A2A adenosine receptor. *Science* 332:322–327.

Yamada EW, and Jakoby WB (1960) Aldehyde oxidation. Direct conversion of malonic semialdehyde to acetyl-coenzyme A. *J Biol Chem* 235:589–594.

Yasgar A, Jadhav A, Simeonov A, and Coussens NP (2016) AlphaScreen-Based Assays: Ultra-High-Throughput Screening for Small-Molecule Inhibitors of Challenging Enzymes and Protein-Protein Interactions. *Methods Mol Biol* 1439:77-98.

Yin H, Chu A, Li W, Wang B, Shelton F, Otero F, Nguyen DG, Caldwell JS, and Chen YA (2009) Lipid G protein-coupled receptor ligand identification using beta-arrestin PathHunter assay. *J Biol Chem* 284:12328-12338.

Yong M, Yu T, Tian S, Liu S, Xu J, Hu J, Hu L (2017) DR2 blocker thioridazine: A promising drug for ovarian cancer therapy. *Oncol Lett* 14:8171-8177.

Yoshida,M, Miyazato,M, and Kangawa,K (2012) Orphan GPCRs and methods for identifyingtheirligands. *Methods Enzymol.* 514:33–44.

Young D, Waitches G, Birchmeier C, Fasano O, and Wigler M (1986) Isolation and characterization of a new cellular oncogene encoding a protein with multiple potential transmembrane domains. *Cell* 45:711–719.

Zanettini C, Wilkinson DS, and Katz JL (2018) Behavioral economic analysis of the effects of N-substituted benztropine analogs on cocaine selfadministration in rats. *Psychopharmacology* 235:47–58.

Zhang C, Srinivasan Y, Arlow DH, Fung JJ, Palmer D, Zheng Y, Green HF, Pandey A, Dror RO, Shaw DE, Weis WI, Coughlin SR, and Kobilka BK (2012a). High-resolution crystal structure of human protease-activated receptor 1. *Nature* 49:387-392.

Zhang D, Zhao Q, and Wu B (2015a) Structural Studies of G Protein-Coupled Receptors. *Mol Cells* 38:836–842.

Zhang D, Gao ZG, Zhang K, Kiselev E, Crane S, Wang J, Paoletta S, Yi C, Ma L, Zhang W, Han GW, Liu H, Cherezov V, Katritch V, Jiang H, Stevens RC, Jacobson KA, Zhao Q, and Wu B (2015b). Two disparate ligand-binding sites in the human P2Y1 receptor. *Nature* 520:317-321.

Zhang K, Zhang J, Gao ZG, Zhang D, Zhu L, Han GW, Moss SM, Paoletta S, Kiselev E, Lu W, Fenalti G, Zhang W, Muller CE, Yang H, Jiang H, Cherezov V, Katritch V, Jacobson KA, Stevens RC, Wu B, Zhao Q (2014) Structure of the human P2Y12 receptor in complex with an antithrombotic drug. *Nature* 509:115-118.

Zhang L, Taylor N, Xie Y, Ford R, Johnson J, Paulsen JE, and Bates B (2005) Cloning and expression of MRG receptors in macaque, mouse, and human. *Brain Res Mol Brain Res* 133:187–197.

Zhang L, Yao K, Fan Y, He P, Wang X, Hu W, and Chen Z (2012c) Carnosine protects brain microvascular endothelial cells against rotenone-induced oxidative stress injury through histamine H_1 and H_2 receptors in vitro. *Clin Exp Pharmacol Physiol* 39:1019-1025.

Zhang R, Yan PK, Zhou CH, Liao JY, and Wang MW (2007) Development of a homogeneous calcium mobilization assay for high throughput screening of mas-related gene receptor agonists. *Acta Pharmacol Sin* 28:125-131.

Zhang T, Li Z, Dang H, Chen R, Liaw C, Tran TA, Boatman PD, Connolly DT, and Adams JW (2012b) Inhibition of Mas G-protein signaling improves coronary blood flow, reduces myocardial infarct size, and provides long-term cardioprotection. *Am J Physiol Heart Circ Physiol* 302:H299–H311.

Zhang Y, Sun B, Feng D, Hu H, Chu M, Qu Q, Tarrasch JT, Li S, Sun Kobilka T, Kobilka BK, and Skiniotis G (2017) Cryo-EM structure of the activated GLP-1 receptor in complex with a G protein. *Nature* 546:248–253.

Zhao J, Deng Y, Jiang Z, and Qing H (2016) G Protein-Coupled Receptors (GPCRs) in Alzheimer's Disease: A Focus on BACE1 Related GPCRs. *Front Aging Neurosci* 8:58.

Zhou XE, He Y, de Waal PW, Gao X, Kang Y, Van Eps N, Yin Y, Pal K, Goswami D, White TA, Barty A, Latorraca NR, Chapman HN, Hubbell WL, Dror RO, Stevens RC, Cherezov V, Gurevich VV, Griffin PR, Ernst OP, Melcher K, and Xu HE (2017) Identification of

phosphorylation codes for arrestin recruitment by G protein-coupled receptors. *Cell* 170:457–469.

Zhu P, Verma A, Prasad T, Li Q (2020) Expression and Function of Mas-Related G Protein-Coupled Receptor D and Its Ligand Alamandine in Retina. *Mol Neurobiol* 57:513-527.

Zhuo RG, Ma XY, Zhou PL, Liu XY, Zhang K, Wei XL, Yan HT, Xu JP, and Zheng JQ (2014) Mas-related G protein-coupled receptor D is coupled to endogenous calcium activated chloride channel in Xenopus oocytes. *J Physiol Biochem* 70:185-191.

Zylka MJ, Dong X, Southwell AL, and Anderson DJ (2003) Atypical expansion in mice of the sensory neuron-specific Mrg G protein-coupled receptor family. *Proc Natl Acad Sci U S A* 100:10043–10048.

Zylka MJ, Rice FL, and Anderson DJ (2005) Topographically distinct epidermal nociceptive circuits revealed by axonal tracers targeted to Mrgprd. *Neuron* 45:17–25.

8. Publications

Poster contributions:

1. Arbogast M, Hanna DMF, Müller S, Sargheini N, Hoffmann K, and von Kügelgen I (2018) Analysis of the ligand binding site of the human Mas-related G protein-coupled receptor D by site-directed mutagenesis. *Naunyn-Schmiedebergs Arch Pharmacol* 391 Supp 1: S32.

2. Hanna DMF, Arbogast M, Müller S, and von Kügelgen I (2020) Coupling of the human Mas-related G protein coupled receptor D to the β-arrestin pathway. *Naunyn-Schmiedebergs Arch Pharmacol* 393 Supp 1: S33.

3. Hanna DMF, Müller S, Arbogast M, and von Kügelgen I (2021) Biased antagonism of the human Mas-related G protein-coupled receptor D. *Naunyn-Schmiedebergs Arch Pharmacol* 394 Supp 1: S41.

9. Acknowledgment

To ***Jesus Christ***, our Lord and Savior, for giving me the wisdom, strength, support, and knowledge to pursue this research and to make this thesis possible.

I would like to express my deepest appreciation and sincere gratitude to my supervisor ***Prof. Dr. med. Ivar von Kügelgen***, for granting me the opportunity to conduct my PhD in his laboratory. His instructive supervision, kind help and generous attitude have been the cornerstone throughout the development of this work.

I would like to especially thank ***Prof. Dr. Christa E. Müller,*** for being my second supervisor.

I would like to acknowledge and sincerely appreciate, ***PD. Dr. Anke Schiedel*** and ***Prof. Dr. Dorothea Bartels*** for giving me the honor of having them in my graduate committee.

I would also like to thank all my colleagues in the Institute of Pharmacology and Toxicology, Pharma Center Bonn for their valuable help, support, and encouragement. A special thanks goes to ***Michael Arbogast, Alina Malov, Elena Bringmann, Nafiseh Sargheini, Katharina Schlomberg, Dorothée Bouschery, Leonie Casimir, Natalie Aster, Rosa Armengol, Mireille Debono, Jonas Richter, Vanessa Hollfoth, Jannis Spintge, and Phillip Koch,*** my dearest officemates.

I would like to cordially thank my dearest friend and sister ***Sara Refaat*** for believing in me and for her continuous support and encouragement.

Finally, I would like to express my deepest thanks to my parents and family, for their patience throughout the whole time of the thesis. A special thanks to my son ***Jovani,*** and my greatest gratitude goes to my husband ***John*** for bearing this load, never doubting me, and continuing to support me even through the hardest times. I will be forever in your debt.